



Universiteit Utrecht



Koninklijk Nederlands
Instituut voor Onderzoek
der Zee

Restratification Structure and Processes in the Irminger Sea

MASTER THESIS

Miriam F. Sterl

Climate Physics



Supervisors:

DR. M.F. DE JONG
Royal Netherlands Institute for Sea Research

DR. E. VAN SEBILLE
Institute for Marine and Atmospheric Research Utrecht

PROF. DR. L.R.M. MAAS
Institute for Marine and Atmospheric Research Utrecht

October 2021

*“Sailing on the ocean, sailing on the sea.
Sailing on a ship is the life for me.”*

RUMAHOY – Pirateship

Abstract

The Irminger Sea is one of the few regions in the global ocean where deep convection occurs. Deep convection is followed by restratification during summer, when the stratification of the water column is reestablished and the convectively formed dense water is exported to the lower limb of the Atlantic Meridional Overturning Circulation (AMOC). We investigate the interannual variability and physical drivers of restratification in the upper 600 m of the Irminger Sea using the CMEMS oceanic reanalysis data for the years 1993–2019. We find that there are distinctly different restratification processes in the upper 100 m of the water column (the upper layer) and the water below it (the lower layer). In the upper layer, the stratification is dominated by the strong seasonal cycle. Restratification starts when the surface heat flux becomes positive, and ends when the heat flux becomes negative. The minimum stratification in winter is always zero, because the mixed layer always extends below the bottom of the upper layer. Interannual variability in the maximum summer stratification is mostly caused by warm and fresh anomalies that cause high stratification, and cold and saline anomalies that cause low stratification. In 2010 and 2019, there were peaks in stratification in the upper layer, which could be related to the combination of surface warming and freshwater gain. In 2010 meltwater from Greenland likely contributed to the high freshwater anomaly. In 2019 an extreme freshwater anomaly circulating through the subpolar North Atlantic added to the freshwater anomaly. By contrast, in the lower layer the seasonal cycle is weaker and there is strong interannual variability. Restratification can continue for up to 5 months after the surface heat flux has become negative, which indicates a role for lateral advection. The maximum summer stratification in this layer is determined by the minimum stratification in the preceding winter as well as the strength of restratification during summer. The minimum winter stratification is related to the mixed layer depth in that winter. The strength of restratification is strongly correlated with eddy kinetic energy in the eastern Irminger Sea. This suggests the lateral advection is driven by warm, saline eddies shed by the Irminger Current. In the future, increased ocean surface temperatures and meltwater from the Greenland Ice Sheet and Arctic sea ice due to anthropogenic climate change are expected to increase upper layer stratification in the Irminger Sea, potentially inhibiting mixing and thereby slowing down deep convection.

Plain Language Summary

The density of sea water is determined by its salinity and temperature. Cold, saline water is denser than warm, fresh water. The ocean at rest is *stratified*: it consists of vertical layers with increasing densities toward the bottom. The larger the density difference between the bottom and top layers, the stronger the stratification. However, stratification can be removed during a process called *deep convection*. If the surface waters become very cold, they may become denser than the layers below, thus sinking and starting to mix with the water below. The mixed part of the water column will then have homogeneous properties, i.e. the same temperature and salinity and thus the same density throughout. If the cooling of the surface continues for a long time, so will this mixing process, resulting in a very deep layer of water with zero or very low stratification. The depth of the mixed layer is partially determined by the initial stratification: if the stratification was already low, it is easier to completely remove it. Once the mixing has stopped, the stratification can come back: this is called *restratification*. Restratification happens for example through heating of the surface. Furthermore, water around the mixed layer which is still stratified can move into the mixed layer, thus also bringing back the stratification.

The cycle of deep convection and restratification occurs only at a few locations in the ocean. An important region where it takes place is the North Atlantic. Here the cycle plays an important role in the Atlantic Meridional Overturning Circulation (AMOC), which is a key component of the climate system because it maintains the relatively mild climate in western Europe, and leads to the North Atlantic storing large amounts of anthropogenic CO₂. At the ocean's surface, the Gulf Stream transports warm waters from the equator northward. When these waters reach the North Atlantic, strong wintertime surface cooling can initiate deep convection, forming mixed layers of more than 1 km deep. In spring, when the surface starts warming again, restratification begins. The dense water mass that was in the mixed layer sinks down to large depths, where it flows back southward.

One of these regions in the North Atlantic where deep convection and restratification happen is the Irminger Sea, southeast of Greenland. In contrast to deep convection, restratification in the Irminger Sea has not been the subject of any major study yet. Therefore the aim of this study is to provide a detailed description of restratification after deep convection in the Irminger Sea.

One of the most important findings is that we can distinguish two vertical layers in the Irminger Sea, which have different restratification behaviour: the upper layer from 0–100 m and the lower layer from 100–600 m.

In the upper layer, the stratification follows a strong seasonal cycle. Stratification is almost zero in winter, when the surface is cooled; then the upper 100 m are completely mixed. In summer, when the surface is warming, the stratification in the upper layer is large. There are yearly fluctuations: for example, in 2010 and 2019 the summer stratification in the upper layer was clearly stronger than in other years. This could be linked to high precipitation and strong solar radiation, which made the surface fresher and warmer, and thus lighter than usual. Additionally, in 2010 there was likely an effect of fresh meltwater from Greenland.

In the lower layer, the stratification also follows a seasonal cycle, but with large differences between years. Deep convection is weak in some winters, so that the mixing does not reach the bottom of the lower layer, leading to high stratification. In the following summer, stratification will also be high. Furthermore, for the lower layer we found that the restratification is driven by warm, saline waters coming from the Irminger Current on the eastern side of the Irminger Sea.

A good understanding of the physical drivers of restratification can help us understand how the cycle of deep convection and restratification in the Irminger Sea might change under the influence of climate change. We know that the ocean surface is currently warming and that the Greenland Ice Sheet is melting, which can lead to strong summertime stratification in the upper layer of the Irminger Sea. Higher stratification might result in shallower mixed layers, because it is harder to remove the stratification and mix down to large depths. Shallower mixed layers mean less sinking of dense waters and thus less storage of CO₂ in the deep ocean. Moreover, there is less dense water which can flow back southward to the equator at large depths. If this part of the AMOC becomes slower, all the other parts will become slower as well, including the Gulf Stream. Changes in stratification in the Irminger Sea may thus have major consequences for the climate system. It is therefore important to understand how the different processes impacting restratification in the Irminger Sea are expected to change in the coming decades.

Contents

Abstract	i
Plain Language Summary	ii
1 Introduction	1
1.1 The Atlantic Meridional Overturning Circulation	1
1.2 Deep Convection and Restratification	1
1.3 Restratification in the Subpolar North Atlantic	3
1.4 The Irminger Sea	3
1.5 Research Questions	4
2 Data and Methods	5
2.1 Data	5
2.1.1 CMEMS Oceanic Reanalysis	5
2.1.2 ERA5 Atmospheric Reanalysis	6
2.2 Methods	6
2.2.1 Defining the Deep Convection Area	6
2.2.2 Making Hydrographic Sections	6
2.2.3 Quantifying Stratification and Restratification	8
2.3 Data Validation	9
2.3.1 Validation with LOCO mooring	9
2.3.2 Validation with CTD data	12
3 Results	14
3.1 Time-Mean Fields	14
3.1.1 Time-Mean and Standard Deviation of Hydrographic Properties over Depth	14
3.1.2 Maps of Mean Hydrographic Properties and Atmospheric Fluxes	15
3.1.3 Mean Hydrographic Sections	16
3.2 Climatology	17
3.2.1 Climatology of Atmospheric Fluxes	17
3.2.2 Climatology of Convection and Stratification	18
3.2.3 Climatology of Hydrographic Sections	20

3.2.4	Climatology of Hydrographic Properties over Depth	20
3.3	Interannual Variability	22
3.3.1	Variability of Hydrographic Properties	23
3.3.2	Variability of Atmospheric Fluxes	24
3.3.3	Variability of Stratification and Restratification	25
4	Interpretation	27
4.1	Case Studies	27
4.1.1	Upper Layer	27
4.1.1.1	High Stratification - 2010 & 2019	27
4.1.1.2	Low Stratification - 2013 & 2015	28
4.1.1.3	Discussion Upper Layer	29
4.1.2	Lower layer	30
4.1.2.1	High Stratification - 2004 & 2006	30
4.1.2.2	Low Stratification - 2009 & 2015	30
4.1.2.3	Discussion Lower Layer	31
4.2	Influence of Salinity and Temperature on (Re)Stratification	33
4.3	Physical Processes Contributing to (Re)Stratification	35
5	Summary and Discussion	37
5.1	Summary	37
5.2	Discussion	38
5.3	Implications for the Future	39
	Data Availability Statement	40
	Acknowledgements	41
	References	42
A	Effect of Averaging CMEMS Data Over DCA	46
A.1	Choosing a DCA Boundary	46
A.2	Comparison of CMEMS Data at Fixed Location and Averaged Over DCA	47

1 Introduction

The Atlantic Meridional Overturning Circulation (AMOC) plays an important role in the global climate system. In the Atlantic ocean, warm and saline waters are transported northward from the equator to high latitudes, where wintertime deep convection transforms them into cold, dense and carbon-rich waters. The deep convection phase is always followed by restratification of the water column during summer. In the subpolar North Atlantic, deep convection and restratification occur in the Nordic Seas, the Labrador Sea, and the Irminger Sea. In the Labrador Sea, both processes have been the subjects of scientific studies. However, for the Irminger Sea, there is no complete study about restratification after deep convection, even though the Irminger Sea was recently found to be one of the regions which contributes the most to overturning in the subpolar gyre (Lozier et al., 2019; Petit et al., 2020; Li et al., 2021). The aim of this project is to provide a detailed study of restratification in the Irminger Sea.

1.1 The Atlantic Meridional Overturning Circulation

The Atlantic Meridional Overturning Circulation (AMOC) is a key component in the climate system. Its pathways are schematically illustrated in Figure 1. In its upper limb, the upper layers of the Atlantic, the AMOC transports warm and saline waters from the equator northward to the subpolar North Atlantic (Lozier, 2010, 2012). There, wintertime air-sea buoyancy loss through strong winds and low air temperatures results in deep convection, which transforms the subtropical waters into cold and dense waters that are rich in carbon and oxygen (Fröb et al., 2016). These dense waters can sink to the southward flowing lower limb of the AMOC in the deep ocean, where they are isolated from the atmosphere for hundreds to thousands of years. Thus the AMOC plays an important role in the ocean’s uptake and storage of heat and anthropogenic CO₂ from the atmosphere (Fröb et al., 2016; Brown et al., 2021). Furthermore, the heat that is released by the ocean at these high latitudes is important for maintaining the relatively mild climate in western Europe, compared to similar latitudes across the ocean (McCarthy et al., 2017). The AMOC will very likely decline over the 21st century as a result of anthropogenic climate change, which may cause a weakening of deep convection (Fox-Kemper et al., 2021). This decline is expected to have a large impact on the global climate, global ocean heat content and transport, global ocean anthropogenic carbon uptake, and sea level (Pérez et al., 2013; McCarthy et al., 2017; Fox-Kemper et al., 2021).

1.2 Deep Convection and Restratification

The process of deep convection resulting in the transformation of warm and light surface waters into cold and dense deep waters can be theoretically described as a three-phase process (Jones and Marshall, 1997; Marshall and Schott, 1999; Gelderloos et al., 2011; de Jong et al., 2018). These three phases are sketched in Figure 2. The first phase is the *preconditioning* phase, which consists of a large-scale (order of 100 km) cyclonic circulation with ‘doming’ isopycnals, bringing weakly stratified waters of the interior close to the surface. The second phase is the *deep convection* phase. It is initiated by vigorous winter buoyancy loss which erodes the near-surface stratification of the cyclonic dome, exposing the weakly stratified water mass beneath directly to the surface forcing. This occurs over an area of several hundred kilometers. Further surface buoyancy loss then makes the surface water cooler and thus denser, until it become denser than the water below, and is mixed downward. This mixing happens in numerous convective plumes. These plumes have horizontal and vertical dimensions in the order of 1 km. Together they eventually form a large and deep ‘mixed patch’ or ‘convective patch’ with homogeneous properties, with a diameter in the order of 100 km. The third phase is the *restratification phase*, which occurs in summer. During this phase the stratification of the convective patch is reestablished by surface buoyancy gain and by lateral exchange between the convective patch and its environment through eddies, which are the result of instability of the density front between the two regions. The cold, dense, convective water mass is then exported to large depths. The restratification occurs on a time scale of weeks to months.

There are only a few areas in the world ocean where the cycle of deep convection and restratification occurs. In the North Atlantic, deep convection occurs in the Labrador Sea (e.g. Lilly et al., 1999; Lazier et al., 2002; Straneo, 2006a; Yashayaev and Loder, 2017) and in the Irminger Sea (e.g. Pickart et al., 2003; Våge et al., 2011; De Jong et al., 2012; de Jong et al., 2018). Here the convectively formed dense waters can be exported to the

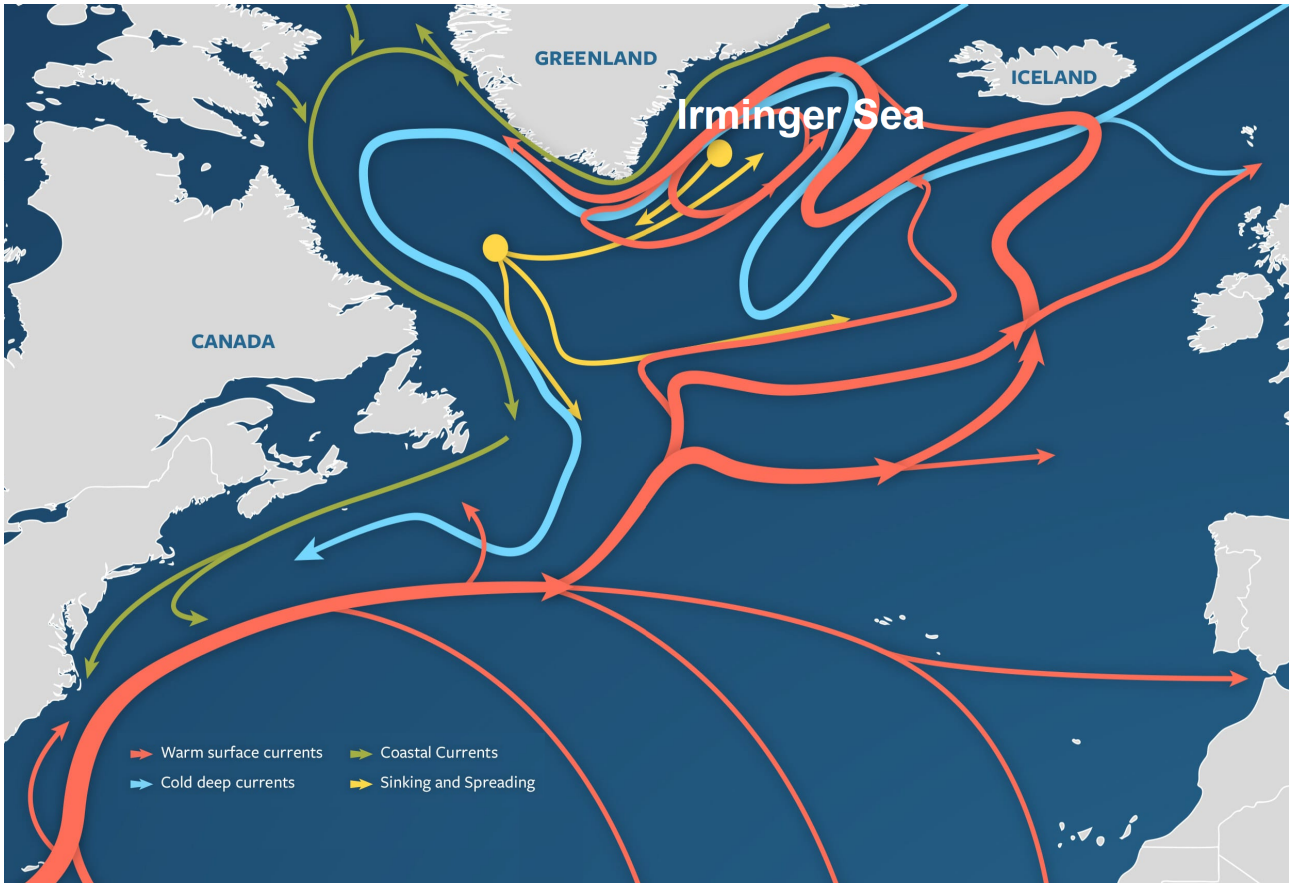


Figure 1: Schematic overview of the Atlantic Meridional Overturning Circulation (AMOC). Adapted from Eric S. Taylor, ©Woods Hole Oceanographic Institution, source: <https://www.whoi.edu/news-insights/content/the-future-of-the-oceans-conveyor-belt/>.

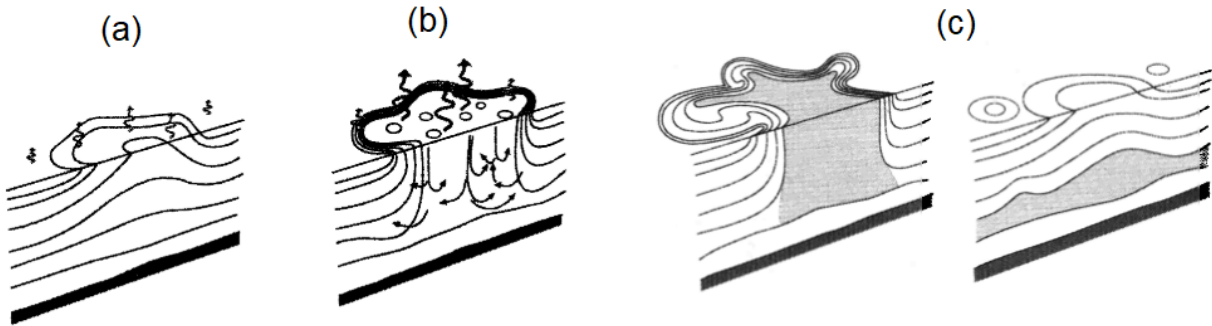


Figure 2: Schematic diagram of the three phases of open-ocean deep convection: (a) preconditioning, (b) deep convection, and (c) restratification and spreading. Buoyancy flux through the sea surface is represented by curly arrows, and the underlying stratification/outcrops is shown by continuous lines. The volume of fluid mixed by convection is shaded. Adapted from Marshall and Schott (1999) (their Figure 3).

perimeter of these seas and downwell to enter the lower limb of the AMOC (Straneo, 2006b; Georgiou et al., 2019; Le Bras et al., 2020). Furthermore deep convection occurs in the Greenland Sea (e.g. Bashmachnikov et al., 2021), the Gulf of Lyon in the Mediterranean (e.g. L'Hévéder et al., 2013; Somot et al., 2018), and the Weddell and Ross Seas in the Southern Ocean (e.g. Assmann and Timmermann, 2005; Pedro et al., 2016; Wang et al., 2017).

1.3 Restratification in the Subpolar North Atlantic

In this study we focus specifically on the restratification phase in the North Atlantic. The North Atlantic stores 23% of global oceanic anthropogenic CO₂ (Sabine et al., 2004) and thus has an important influence on the climate system. There are multiple studies addressing restratification in the Labrador Sea. It was found that there is interannual variability in the deep convection as well as the restratification in the Labrador Sea (e.g. Lazier et al., 2002; Straneo, 2006a; de Jong et al., 2016). Furthermore it was shown that surface buoyancy gain during summer alone cannot account for restratification. Instead, lateral exchange between the interior, where deep convection occurs, and the cyclonic boundary current in the Labrador Sea plays an important role in restratifying the water column (e.g. Jones and Marshall, 1997; Straneo, 2006a). Many studies have focused on this lateral exchange. Straneo (2006a) found that there are distinct behaviours in the surface layer between 0–200 m and the lower layer between 200–1300 m in the Labrador Sea interior. The surface layer properties follow a strong seasonal cycle and changes are mainly affected by surface fluxes, whereas the lower layer properties show strong interannual variability and changes are mainly driven by lateral fluxes. Furthermore, in the same study it was found that the lateral exchange in the Labrador Sea is controlled by the lateral density gradient between the interior and the boundary current. This gradient governs the boundary current instability which results in eddies that can suppress the lateral density gradient. Straneo (2006a) found a quadratic relation between the restratification rate and the lateral density gradient, defined as the thickness difference of convectively formed water (Labrador Sea Water) between the interior and the boundary current at the start of the restratification phase. Moreover, de Jong et al. (2016) found a significant correlation between the eddy kinetic energy (EKE) in the Labrador Sea and the lateral density gradient, measured as the difference in density averaged over the upper 1000 m of the water column between the interior and the boundary current. Multiple studies found that a certain type of eddies, namely Irminger rings shed by the boundary current near the west coast of Greenland, strongly contribute to restratification of the Labrador Sea (e.g. Katsman et al., 2004; Chanut et al., 2008; Gelderloos et al., 2011). Observations from a mooring located between the boundary current and the interior of the Labrador Sea as described in De Jong et al. (2014) show that these Irminger rings consist of a warm and saline core topped by a colder and fresher surface layer. So these eddies can be divided in an upper layer and a lower layer with distinct contributions to restratification of the Labrador Sea interior. This can be linked to the distinct behaviour between the upper and lower layer in the interior Labrador Sea found by Straneo (2006a). However, de Jong et al. (2016) found in a model study that most of the heat transport from the boundary current to the interior of the Labrador Sea occurs through noncoherent anomalies rather than coherent Irminger rings.

For the Irminger Sea there exist many studies addressing deep convection (e.g. Pickart et al., 2003; Våge et al., 2011; De Jong et al., 2012; de Jong and de Steur, 2016; Fröb et al., 2016; de Jong et al., 2018; Le Bras et al., 2020; Petit et al., 2020). It is known that deep convection occurs in every winter in the Irminger Sea, but the convection strength can differ per year. However, restratification in the Irminger Sea has not been the subject of any major study yet. The most likely explanation for this is that for a long time it was unclear whether deep convection also occurred in the Irminger Sea, or whether dense water masses found there were just exported from the Labrador Sea (Pickart et al., 2003; Våge et al., 2011). However, recent studies by Lozier et al. (2019), Petit et al. (2020) and Li et al. (2021) found that deep convection in the Irminger Sea is a major contributor to overturning, whereas the strength of Labrador Sea convection contributes minimally to the total overturning of the subpolar gyre. Moreover, the Irminger Sea is found to be an important region for anthropogenic carbon uptake. Fröb et al. (2016) showed that in the winter of 2014–2015, when deep convection in the Irminger Sea was strong, anthropogenic carbon storage rates almost tripled compared with the years 1997 and 2003, in which deep convection was much weaker. In the light of these results, restratification in the Irminger Sea is a very relevant research subject.

1.4 The Irminger Sea

The Irminger Sea is located southeast of Greenland. It can be partitioned into an interior and a boundary current system. In the interior there is a cyclonic gyre, the Irminger Gyre (Våge et al., 2011), shown in Figure 3. This is the region where deep convection occurs. The cyclonic circulation corresponding with doming isopycnals contributes to preconditioning. In addition, intense wintertime wind events just south of Greenland, the so-called Greenland tip jets, drive strong air-sea heat fluxes in the Irminger Sea, and thus contribute strongly to deep convection (Våge et al., 2008). The boundary currents are shown in Figure 4. On the eastern side of the

Irminger Sea, along the western flank of Reykjanes Ridge, we find the northward-flowing Irminger Current (IC; Våge et al., 2011; de Jong et al., 2020). It transports water from the North Atlantic Current and is therefore warm and saline. Near the IC path along Reykjanes Ridge, warm and saline core eddies are found that travel westward to the interior of the Irminger Sea (Fratantoni, 2001; Volkov, 2005; Fan et al., 2013). These eddies are anticyclonic, indicating that they are buoyant, and mainly occur in summer (Fan et al., 2013). The IC follows the bathymetry, so around 65°N, it continues southward along the East Greenland Shelf. Alongside this part of the IC we find a current of Arctic origin, which is thus fresher and colder: the East Greenland Current (EGC). The merged EGC and IC together are sometimes also referred to as the EGIC (Le Bras et al., 2018). Finally, on the inner shelf there is southward transport of very cold and fresh water; this is the East Greenland Coastal Current (EGCC), which advects a combination of coastal runoff and Arctic-origin water (Sutherland and Pickart, 2008; Le Bras et al., 2018). The figure also shows some currents in the deep ocean; the Deep Western Boundary Current (DWBC) which is part of the lower limb of the AMOC (Hopkins et al., 2019), Denmark Strait Overflow Water (DSOW) entering the Irminger Sea from the north and Iceland Scotland Overflow Water (ISOW) entering from the south along Reykjanes Ridge (Swift, 1984).

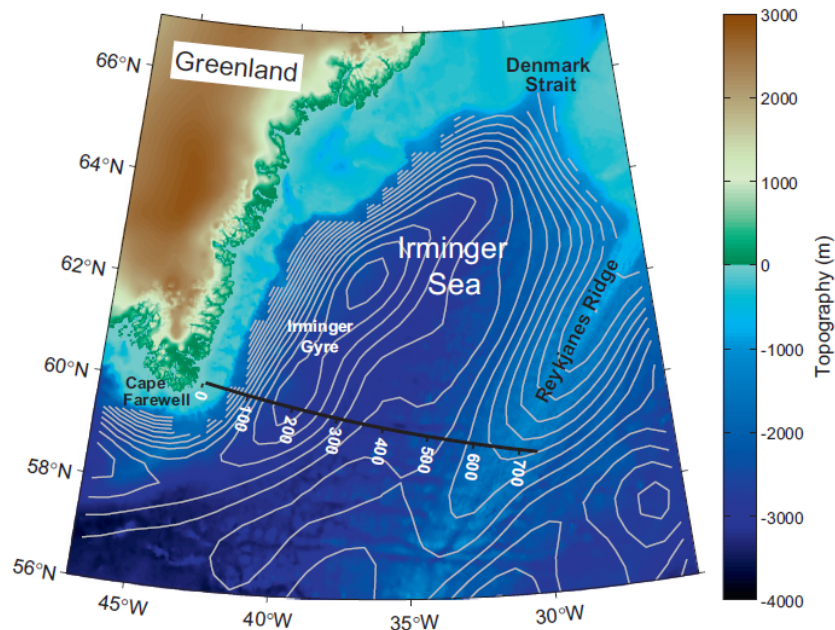


Figure 3: Topography (colour) of southeast Greenland and the Irminger Sea. The grey lines are contours of geostrophic pressure at 700 db. The closed contours in the western Irminger Sea reveal the location of the Irminger Gyre. The black line identifies the WOCE AR7E line which is used for hydrographic sections, and the white numbers indicate distance in km. Figure from Våge et al. (2011) (their Figure 1).

1.5 Research Questions

The main objective of this study is to provide a description of restratification after deep convection in the Irminger Sea. More precisely, we aim to answer the following questions:

1. What is the vertical structure of restratification in the Irminger Sea?
2. What are the characteristics of interannual variability in restratification in the Irminger Sea?
3. What is the influence of salinity and temperature on restratification in the Irminger Sea?
4. Which physical processes contribute to restratification in the Irminger Sea?

Finally, we will compare the results for the Irminger Sea with results about restratification in the Labrador Sea from previous studies.

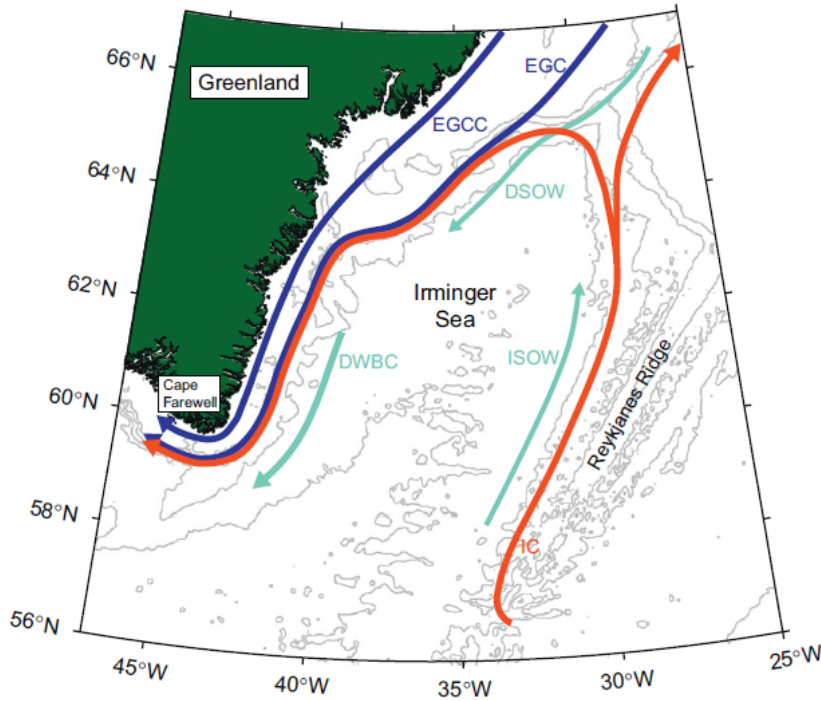


Figure 4: The boundary currents of the Irminger Sea. The acronyms are: IC = Irminger Current; EGC = East Greenland Current; EGCC = East Greenland Coastal Current; DWBC = Deep Western Boundary Current; DSOW = Denmark Strait Overflow Water; ISOW = Iceland Scotland Overflow Water. Red (blue) arrows indicate upper-layer transport of warm (cold) water, while green arrows denote deep currents. The 500, 1000, 1500, 2000, and 3000 m isobaths are plotted. Figure from Våge et al. (2011) (their Figure 2).

2 Data and Methods

2.1 Data

2.1.1 CMEMS Oceanic Reanalysis

For oceanic variables we used the GLORYS12V1 global ocean physics reanalysis from the Copernicus Marine Environment Monitoring Service (CMEMS). It is based largely on the current real-time global forecasting CMEMS system. It uses the NEMO model component and is forced at the surface by ECMWF ERA-Interim reanalysis from 1993–2017, and ERA5 reanalysis for recent years. Detailed information about the CMEMS data set can be found in Fernandez and Lellouche (2018), and information about NEMO can be found in Madec (2016). The data is available for the period from January 1993 until December 2019. We used the monthly mean data for this time period. It should be noted that from 2000 onward, data from the ARGO programme was included in the CMEMS reanalysis. In 2001, the first ARGO floats were deployed in the Irminger Sea (see fleetmonitoring.euro-argo.eu). Therefore we have most confidence in the data from 2001 onward in the accurate representation of the variability in the Irminger Sea. Note that in 2001 there was still only one ARGO float in the Irminger Gyre region, where deep convection occurs. The data set has a spatial resolution of $1/12^\circ$ and has 50 vertical levels, with a vertical resolution of 1 m at the surface decreasing to 450 m at the bottom. The temporal and spatial resolution of this data set are sufficient for our study since convection and restratification are processes occurring over the course of months, and affecting a region in the order of 100 km (see also Section 1.2). Moreover, the reanalysis data were previously validated against two years of mooring data in the Irminger Sea in de Jong et al. (2020). In this report we will also show validation of the reanalysis data against mooring data and CTD data (Section 2.3). The variables we use are the potential temperature (`thetao`), practical salinity (`so`), eastward and northward ocean current velocity (`uo` and `vo`), and mixed layer depth (`m1otst`). The mixed layer depth (MLD) in CMEMS is defined as the depth where the density difference

compared to a reference level is 0.01 kg/m^3 (Madec, 2016, p. 246). We use the GSW Oceanographic Toolbox in Python (`gsw` version 3.4.0) to recompute practical salinity to absolute salinity, and potential temperature to conservative temperature (McDougall and Barker, 2011). From these properties we can then also compute the potential density anomaly referenced to the surface (being the potential density referenced to the surface minus 1000 kg/m^2). From now on, unless explicitly stated otherwise, every mention of salinity, temperature, and density from the CMEMS data will refer to absolute salinity, conservative temperature, and potential density anomaly referenced to the surface, respectively.

2.1.2 ERA5 Atmospheric Reanalysis

For atmospheric variables we used the ERA5 reanalysis from the Copernicus Climate Change Service (C3S) Climate Data Store (CDS) (Hersbach et al., 2020), which replaces the ERA-Interim reanalysis. We used the monthly averaged data on single levels. The data set has a horizontal resolution of 0.25° . The data set spans the period from January 1979 to present, but to make it compatible with the CMEMS data we only used the data from January 1993 until December 2019. For freshwater fluxes we used the evaporation (`e`) and total precipitation (`tp`); the sum of these two yields the net atmospheric freshwater flux. For heat fluxes we used the surface net solar radiation (`ssr`), surface net thermal radiation (`str`), surface latent heat flux (`slhf`) and surface sensible heat flux (`sshf`), and summed these together to get the net atmospheric heat flux.

2.2 Methods

2.2.1 Defining the Deep Convection Area

As we are interested in restratification after deep convection, we need to identify the area within the Irminger Sea where deep convection occurs to study its hydrographic properties. In other words, we look for the region with the deepest mixed layers. Since the Irminger Sea is preconditioned for deep convection by cyclonic circulation with its doming isopycnals (Section 1.2), we can focus on the southwestern part of the Irminger Sea, where the cyclonic Irminger Gyre is located (Section 1.4). We take the region $[45^\circ\text{W}, 35^\circ\text{W}] \times [58^\circ\text{N}, 65^\circ\text{N}]$ and select all months from the monthly 1993–2019 CMEMS data set in which the maximum MLD within this region exceeds 1000 m. Then we average the MLD field over these months. The result is shown in Figure 5. The center where the deepest mixed layers are found is clearly visible. To define a boundary for the area of deep convection, we first smooth this averaged MLD field using a Gaussian filter with $\sigma = 5$ grid cells. Then we take a contour of this smoothed field that encloses the region with the highest MLD values. The chosen contour is also shown in Figure 5 and corresponds with a value of 650 m of the smoothed MLD field. This particular contour was chosen because it contains most of the high MLD region, without extending so far northward that it contains part of the warm Irminger Current, which should not be part of the cold region of convection (see Appendix A.1 for a comparison with different contours). The part of the Irminger Sea enclosed by this contour will henceforth be referred to as the Deep Convection Area, abbreviated as DCA.

We averaged the data from the CMEMS and ERA5 reanalyses over the DCA to get time series of surface freshwater and heat fluxes and mixed layer depth in the DCA, and also time series of salinity, temperature, and density profiles. These time series were used to study convection and stratification in the DCA. The effect of averaging over the DCA on the representation of interannual variability in hydrographic properties is discussed in Appendix A.

2.2.2 Making Hydrographic Sections

To get an impression of the entire water column in and around the DCA, we study hydrographic properties along a section through the Irminger Sea. For this section we choose part of the WOCE AR7E line (Koltermann et al., 2011), shown in Figure 6. Along this line we define points at 5 km intervals. We can then interpolate fields derived from the CMEMS reanalysis to these points to get hydrographic sections (using the Python `scipy` version 1.5.2 package).

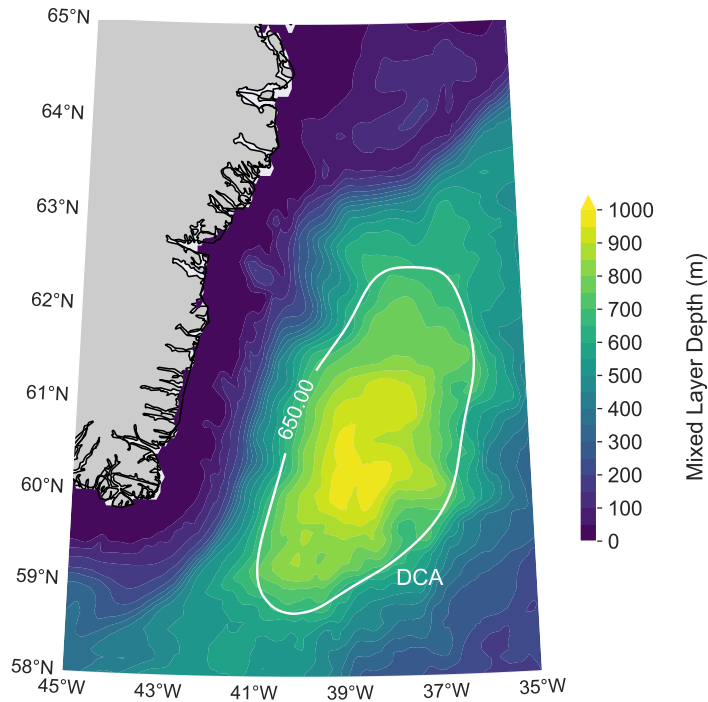


Figure 5: The MLD field averaged over the months from the monthly 1993–2019 CMEMS data set in which the maximum MLD within the region $[45^{\circ}\text{W}, 35^{\circ}\text{W}] \times [58^{\circ}\text{N}, 65^{\circ}\text{N}]$ exceeds 1000 m. In white, the 650 m contour of the MLD field smoothed with with a Gaussian filter ($\sigma = 5$ grid cells) is shown, representing the boundary of the Deep Convection Area (DCA).

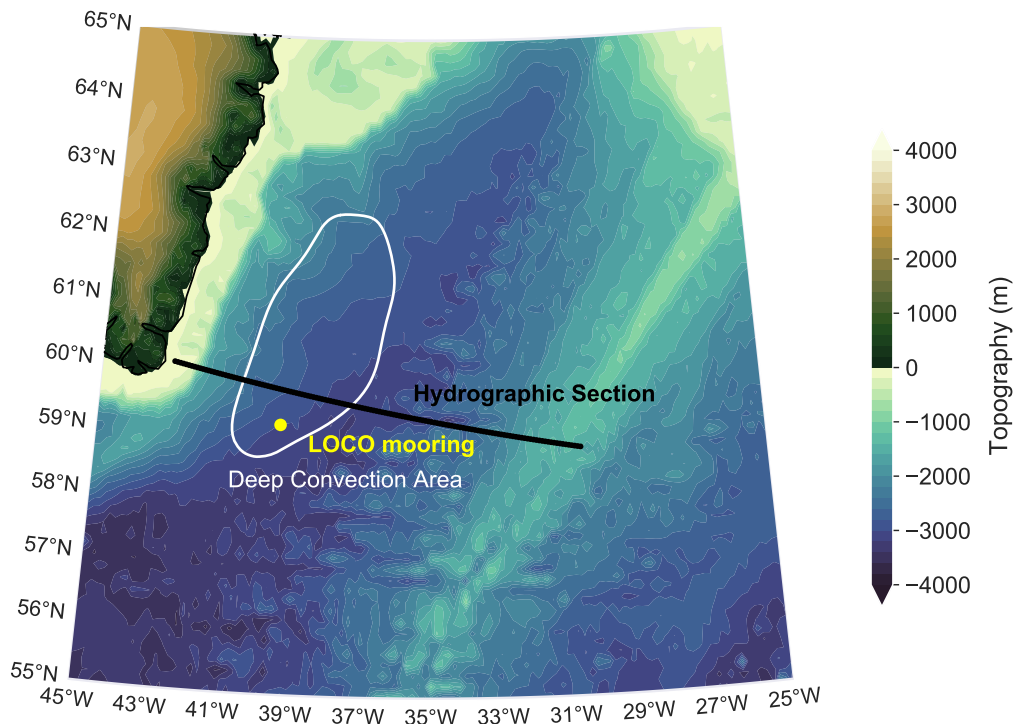


Figure 6: The hydrographic section line along which we study properties (black), the boundary of the Deep Convection Area (white), and the location of the LOCO mooring used for data validation (yellow), plotted on top of the bathymetry in the Irminger Sea derived from ETOPO.

2.2.3 Quantifying Stratification and Restratification

As a quantitative measure of the stratification of the water column between depths $-h_1$ and $-h_2$ (where $0 \leq h_1 < h_2$), we use the stratification index (SI), defined as the integral of potential density gradient times depth:

$$\text{SI} = \int_{-h_2}^{-h_1} \frac{\partial \sigma}{\partial z} z \, dz, \quad (1)$$

with units of kg/m^2 . Note that it does not matter whether the potential density or the potential density anomaly is used to calculate the SI. Partial integration of Equation (1) yields an expression of the SI in terms of the density profile $\sigma(z)$ (rather than the density *gradient* profile):

$$\text{SI} = -h_1 \sigma(-h_1) + h_2 \sigma(-h_2) - \int_{-h_2}^{-h_1} \sigma(z) \, dz. \quad (2)$$

The SI indicates the ability of mixing the water column; it is the amount of buoyancy that must be removed in order for the water column to mix down from depth $-h_1$ to depth $-h_2$ with subsequent uniform density. A stratified layer has a positive SI, a perfectly mixed layer has an SI of zero, and an unstable layer about to overturn has a negative SI. The SI has been used as a measure for stratification in various Mediterranean studies, where it is usually defined with a factor g/ρ_0 so that it is the integral of the Brunt-Väisälä frequency (e.g. Herrmann et al., 2010; L'Hévéder et al., 2013; Somot et al., 2018; Margirier et al., 2020). The partial integration expression (2) multiplied by -1 has also been used in North Atlantic Studies; Bailey et al. (2005) referred to it as the integrated buoyancy anomaly and Frajka-Williams et al. (2014) as the Convection Resistance.

To study the influence of temperature and salinity on the stratification, we compute two additional values of the SI: SI_T and SI_S , which only take into account the contribution of temperature and salinity to stratification, respectively. We do this by using the linear approximation for the density of seawater (Dijkstra, 2008):

$$\rho = \rho_0 [1 - \alpha (T - T_0) + \beta (S - S_0)], \quad (3)$$

where T_0 and S_0 are a reference temperature and salinity and $\rho_0 = \rho(T_0, S_0)$ is a reference density. In this expression ρ is in-situ density, not potential density or potential density anomaly. Furthermore,

$$\alpha = -\frac{\partial \rho}{\partial T} \quad (4)$$

is the thermal expansion coefficient with units $1/\text{K}$, and

$$\beta = \frac{\partial \rho}{\partial S} \quad (5)$$

is the saline contraction coefficient in kg/g . We can estimate the error of this approximation by applying it to the CMEMS reanalysis data averaged over the DCA for each depth level and each month of the time series. We let S_0 and T_0 be the time-mean salinity and temperature per depth level, and compute α and β with the `gsw.alpha` and `gsw.beta` functions. We can then compare it with the value of ρ as computed from salinity and temperature using the `gsw.rho` function (Roquet et al., 2015). The difference between the two different values of ρ averaged over time and depth is in the order of 10^{-3} kg/m^3 . This is very small compared to the values of ρ itself, which are in the order of 10^3 kg/m^3 . Thus we can conclude that Equation (3) provides a good approximation for ρ . Based on this equation, we can view $-\alpha T$ as a first approximation of the temperature contribution to density, and similarly βS as the salinity contribution. Hence, if we replace σ in Equation (2) by $-\alpha T$ and βS , respectively, we get an approximation of the temperature and salinity contribution to stratification. Note that $-\alpha T$ and βS are unitless, so that SI_T and SI_S are given in m instead of kg/m^2 . Therefore the magnitudes of SI_T and SI_S cannot be directly compared with the magnitude of the actual SI; however, the magnitudes of SI_T and SI_S can be compared with each other, and the trends in their time series can be compared with the trends in the SI time series. As we are interested in variability in stratification, these trends are the most important, and exact magnitudes are less interesting.

As explained in Section 2.2.1, we compute time series of salinity, temperature, and density profiles averaged over the DCA. Using Equation (2) we can then compute the SI from the potential density anomaly profile for every month of the time series. Furthermore, for each month we compute the thermal expansion coefficient and

saline contraction coefficient from the averaged salinity and temperature profiles, and from that the profiles of $-\alpha T$ and βS (where T is conservative temperature and S is absolute salinity) to compute monthly values of SI_T and SI_S .

From the monthly values of the stratification index we can then compute annual values for restratification, which we define to be the difference between the maximum SI reached in the summer of a certain year and the minimum SI of the preceding winter.

2.3 Data Validation

To see how accurately the CMEMS reanalysis data represents the vertical structure and interannual variability of properties in the Irminger Sea, we compare it with observational data.

2.3.1 Validation with LOCO mooring

First, we compare hydrographic properties over depth from the reanalysis and from a mooring in the Irminger Sea. The mooring we use for this validation is the LOCO (Long-term Ocean Climate Observations) mooring, located at 39.5°W, 59.2°N, at the southern end of the DCA. Its location is shown in Figure 6. A detailed description of the LOCO mooring can be found in De Jong et al. (2012). The LOCO data is not assimilated in the CMEMS reanalysis and can therefore be used for an independent comparison of the reanalysis data with observational data. LOCO provides daily data and has a vertical resolution of 1 dbar, which is much higher than the resolution of the CMEMS reanalysis. However, LOCO has no data above 100 m depth. For the comparison of the two data sets, we can therefore only consider deeper waters. Processed LOCO data is available for the period from September 2003 until July 2015, although there is missing data for parts of this period. For the comparison of LOCO and CMEMS, we converted the LOCO data to monthly averaged data and interpolated the CMEMS data to the LOCO mooring location.

In Figure 7, the full time series from September 2003 until July 2015 of salinity, temperature, and density from CMEMS and LOCO are shown. The time series will be discussed in detail in Section 3.3.1; here we only focus on the comparison of CMEMS with LOCO. From these figures we see that the CMEMS reanalysis data accurately represents the interannual variability in salinity, temperature, density and mixed layer depth. Values of all properties are very similar in the CMEMS and LOCO time series. A mid-depth salinity minimum is clearly visible in both time series, as is a continuously layered structure of temperature and density. The MLD follows the same temporal trends in both data sets, with the MLD extending below 100 m in every winter, and with local maxima in 2008, 2009 and 2015 clearly visible in both time series. Also, features of individual years such as the salinity and density maximum in the 2010–2011 winter are visible in both the CMEMS and the LOCO data. Thus we conclude that the CMEMS reanalysis accurately represents the interannual variability of hydrographic properties at the LOCO mooring location. Furthermore, the time series of the CMEMS data averaged over the DCA are very similar to the time series of CMEMS interpolated to the mooring location, as is shown in Appendix A.2. Therefore we may assume that the CMEMS data averaged over the DCA, which we use throughout this study, accurately represents the hydrography and the restratification behaviour in the convection region of the Irminger Sea.

We can also compare climatological profiles based on the time series from Figure 7. Here we focus only on the part of the water column above 600 m depth, since we will not study stratification in deeper waters, as will be explained in Section 3.1.1. Because LOCO data above 200 m is very sparse, we only consider the part of the water column from 200–600 m. Furthermore, for the LOCO climatology only monthly profiles which have data for all depth levels in this part are taken into account. Interpretation of the climatologies will be discussed in Section 3.2.4.

The figures show that the magnitudes of the climatological properties are very similar for the CMEMS and the LOCO data. Also the position of the profiles of the different months with respect to each other are mostly the same for both data sets. However, there are also some differences, most notably in the salinity. The salinity profiles of the LOCO data lie closer to each other than those of the CMEMS data. Also, at the bottom of the layer the salinity of the summer months is larger in the LOCO data than in the CMEMS data. It should be

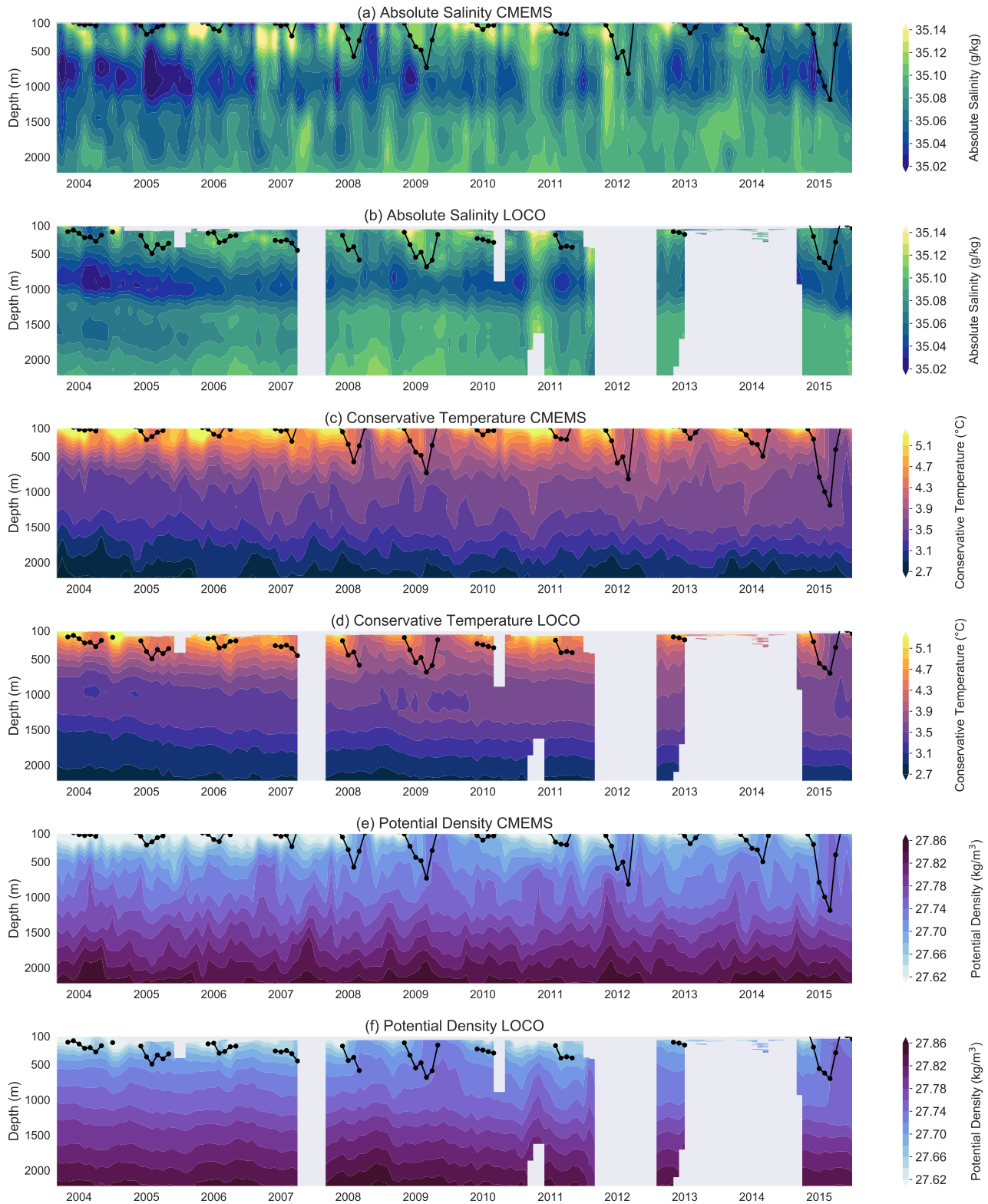


Figure 7: The temporal evolution of profiles of (a)-(b) absolute salinity, (c)-(d) conservative temperature and (e)-(f) potential density at the LOCO mooring (location shown in Figure 6). The mixed layer depth is shown in black. Panels (a), (c) and (e) show the data from the CMEMS reanalysis interpolated to the mooring location. Panels (b), (d) and (f) show the data from the LOCO mooring.

noted that some of the LOCO profiles have a lot of noise, especially the January–May profiles. This is likely the result of missing data as can be seen in Figure 7. Furthermore, the CMEMS data has a much lower vertical resolution than the LOCO data. In the vertical range depicted in Figure 8, only 7 vertical levels from CMEMS are included, as opposed to 347 vertical levels from LOCO. The lower vertical resolution of CMEMS makes the CMEMS data appear smoother than the LOCO data.

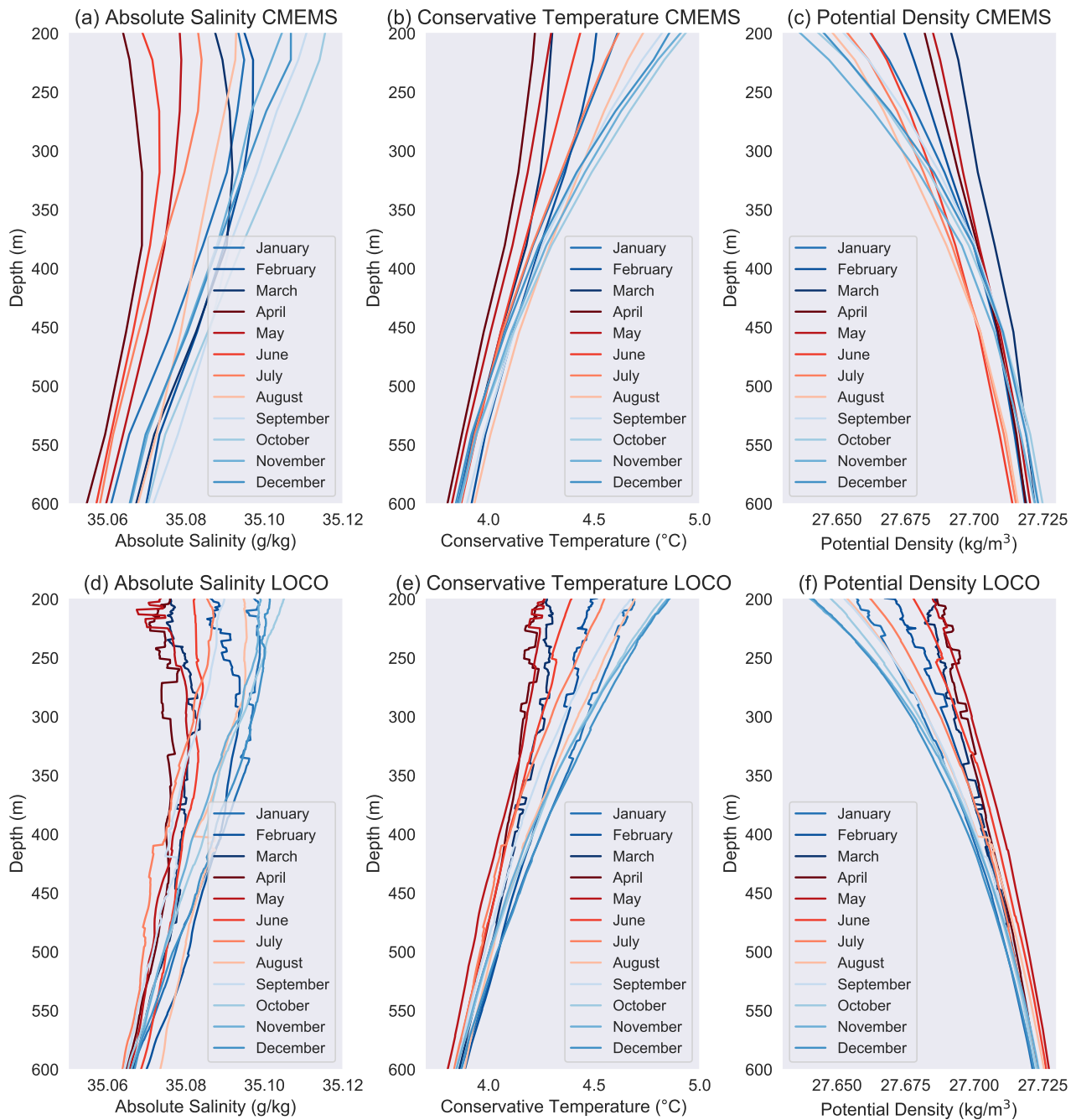


Figure 8: Climatologies of (a),(d) absolute salinity, (b),(e) conservative temperature and (c),(f) potential density profiles in the lower layer at the LOCO mooring (location shown in Figure 6). Panels (a)–(c) show the data from the CMEMS reanalysis interpolated to the mooring location. Panels (d)–(f) show the data from the LOCO mooring. The climatologies are made from data for the period September 2003–July 2015.

2.3.2 Validation with CTD data

Next, we compare CMEMS hydrographic sections interpolated to the WOCE AR7E line (see Section 2.2.2) with CTD data from hydrographic surveys in the Irminger Sea. Interpretation of the hydrographic sections will be discussed in Section 3.1.3 and in Section 3.2.3. It should be noted that the CTD data shown here is likely also assimilated in the CMEMS reanalysis. Therefore the validation might not be entirely independent.

The first survey is from September 2005 and has 14 points along the AR7E section at approximately 55 km intervals, with a vertical resolution of 1 dbar (Veth, 2005). In the 2004/2005 winter deep convection was weak (as will be shown in Figure 19 in Section 3.3.1). The CTD results from this survey together with the CMEMS data from September 2005 are shown in Figure 9. From this figure it can be seen that the CMEMS and CTD data both show the same characteristics. In terms of salinity, we see a thin, fresh surface layer, then a layer with high salinity west and east of the DCA, and a salinity minimum around 1 km depth in the DCA. In terms of temperature and density, we see a continuously layered structure with very warm and light water at the surface.

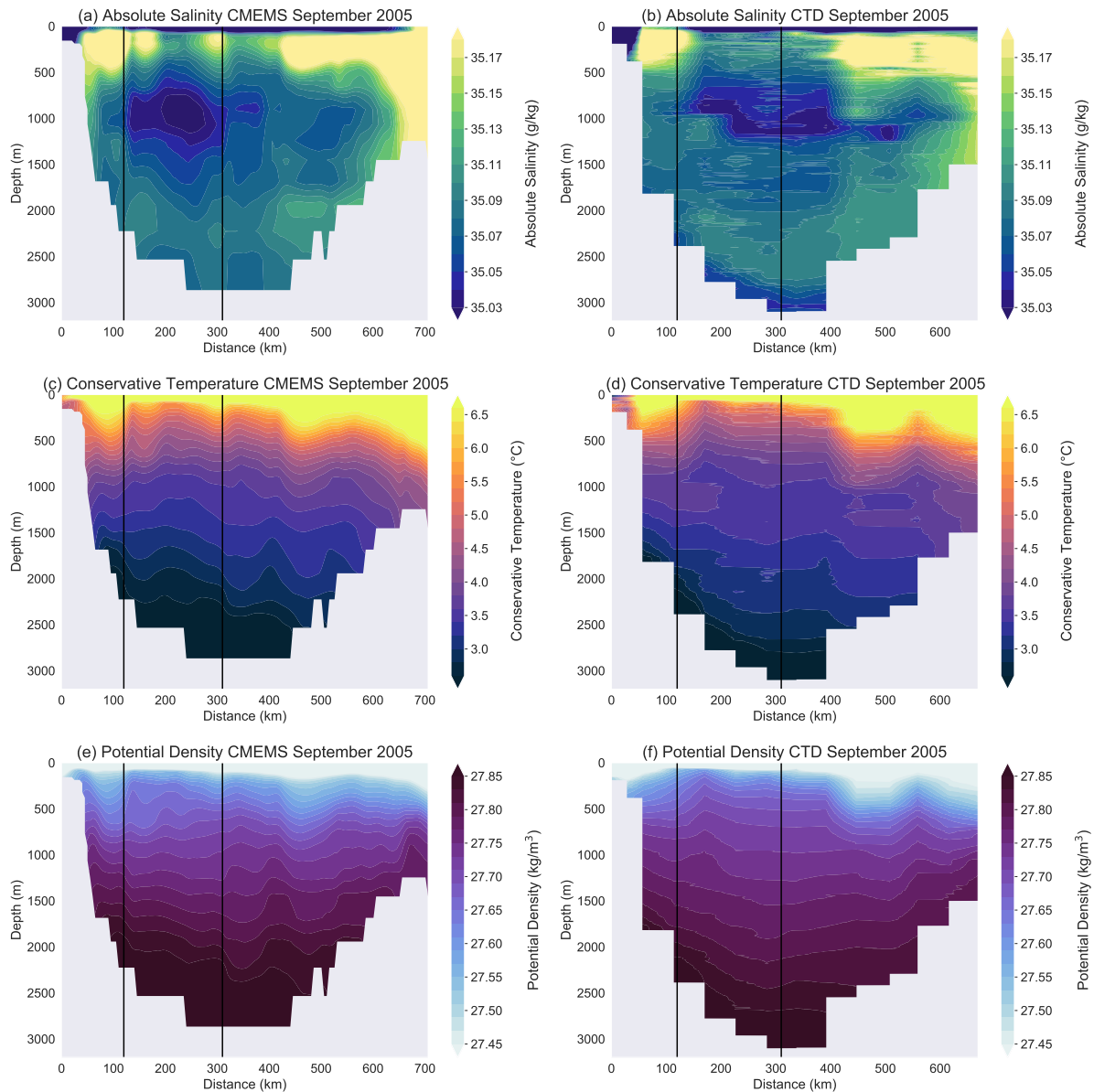


Figure 9: Hydrographic sections of the September 2005 (a)-(b) absolute salinity, (c)-(d) conservative temperature, and (e)-(f) potential density along the WOCE AR7E section in the Irminger Sea. Panels (a), (c) and (e) show the data from the CMEMS reanalysis interpolated to the section. Panels (b), (d) and (f) show the data from a ship CTD. The vertical black lines mark the points where the section intersects the DCA boundary.

The second survey is from August 2016 and has 34 points along the AR7E section with an average spacing of 20 km, and a vertical resolution of 2 dbar (Holliday, 2016). The results for this month are shown in Figure 10. Again, we see that the CMEMS data clearly shows the same spatial patterns as the CTD data. In both the 2014/2015 and the 2015/2016 winter, deep convection was strong (again, see Figure 19 in Section 3.3.1). Indeed, we see signatures of convectively formed water in the Irminger Sea in August 2016, most notably within the DCA: a strong mid-depth salinity and temperature minimum (see also Section 3.1.1) and isopycnals that lie very far from each other in the vertical, indicating low stratification.

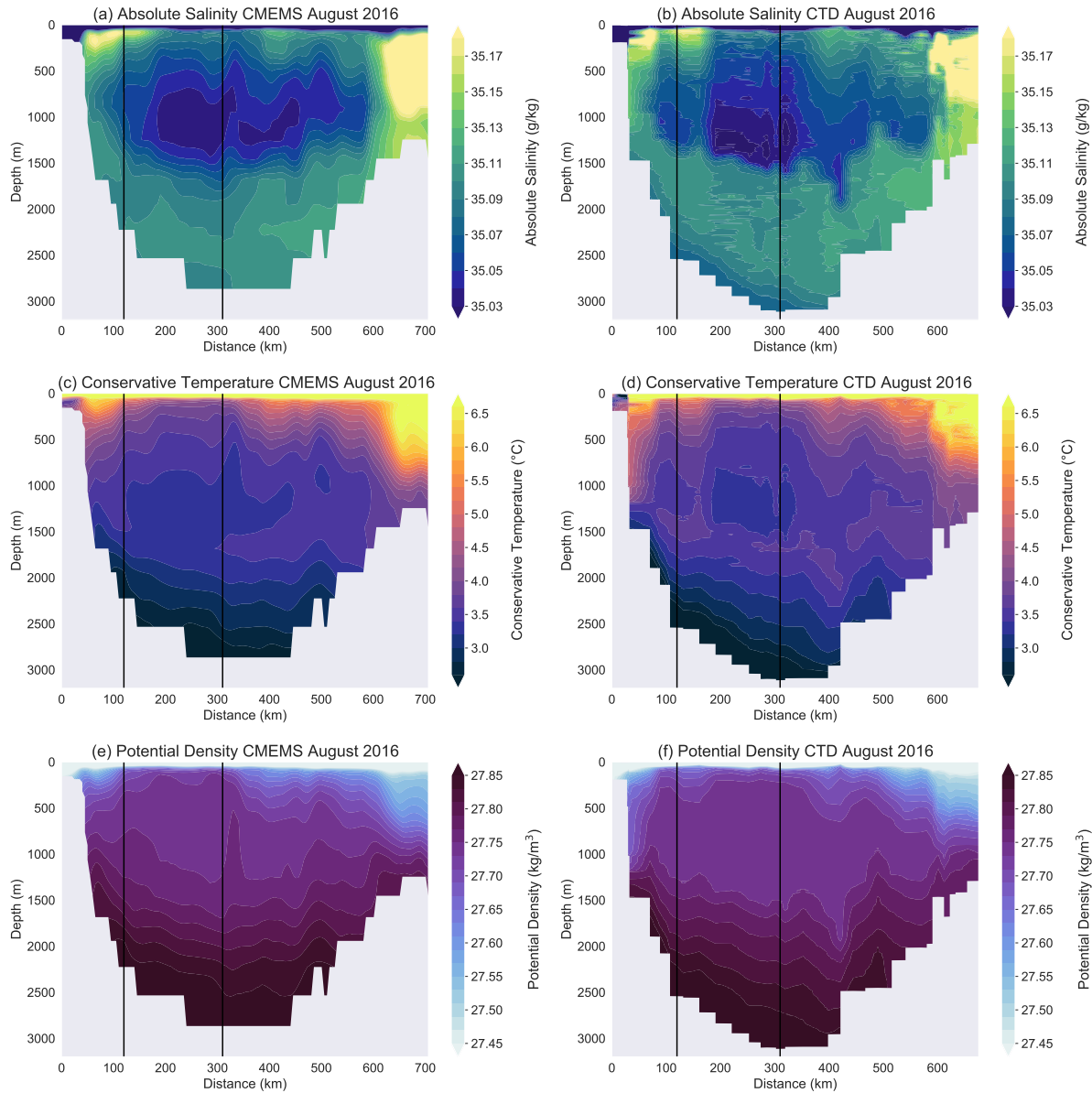


Figure 10: Hydrographic sections of the August 2016 (a)-(b) absolute salinity, (c)-(d) conservative temperature, and (e)-(f) potential density along the WOCE AR7E section in the Irminger Sea. Panels (a), (c) and (e) show the data from the CMEMS reanalysis interpolated to the section. Panels (b), (d) and (f) show the data from a ship CTD. The vertical black lines mark the points where the section intersects the DCA boundary.

From these figures we conclude that the CMEMS reanalysis data accurately represents hydrographic properties along the AR7E section in the Irminger Sea, for summers after weak deep convection as well as summers after strong deep convection.

3 Results

3.1 Time-Mean Fields

To familiarise ourselves with the study area, we will first study time-mean properties within the Deep Convection Area and throughout the Irminger Sea.

3.1.1 Time-Mean and Standard Deviation of Hydrographic Properties over Depth

Since this study is on stratification, we start with focusing on the vertical structure of the water column. Of the profiles of salinity, temperature and density averaged over the Deep Convection Area, the time-mean and standard deviation per depth level over the 1993–2019 time series are shown in Figure 11. For all three properties, we observe a strong gradient near the surface (halocline, thermocline or pycnocline, respectively). Below that, the temperature continues to decrease more gradually, and the density continues to increase. The salinity first decreases below the halocline until approximately 1000 m depth and then increases again. This mid-depth minimum in salinity is a signature of convectively formed water, since convection occurs in the freshest part of the Irminger Sea (see Section 3.1.2).

In all three profiles, we see that the standard deviation is largest near the surface. For salinity, it is decreasing downward until approximately 1000 m, then increasing between 1000 and 2000 m depth. For the temperature and density, the standard deviation keeps steadily decreasing with depth. In studying the process of restratification, we are interested in that part of the water column with large density variations in time. Therefore we choose to only study the salinity, temperature, and density profiles in this top part of the water column. We define this top part from the surface to 600 m depth. Below this depth the temporal variations in density become very small; at 600 m the standard deviation in density is only 7.3% of the standard deviation at the surface.

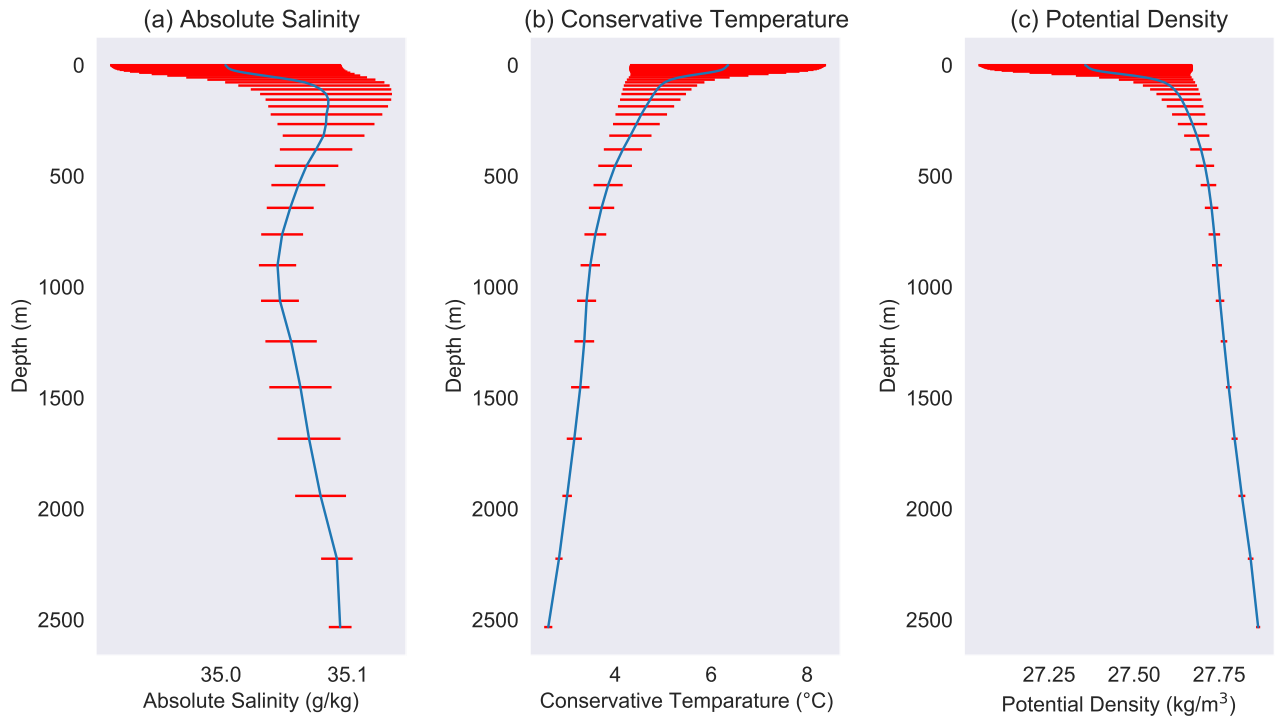


Figure 11: The 1993–2019 mean and standard deviation per depth level of (a) absolute salinity, (b) conservative temperature, and (c) potential density from the CMEMS reanalysis averaged over the Deep Convection Area. The blue curves show the time-mean; the red bars indicate the standard deviations for each depth level.

3.1.2 Maps of Mean Hydrographic Properties and Atmospheric Fluxes

To get an overview of the currents and water mass properties around the DCA, we will now look at time-mean hydrographic properties throughout the whole Irminger Sea, shown in Figure 12. All of these properties are depth-averaged until a depth of 600 m. Figures 12a and 12b show the salinity and temperature, respectively. Figure 12c shows the mean flow velocity; the arrows show the magnitude and direction of the mean flow. Here two different scales are used, which are shown in the upper left corner of Figure 12c: black arrows for velocities smaller than 0.07 m/s and white arrows for larger velocities. Figure 12d shows the mean eddy kinetic energy (EKE) in the Irminger Sea. The EKE is computed as

$$\text{EKE} = \frac{1}{2} \left[(u - \bar{u})^2 + (v - \bar{v})^2 \right], \quad (6)$$

where \bar{u} and \bar{v} are the time-mean zonal and meridional velocity components over the whole time series.

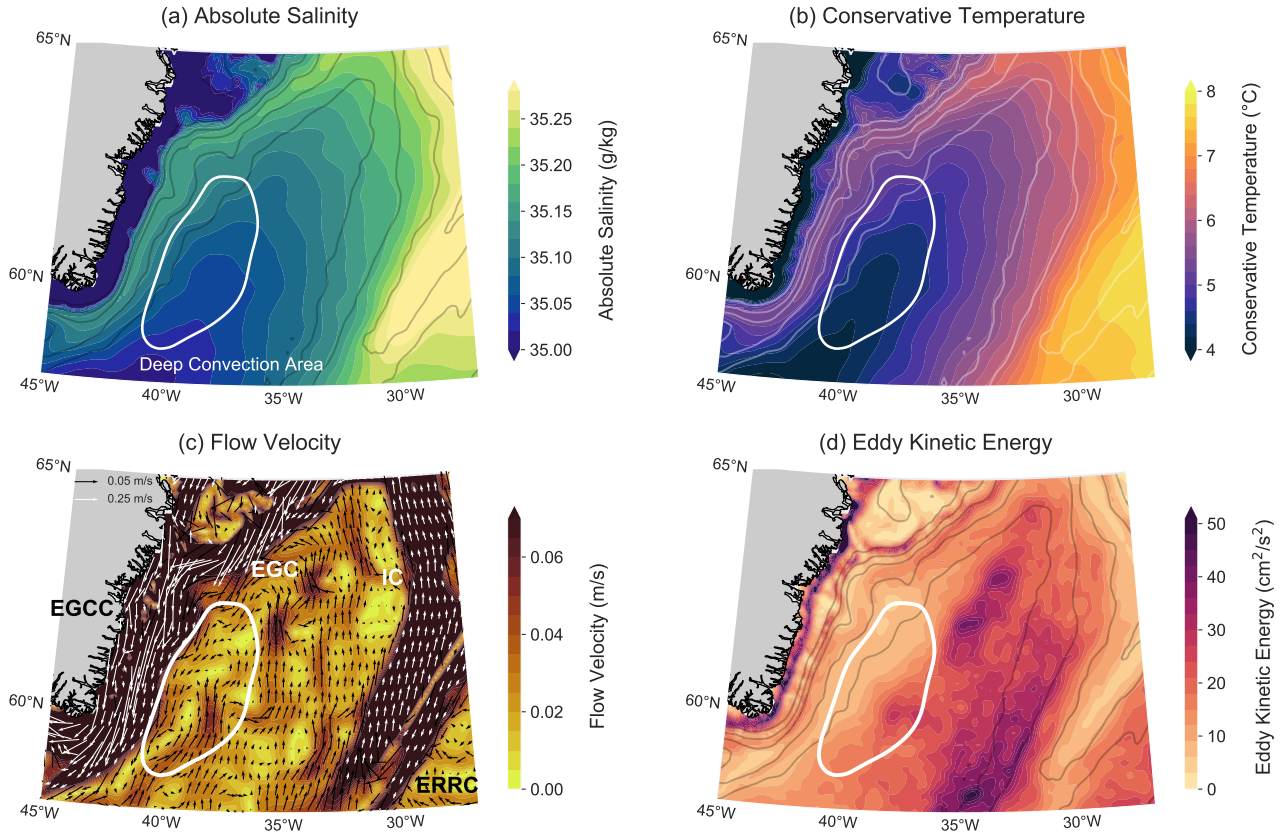


Figure 12: The 1993–2019 mean from the CMEMS reanalysis of the (a) absolute salinity, (b) conservative temperature, (c) flow velocity and (d) eddy kinetic energy in the Irminger Sea, averaged over the upper 600 m of the ocean. In panels (a), (b) and (d), smoothed contours of the bathymetry between 500 m and 2500 m are shown at 500 m intervals. In panel (c), velocity direction and magnitude are indicated by vectors. Velocities smaller than 0.07 m/s are indicated by black arrows, larger velocities by white arrows. The black and white vectors have different scalings, as shown by the reference vectors in the top right of the panel. In this panel, also the different currents are indicated: EGCC = East Greenland Coastal Current; EGC = East Greenland Current; IC = Irminger Current; ERRC = East Reykjanes Ridge Current.

From these figures, we can identify the main currents in this region and their characteristics, which were already introduced in Section 1.4; the warm and saline Irminger Current, the cold and fresh East Greenland Current, and the even colder and fresher East Greenland Coastal Current. The highest flow velocities are found along the shelfbreak where the IC and EGC flow next to each other. The EKE in the Irminger Sea is highest along the East Greenland shelf, along the Irminger Current west of Reykjanes Ridge, and to the northeast of the DCA. These regions are in agreement with the maximum EKE regions that were derived from satellite altimetry data by Volkov (2005) and Fan et al. (2013). In the region just west of Reykjanes Ridge, Fratantoni (2001) also

found high EKE using data from surface drifters. The eddies travel westward and have a warm and saline core (Fan et al., 2013); this signature suggests that they are shed by the Irminger Current.

In each panel of Figure 12, the boundary of the Deep Convection Area is also indicated. The flow is cyclonic within the DCA: the signature of the Irminger Gyre (Våge et al., 2011). The DCA lies between the EGC and the IC and is the coldest and freshest part of the Irminger Sea (apart from the EGCC). The low temperatures can be explained by the upwelling due to the cyclonic circulation. The low salinity is a result of freshwater accumulation due to precipitation and wind-driven exchange with the EGC, which then stays within the Irminger Gyre as the flow cannot cross streamlines (Duyck and De Jong, 2021; Duyck et al., prep). EKE is high to the east of the DCA, but very low on its western side.

Finally, to also get an impression of the air-sea freshwater and heat fluxes over the Irminger Sea, we consider the 1993–2019 time-mean net freshwater and heat fluxes. These are shown in Figure 13. Positive values indicate fluxes from the atmosphere to the ocean, negative values are for fluxes from the ocean to the atmosphere. The figures reveal that on average, there is a net gain of freshwater and a net loss of heat from the ocean to the atmosphere. Only in a narrow region along the East Greenland shelf there is a net gain of heat since here sea surface temperatures are lower than air temperatures. The freshwater gain is largest near Greenland and decreases with the distance to the land. The heat loss is largest along the main path of the Irminger Current, because the IC is very warm and the temperature difference between ocean and atmosphere is large here. The heat loss is smallest in the DCA. This might seem surprising given that the DCA is the region where deep convection occurs. However, as was discussed in Section 1.2, deep convection requires more than just strong heat fluxes; the preconditioning involves a cyclonic circulation gyre, which is only present in this part of the Irminger Sea.

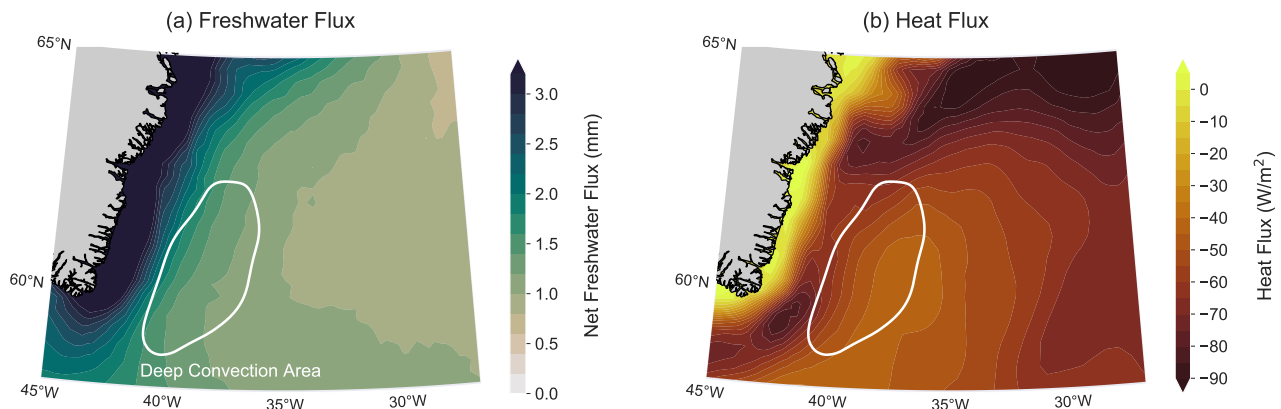


Figure 13: The 1993–2019 mean from the ERA5 reanalysis of the (a) net surface freshwater flux and (b) net surface heat flux in the Irminger Sea.

3.1.3 Mean Hydrographic Sections

Along the hydrographic section described in Section 2.2.2, we interpolate absolute salinity, conservative temperature, potential density anomaly, and EKE (computed from the velocity anomalies, Equation (6)) from the CMEMS reanalysis. The time-mean properties over the 1993–2019 period are shown in Figure 14. In each panel, two vertical black lines mark the DCA boundaries (Figure 6).

In these hydrographic sections, we can observe the signatures of the cold and fresh EGCC on the western side above the East Greenland shelf, and the warm and saline IC on the eastern side along Reykjanes Ridge. Between 500 and 1500 m depth, convectively formed water can be identified by its mid-depth salinity minimum signature (recall that the DCA is very fresh; during deep convection this low salinity is mixed down). Most of the convectively formed water along this section is contained within the DCA, but some of it is found outside the eastern DCA boundary. Part of it is formed locally in the Irminger Sea and part likely originates from either the Labrador Sea or just south of Cape Farewell (Yashayaev et al., 2007; De Jong et al., 2012; Petit et al., 2019).

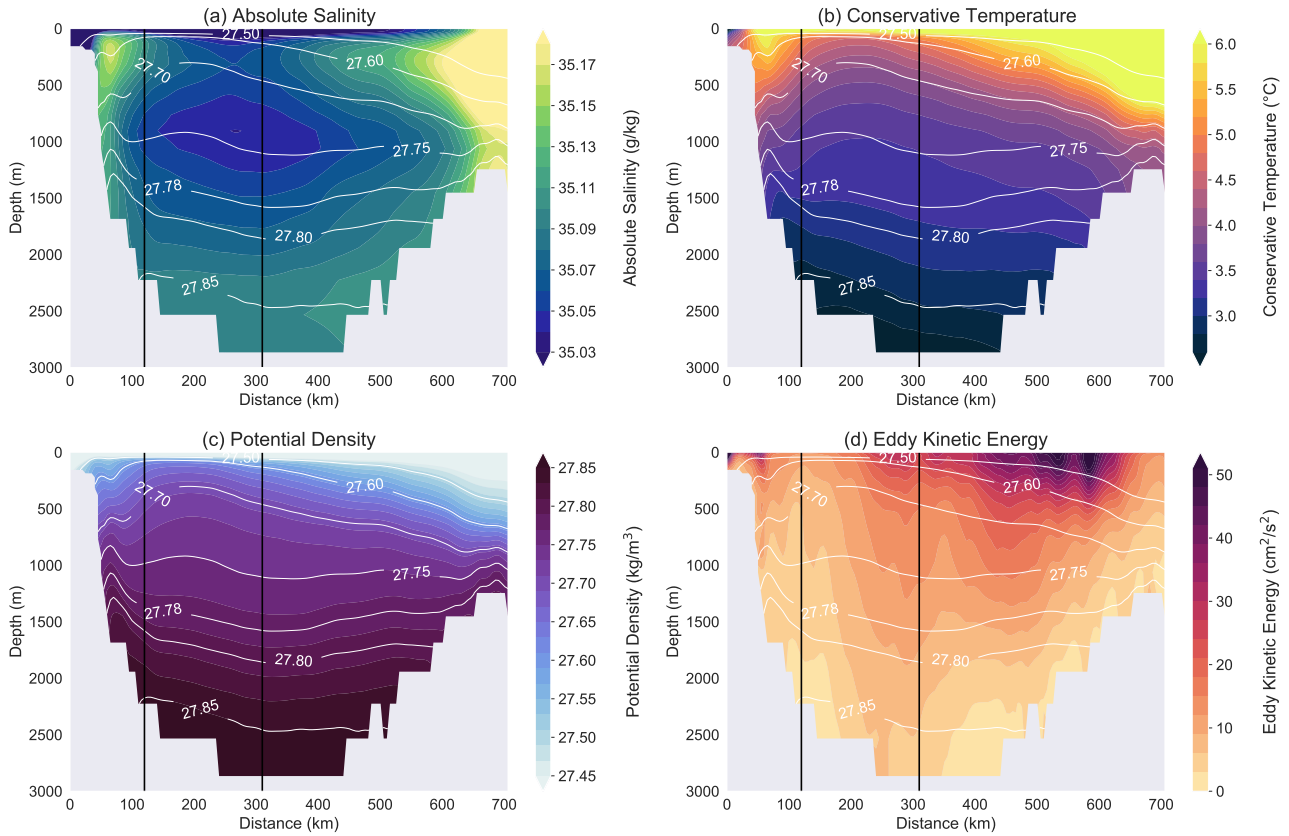


Figure 14: The 1993–2019 mean from the CMEMS reanalysis of the (a) absolute salinity, (b) conservative temperature, (c) potential density and (d) eddy kinetic energy along the WOCE AR7E section in the Irminger Sea (shown in Figure 6). The vertical black lines mark the points where the section intersects the Deep Convection Area boundary. The white curves are isopycnals.

The EKE is highest just west of Reykjanes Ridge, as we already saw in Figure 12. Within the DCA, the EKE is relatively small, with a minimum along the western DCA boundary. The EKE is everywhere highest at the surface and decreases with depth; this illustrates the vertical and surface-intensified structure of eddies (Robinson, 2010; Fan et al., 2013).

Within the DCA, until a depth of around 1000 m, we observe the doming of isopycnals which is associated with the cyclonic circulation of the Irminger Gyre and which is part of the preconditioning facilitating deep convection. The doming indicates a lateral density gradient between the DCA and its surroundings.

3.2 Climatology

Now that we have an overview of the time-mean situation, we will move on to study the seasonal cycle of convection and stratification.

3.2.1 Climatology of Atmospheric Fluxes

First of all we will look at climatologies of surface fluxes and surface properties over the DCA to learn something about their timing and influence on deep convection. Figure 15 shows climatologies of the surface freshwater fluxes, surface heat flux, surface salinity and surface temperature averaged over the DCA, based on data from the ERA5 and CMEMS 1993–2019 monthly reanalysis data. In each of these figures, we can identify a seasonal cycle in the surface fluxes and properties of the DCA. First of all, Figure 15a shows the climatology of precipitation P , evaporation E , and net freshwater flux $E + P$, all measured in mm of water equivalent. We see that

both precipitation and evaporation are weakest in summer and strongest in winter. The winter maximum in evaporation can be explained by the fact that evaporation in this region is mainly wind-driven (sensible and latent heat fluxes are very strong), and that the wind is strongest in winter (Sampe and Xie, 2007). The net effect of evaporation and precipitation is always a net gain of freshwater in the climatology, with a maximum in September and a minimum in March.

Next, Figure 15b shows the surface heat flux climatology. Positive values indicate a heat flux from the atmosphere into the ocean. From April until August, the ocean is gaining heat from the atmosphere, mainly due to incoming solar shortwave radiation which is maximum during summer. The ocean loses heat to the atmosphere from September until March, mainly through sensible and latent heat fluxes which are wind-driven and thus maximum in winter. The surface heat flux is minimum in January and maximum in June. The negative heat fluxes are on average stronger than the positive ones; the magnitude of the winter minimum is approximately twice as large as the magnitude of the summer maximum.

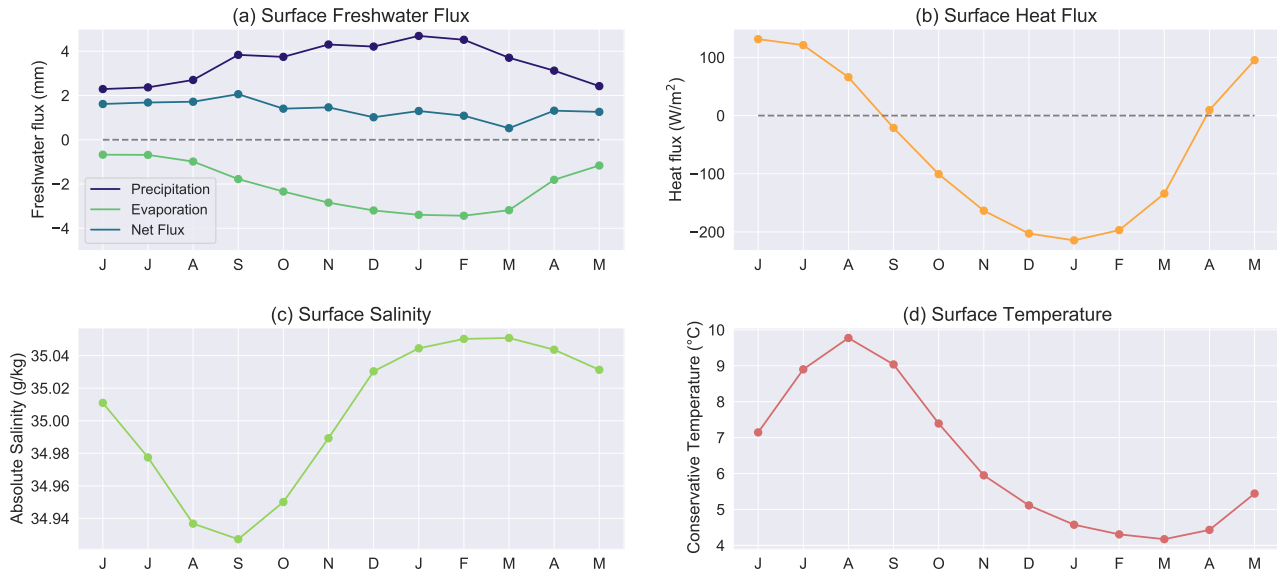


Figure 15: Climatologies of (a) surface freshwater fluxes (evaporation, precipitation, net freshwater flux), (b) surface heat flux, (c) surface absolute salinity and (d) surface conservative temperature over 1993–2019, averaged over the Deep Convection Area. Monthly ERA5 reanalysis data is used for (a) and (b) and monthly CMEMS reanalysis data is used for (c) and (d).

Figures 15c and d show the surface salinity and temperature climatology. Again we see a clear seasonal cycle with fresh, warm surface waters in summer and cold, saline waters in winter. The timing of increase and decrease in surface temperature corresponds with the timing of the surface heat flux being positive or negative. As the net surface freshwater flux is always positive, this alone cannot explain the trends in surface salinity; during winter, mixing with more saline waters from below plays a role, as will be explained below.

The fact that high temperature and low salinity go hand in hand, as do low temperature and high salinity, can be explained as follows. In summer, the surface heat flux is positive, and the surface layer warms. This increases the stratification in the top layer of the water column and restricts mixing to only a thin layer. Therefore the surface freshwater flux, which is positive throughout the whole year, is also restricted to only this thin layer, which can therefore become very fresh. This surface freshening increases the stratification even further and also restricts the surface warming to a thin layer, which thus becomes very warm. During the winter months, the surface heat flux is negative and the surface cools. This surface cooling drives deep convection. Vertical exchange between the surface layer and the water below it will make the surface even colder and also saltier (see Fig. 11 and 14: the surface is fresher and warmer than all the water below it).

3.2.2 Climatology of Convection and Stratification

To visualise the annual cycle of convection and restratification, we can look at the climatology of mixed layer depth and stratification index averaged over the DCA, shown in Figure 16. During the autumn and winter

months, the MLD is increasing and the SI is decreasing, until they reach their maximum and minimum, respectively, in late winter or early spring: this is the convection period. The stratification has its minimum in March, whereas the MLD has its maximum in February. Note, though, that the February and March MLD values are very close; in February it is 480 m, in March 470 m. Note that this maximum MLD value of 480 m is not a value we would expect for winters with strong deep convection, when the MLD can be more than 1 km deep. The reason for this is that the strength of convection differs per year (e.g. De Jong et al., 2012), and there are also years with shallow mixed layers included in this 27-year climatology (this could already be seen in Figure 7 and will be further discussed in Section 3.3.1). This interannual variability in maximum MLD is reflected in the large standard deviation in the months December–April. For the rest of the year, roughly from April until September, the trends in SI and MLD are reversed and the water column is restratifying. The stratification has its maximum in September. The minimum MLD occurs in July, but the June, July, and August MLD values are virtually the same, all approximately 15 m, with very low standard deviations. For the SI, the standard deviation is approximately the same for all months.

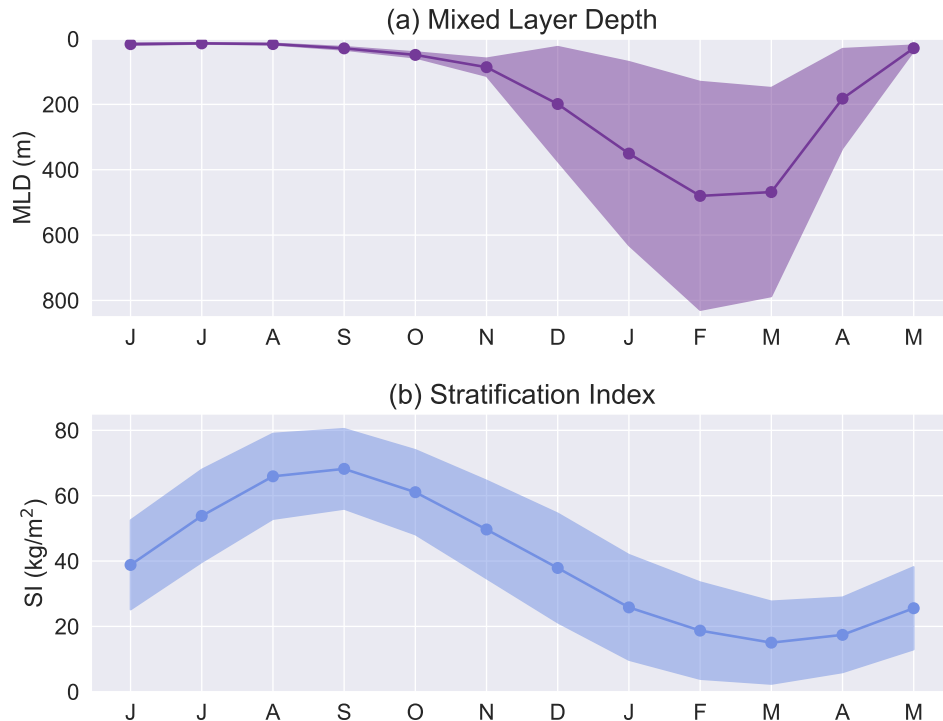


Figure 16: Climatology of (a) mixed layer depth and (b) stratification index over the upper 600 m in the Deep Convection Area, from the monthly 1993–2019 CMEMS reanalysis. The shaded areas indicate the standard deviation of the indicated month.

Over the course of the convection period, the MLD increase is accelerating whereas the SI decrease is decelerating. An explanation for this is that at the end of the summer, the surface waters are very warm and fresh (Fig. 15c,d) and there is a steep pycnocline in the upper 100 m of the water column (Fig. 18c). Therefore a lot of energy is required to mix down through the pycnocline, resulting in a strong decrease in stratification but only a small increase in MLD. Once the pycnocline has disappeared (November–December), further mixing will have less impact on the already weak stratification in the upper 600 m, but the mixed layer can continue to reach large depths beyond 600 m.

Comparing the convection and stratification climatology with the surface heat flux and temperature climatology from Figure 15, we see that the ocean first starts losing heat to the atmosphere in September; surface temperature starts decreasing in this month, MLD starts increasing, SI starts to decrease one month later. The surface heat fluxes become negative again from April onward, which is also when the MLD first shows a strong decrease and the surface temperature and SI begin to slowly increase. So we conclude that the timing of the surface heat fluxes becoming negative or positive coincides with the onset of convection and of restratification, respectively. Keep in mind that this applies to the climatology and that the exact timing might differ from year to year.

3.2.3 Climatology of Hydrographic Sections

To compare the properties in the Irminger Sea during convection and restratification, we look at mean winter and summer hydrographic sections. We consider climatologies of March and September, when the stratification climatology reaches its minimum and maximum, respectively (Fig. 16). These hydrographic sections are shown in Figure 17. This figure clearly shows the differences between the convection and restratification phase. In March, during deep convection, cold and dense water comes to the surface, with the lowest temperatures and highest densities in the DCA. Isopycnals and isotherms outcrop and lie far from each other in the vertical direction, indicating low stratification. The top of the DCA is very fresh, as we already saw in Figure 12a. The temperature is homogeneous until approximately 500 m depth, but the salinity has a local minimum around this depth, as it also has in the time-mean section (Fig. 14a). By contrast, in September, there is a warm and fresh (and thus light) layer on top along the entire section line. The high stratification is visible in the small vertical distance between isopycnals in the upper 1000 m. Below 1000 m, there are no clear differences between the March and September climatologies of salinity, temperature and density; as we already saw in Figure 11, temporal variations at these depths are small compared to those at the surface. By contrast, in the EKE changes do appear at larger depths. This is because the eddies are surface-intensified vertical phenomena, so changes in EKE at the surface are also visible throughout the water column. Comparing March to September, we see that in both months the EKE is high between 500 and 600 km along the section, as in the time-mean situation (Fig. 14). Furthermore, in March there is also high EKE between 400 and 500 km, whereas in September EKE is enhanced between 250 and 300 km, just inside the DCA.

3.2.4 Climatology of Hydrographic Properties over Depth

To study the seasonal cycle in the vertical structure of the water column within the DCA, we consider climatologies of the salinity, temperature and density profiles in the upper 600 m of the DCA. These are shown in Figure 18. In all three properties the convection-restratification cycle can be identified. In late winter and early spring (February–April), all properties have very weak vertical gradients: these are the months in which convection has reached large depths (see also Fig. 16). A nonzero vertical gradient remains because these climatologies also contain winters with weak convection. After these months the vertical gradients increase and a clear halocline, thermocline, and pycnocline become visible, which steepen throughout spring and summer. Note that even in these months the upper 30–50 m of the water column is well-mixed. This small layer is the wind mixed layer, which is deepest in autumn, when the wind is strongest (Sampe and Xie, 2007).

An interesting observation from the salinity climatology (Fig. 18a) is that there are opposing temporal trends in the upper and lower water column. In the upper 100 m, the salinity is decreasing in summer and increasing in winter. The salinity always increases with depth in this part, indicating stable stratification. Below 100 m, however, the temporal trends are reversed: salinity increases in summer and decreases in winter. Moreover, here we find saltier water overlaying fresher water, which indicates unstable stratification in terms of salinity. A possible explanation is as follows. In summer, the mixed layer is entirely contained within the surface layer. At this time, surface fluxes are not acting on the waters below the shallow wind mixed layer. Therefore, any change in this deeper part of the water column must be dominated by the lateral exchange with the surrounding ocean. For our DCA in the Irminger Sea, this lateral exchange is mainly due to warm and saline eddies shed from the Irminger Current (Fig. 12). During this same period, the surface layer is freshened by precipitation (Fig. 15a) and possibly meltwater from Greenland. Later, during convection, the mixed layer deepens and thus leads to a vertical exchange of properties between the surface layer and the deeper layer, making the former saltier and the latter fresher, until salinity is almost homogeneous over the upper 600 m.

The temperature climatology (Fig. 18b) does not show opposing temporal trends between the layers above and below 100 m. In summer, when the surface gains heat through atmospheric fluxes (Fig. 15b) and there is lateral exchange with the surrounding waters which are all warmer than those in the DCA (Fig. 12b), the temperature as well as the vertical temperature gradient are increasing. In winter, when there is heat loss and vertical mixing, the temperature decreases. There is, however, still a difference: in the upper 100 m, warming continues until August, whereas below, it continues until November. In terms of temperature, the water is always stably stratified, with warmer water above colder water. Note that in the surface layer, high temperature corresponds with low salinity, and low temperature with high salinity, as was already discussed for the surface values in Section 3.2.1.

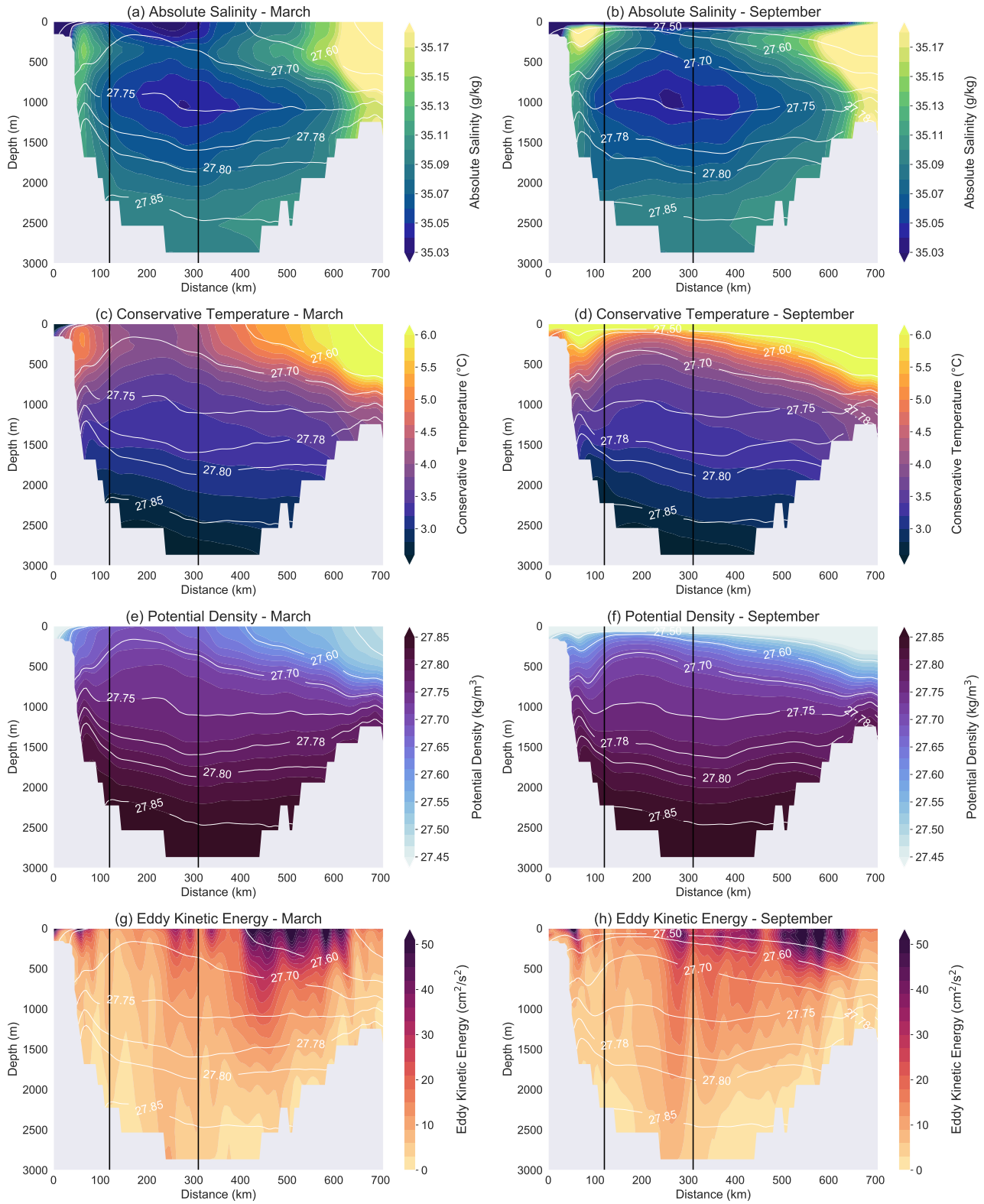


Figure 17: The 1993–2019 March (left column) and September (right column) climatologies from the CMEMS reanalysis of the (a)-(b) absolute salinity, (c)-(d) conservative temperature, (e)-(f) potential density and (g)-(h) eddy kinetic energy along the WOCE AR7E section in the Irminger Sea. The vertical black lines mark the points where the section intersects the Deep Convection Area boundary. The white curves are isopycnals.

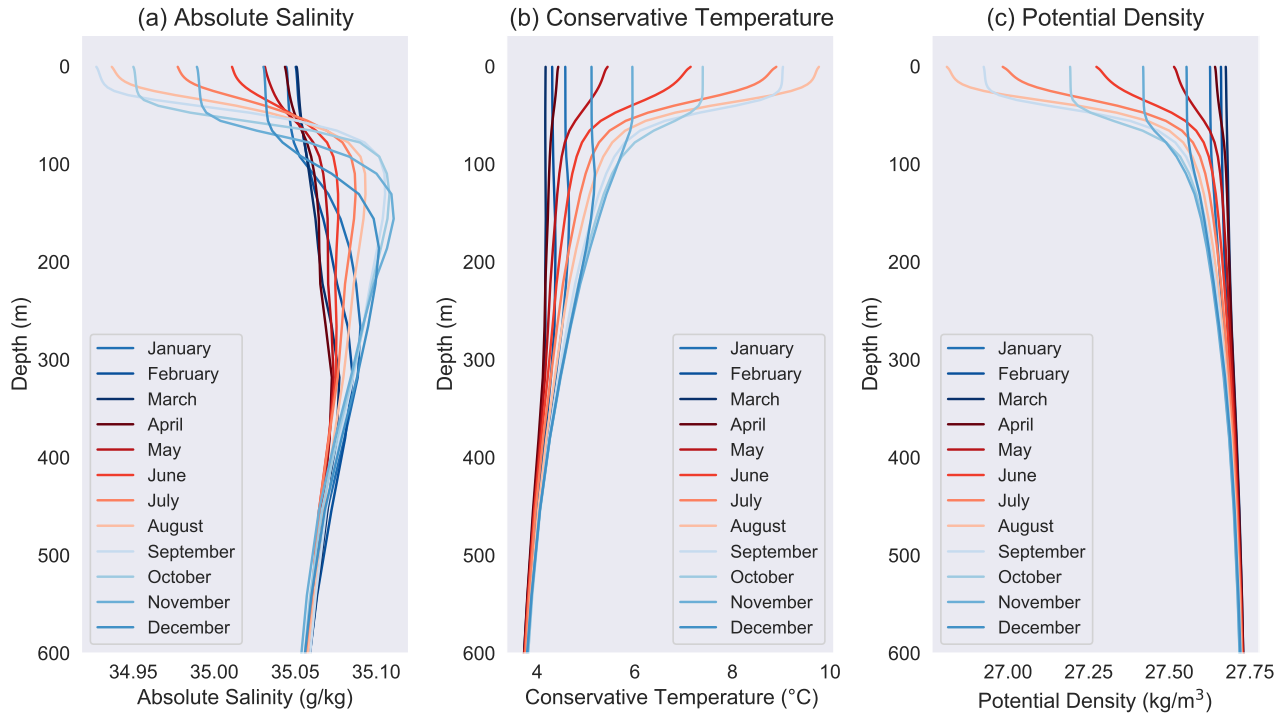


Figure 18: Climatologies of the (a) absolute salinity, (b) conservative temperature and (c) potential density profiles averaged over the Deep Convection Area, from the monthly 1993–2019 CMEMS reanalysis.

The annual cycle in the density profile (Fig. 18c) strongly reflects the temperature profile climatology. From April until August, surface density is decreasing, and the vertical density gradient increases throughout the whole upper 600 m. After this restratification phase density starts decreasing again in the upper 100 m, but below that, the density gradient continues to increase until November: here restratification goes on for longer. In the upper 100 m, the water becomes fresher and warmer and thus lighter in summer, and saltier and colder and thus denser in winter. By contrast, the layer below 100 m gets warmer and more saline in summer, and colder and fresher in winter. The fact that the density in this layer increases in summer and decreases in winter shows that the temperature is the dominant contributor to density here.

Based on the observation that salinity trends in the upper part of the water are opposite to those in the lower part, and that restratification ends earlier in the upper than in the lower part, we will study the interannual variability in (re)stratification in two separate layers in the next part. For this we define an upper layer from 0–100 m and a lower layer from 100–600 m. Based on this partition, we expect different interannual variability in the two layers. We hypothesise that atmospheric fluxes are the main forcing mechanism for the upper layer. This hypothesis is based on our previous finding that the timing of negative and positive heat fluxes matches the timing of convection and restratification in the climatology (Section 3.2.2). As these atmospheric fluxes occur at the air-sea interface, we don't expect them to play a role for restratification the lower layer; during restratification the mixed layer does not penetrate into the lower layer (Fig. 16) and so the surface fluxes do not affect this part. Instead, we expect the (re)stratification in the lower layer to be mainly determined by lateral exchange with other water masses and by the strength of convection. This strength in convection is not expected to play a role for the upper layer since the mixed layer always extends deeper than 100 m in winter (Fig. 19, 28a) and thus always contains the upper layer.

3.3 Interannual Variability

With our knowledge of the time-mean situation and the mean seasonal cycle throughout a year, we will now consider full time series of properties in the DCA, to study the interannual variability in (re)stratification.

3.3.1 Variability of Hydrographic Properties

To study interannual variability in hydrographic properties throughout the water column, we consider the full 1993–2019 time series of salinity, temperature, and density over depth within the DCA, shown in Figure 19. The mean MLD as well as the maximum MLD over the DCA are plotted in black and white, respectively. From the evolution of the MLD, we see that there is not only a clear seasonal cycle (Fig. 16), but also strong interannual variability in the deep convection strength. Also we see interannual variability in (re)stratification: some years have much weaker vertical density gradients than other years. In years with deep mixed layers, we see outcropping of isopycnals: dense, cold and saline water comes close to the surface. The deepest mixed layers were found in the 1990s, which were forced by cold and stormy winters (Våge et al., 2011). In these years we see cold, dense waters extending quite high in the water column. In the 2000s, convection was less strong, and stratification was high. From 2015 until 2019, MLD increased again, and we observe a thickening of deep cold and dense layers and thus a decrease in stratification. The deep mixed layers in these years were also observed from moorings within the DCA by de Jong and de Steur (2016) and de Jong et al. (2018).

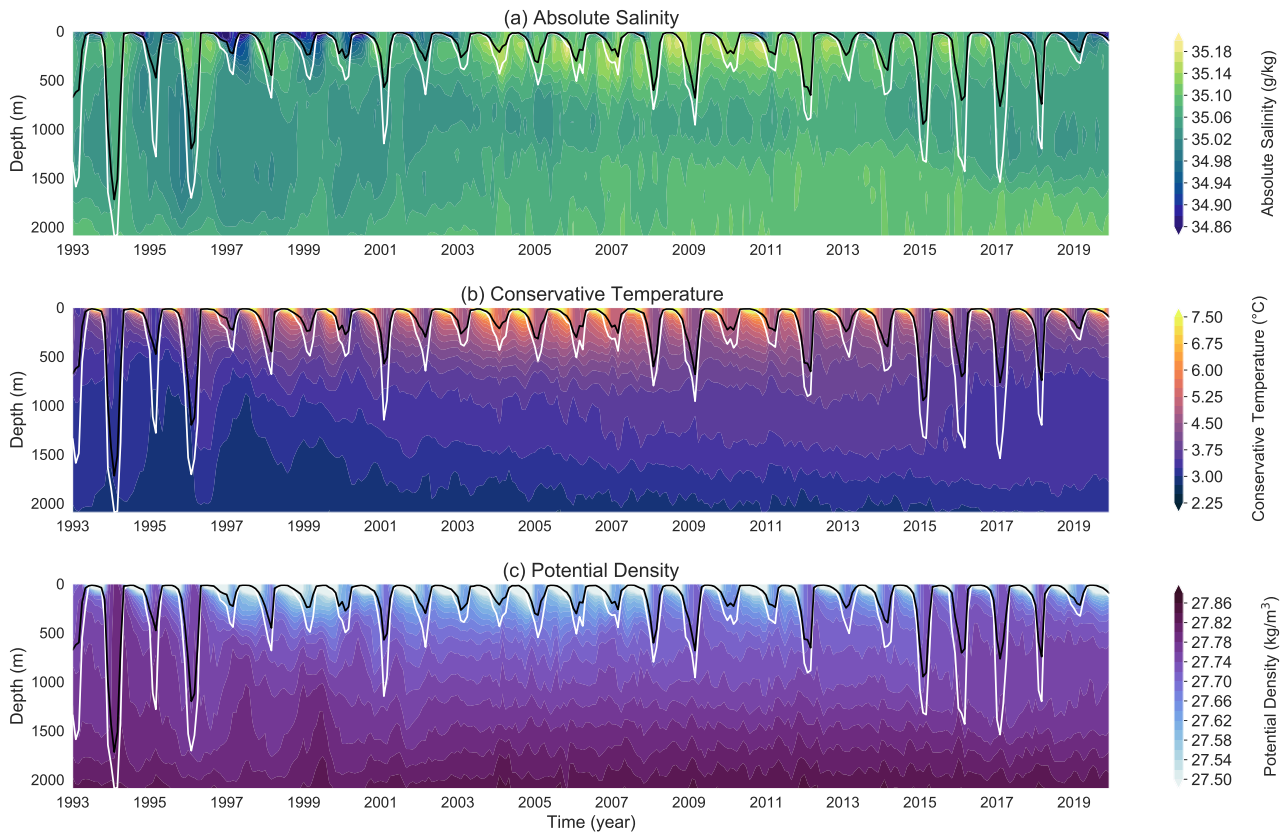


Figure 19: The temporal evolution of profiles of (a) absolute salinity, (b) conservative temperature and (c) potential density from the CMEMS reanalysis averaged over the DCA. The mixed layer depth averaged over the DCA is shown in black; the maximum mixed layer depth reached within the DCA is shown in white.

The temperature and density have continuously layered structures, with warm, light layers above cold, dense ones. By contrast, a different layered structure is present in the salinity profiles; in the layer between approximately 500 and 1500 m we find the fresh signature of convectively formed water, as also seen in the mean hydrographic section through the Irminger Sea (Fig. 14). From roughly 2002 until 2012, the surface waters became more saline. From 2017 onward, a freshening of upper and intermediate layers can be observed. This is the result of a freshwater anomaly which formed in the eastern subpolar North Atlantic between 2012 and 2016 and went on to propagate northward into the Irminger and Labrador Sea and the Nordic Seas (Holliday et al., 2020).

3.3.2 Variability of Atmospheric Fluxes

Next, we will study the interannual variability in atmospheric forcing above the DCA. The full 1993–2019 time series of surface freshwater and heat fluxes from ERA5 and of surface salinity and temperature from CMEMS averaged over the DCA are shown in Figure 20. A strong seasonal cycle is visible in the evaporation, surface heat flux, and surface temperature. The precipitation and surface salinity also have some seasonal signature, but with strong interannual variability. The net freshwater flux, precipitation minus evaporation, is positive almost throughout the whole period, and has no clear seasonality. The surface heat flux is negative during winter and positive during summer, with larger values in winter, so that over an entire year the net heat flux is always negative. This means that each year there is a net gain of freshwater and loss of heat to the atmosphere (see also Fig. 13). Since, however, the surface waters in the DCA are not getting fresher and colder each year (Fig. 20d,e), lateral exchanges with surrounding water masses must play an important role in supplying the DCA with heat and salt. This lateral exchange is probably mainly facilitated through warm and saline eddies shed from the Irminger Current, as seen from the locations of high EKE in Figure 12.

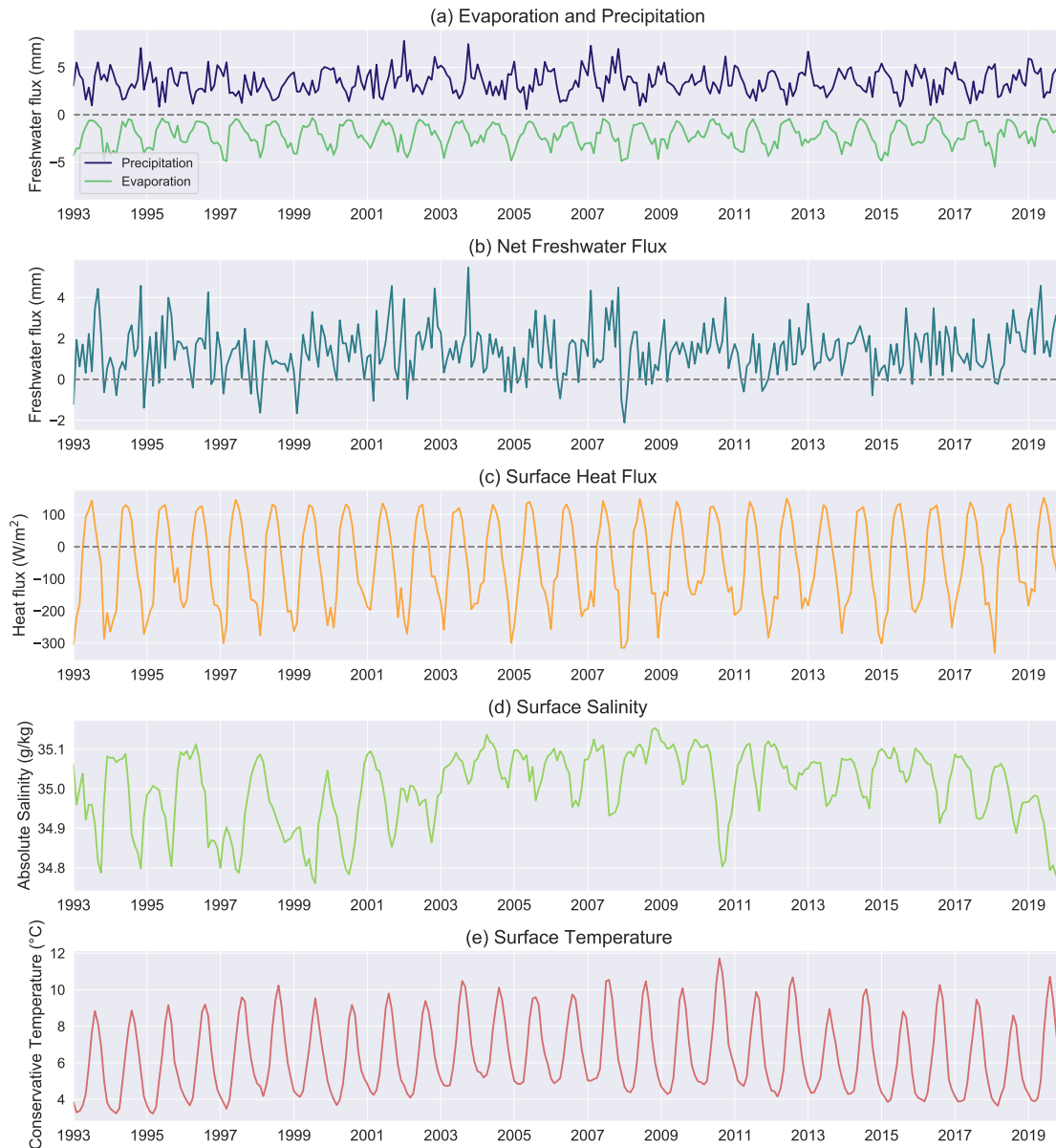


Figure 20: Time series of (a) evaporation and precipitation, (b) net freshwater flux, (c) surface heat flux, (d) surface absolute salinity and (e) surface conservative temperature over 1993–2019, averaged over the DCA. Monthly ERA5 reanalysis data is used for (a)–(c) and monthly CMEMS reanalysis data is used for (d) and (e).

3.3.3 Variability of Stratification and Restratification

We have seen that there is interannual variability in the hydrographic as well as atmospheric properties in the DCA, and also in the strength of deep convection. Now, we will study the interannual variability in stratification and restratification in the DCA. As was argued at the end of Section 3.2.4 we expect different behaviour for the upper layer from 0–100 m and the lower layer from 100–600 m, as we observed different behaviour of salinity and temperature in both layers. Therefore we will study the (re)stratification in these layers separately.

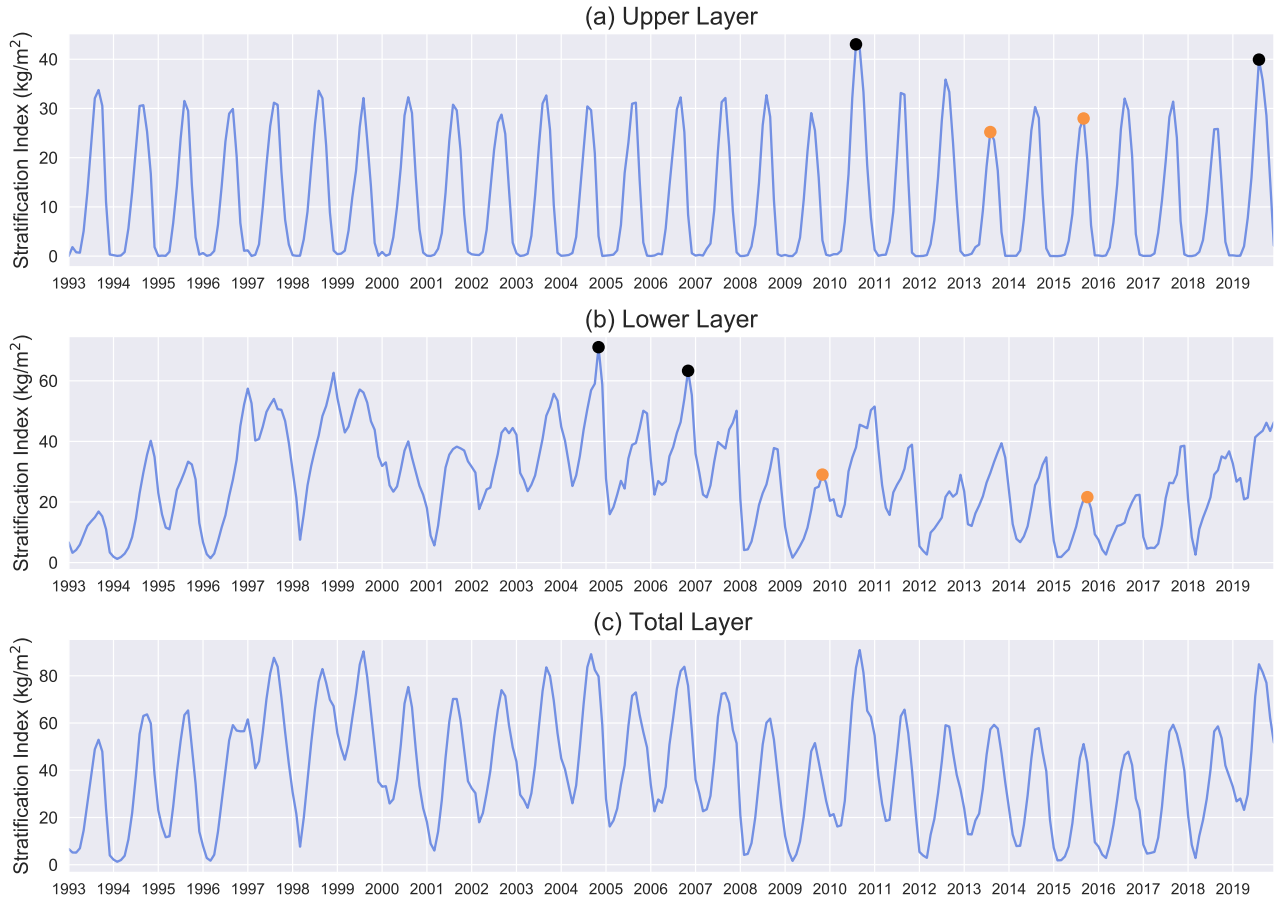


Figure 21: The stratification index in the DCA for (a) the upper layer from 0–100 m, (b) the lower layer from 100–600 m, and (c) the total water layer from 0–600 m. Black dots mark years with high stratification and orange dots mark years with low stratification that will be used in case studies.

Figure 21 shows the full 1993–2019 time series of stratification in the DCA, measured by the stratification index (SI) as introduced in Section 2.2.3, for the upper, lower and total layer. It is clear that the upper and lower layer exhibit very different behaviour. Firstly, in the upper layer the stratification has a very clear seasonal cycle, with high values in summer and low values in winter. There is little interannual variability in this layer, although there are a few years with notably higher or lower summer maxima (e.g. exceptionally strong stratification in 2010 and 2019). The seasonal cycle of the stratification is similar to that of surface heat flux and surface temperature (Fig. 20). By contrast, in the lower layer interannual variability dominates over seasonality. Still a seasonal cycle with minima in winter and maxima in summer can be identified, but the values of these minima and maxima can differ strongly between years. Moreover, the timing of maximum and minimum stratification differs between the two layers. In the upper layer, the minimum stratification almost always occurs in January or February (though the values are approximately constant from December–April), and the maximum stratification is always reached in August or September. In almost all years, the stratification in the upper layer starts to increase at the same time as when the surface heat flux first becomes positive. Also, in most years the stratification starts to decrease once the surface heat flux becomes negative. In 8 of the 27 years the stratification only starts to decrease one month after the heat flux has become negative. In the lower layer, there is more variation in the timing of minima and maxima between the years. The minimum stratification is most often in March, but also

frequently occurs in February or April; this is always either in the same month or one or two months after the maximum MLD is reached. The maximum stratification can occur in any month from July until January in this time series, with the highest frequencies in November and December. Thus both the minima and maxima occur later in the lower layer than in the upper layer. The stratification almost always continues to increase until after the surface heat flux has become negative, with lags of up to 5 months.

The stratification over the total layer from 0–600 m is the superposition of the strong seasonal cycle in the upper layer and the interannual variability in the lower layer.

Figure 22 shows the annual values of restratification (difference maximum and minimum SI per year), again for the upper, lower and total layer separately. Again we observe strong interannual variability, in the upper as well as the lower layer. In the upper layer there are clear peaks in restratification in 2010 and 2019, which were also the years in which stratification in the upper layer was very high (Fig. 21). These peaks are also clearly visible in the stratification and restratification of the total layer. In the lower layer the strongest restratification values are observed in 1996 and 1998. Note, however, that in the CMEMS reanalysis data from these years no ARGO data was yet assimilated, so these values may be less accurate than the values from 2001 and later (see Section 2.1.1).

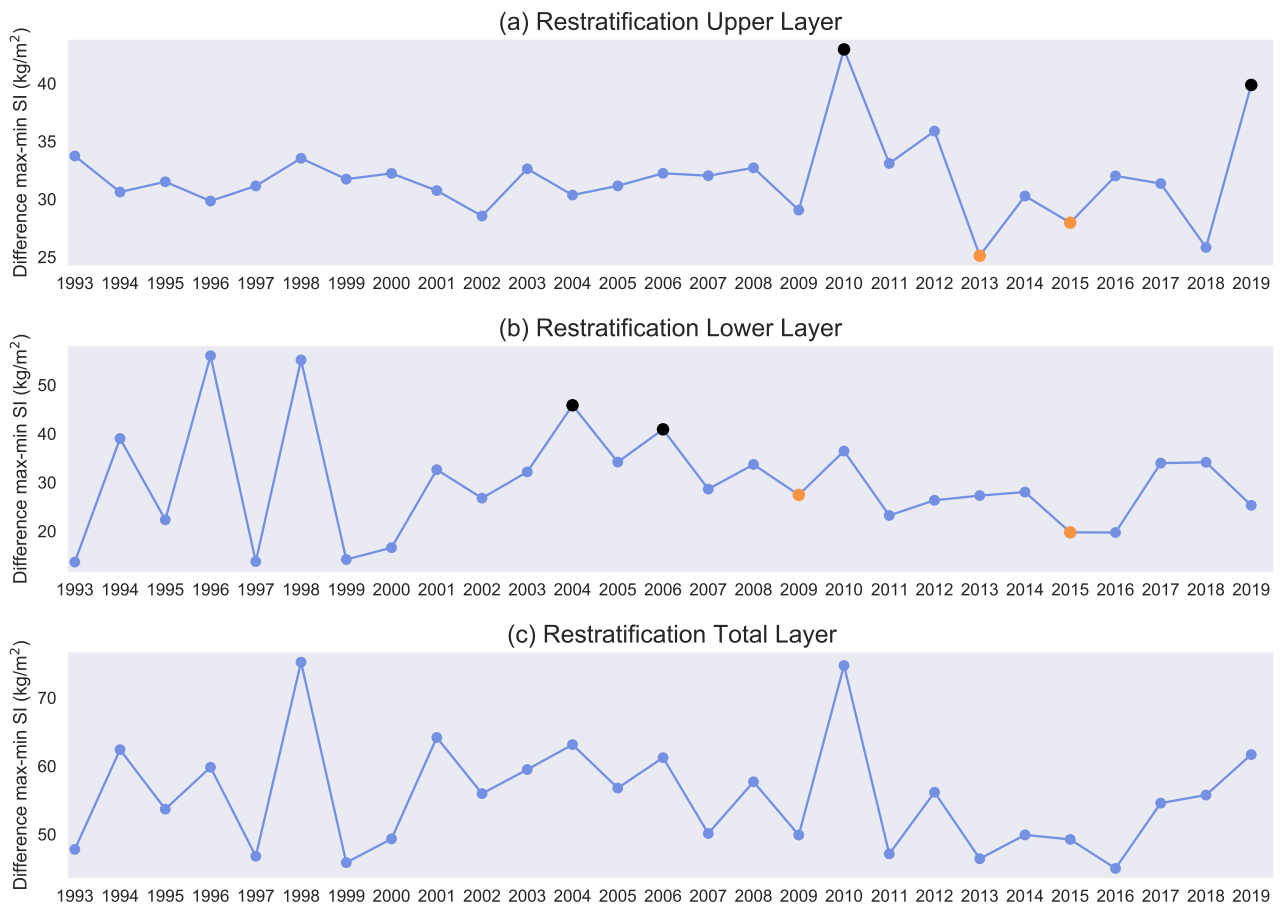


Figure 22: The annual restratification in the DCA, defined as the difference between the maximum stratification index (SI) reached in the summer of a certain year and the minimum stratification index reached in the preceding winter, for (a) the upper layer from 0–100 m, (b) the lower layer from 100–600 m, and (c) the total water layer from 0–600 m. Black dots mark years with high stratification and orange dots mark years with low stratification that will be used in case studies.

4 Interpretation

In this section we give a physical interpretation of the results and aim to identify drivers of the interannual variability in (re)stratification.

4.1 Case Studies

As we have seen, there is clear interannual variability in the stratification and restratification within the DCA. In order to learn something about the physical processes determining the strength of (re)stratification in a certain year, we will perform a number of case studies for years with exceptionally high or low maximum stratification. We found that the upper and lower layer have distinct (re)stratification behaviour (Section 3.3.3). Therefore, we will make a distinction between both layers in our case studies. After the case studies we will try to generalise the results regarding the physical processes determining (re)stratification.

Based on Figure 21, we choose the years to study. We do not consider years before 2001 since in that time there was no ARGO data to be used for the CMEMS reanalysis. The upper layer shows little interannual variability, but the years 2010 and 2019 have clear peaks in the maximum stratification, whereas 2013 and 2015 have small peaks compared to other years. In the lower layer, interannual variability is much stronger. We choose 2004 and 2006 as years with high stratification and 2009 and 2015 as years with low stratification in the lower layer. All these years are also indicated in Figures 21 and 22.

For these years, we will study the vertical profiles of salinity, temperature, and density in the months of minimum and maximum stratification, as shown in Figures 23–27. In addition, we will consider the 1993–2019 climatological profiles of salinity, temperature, and density, to see how the conditions in the year of interest deviate from the climatology. As mentioned in Section 3.3.3, the timing of minimum and maximum stratification differs between the upper and lower layer. For the upper layer, we will look at the months February and August; for the lower layer, we consider March and November as months for minimum and maximum stratification. In some years the minimum or maximum stratification occurs one month earlier or later than the months chosen here, but the different profiles do not yield qualitatively different results. Although the exact months of minima and maxima differ from year to year, we choose these fixed months to be able to compare the different years of the case studies with the same climatologies, and to not overload the figures. Apart from studying these profiles, we will look at the surface fluxes of heat and freshwater, the strength of convection, and the EKE in the indicated years, to see if these might explain the high or low stratification. We will first discuss the case studies in the upper layer, and then those in the lower layer.

4.1.1 Upper Layer

4.1.1.1 High Stratification - 2010 & 2019

Figure 23 shows the vertical profiles of salinity, temperature, and density in the upper layer in the months February and August of the high stratification years 2010 and 2019, as well as the 1993–2019 climatological profiles of those months as a reference. February was more saline and warmer than usual in 2010, whereas it was fresher and colder than usual in 2019. Then in August, both years had a warm anomaly and an increased vertical temperature gradient. In terms of salinity there is a difference: in August 2019 there was a fresh anomaly in the upper layer, but in August 2010 there was a saline anomaly between 40–100 m and a fresh anomaly in the top 40 m. In both years there was also an increased vertical salinity gradient. Density was anomalously low in August of both years and had an anomalously large vertical gradient, indicating increased stratification. As both salinity and temperature had increased vertical gradients compared to the climatology in August 2010 and 2019, both properties contributed to this increased stratification.

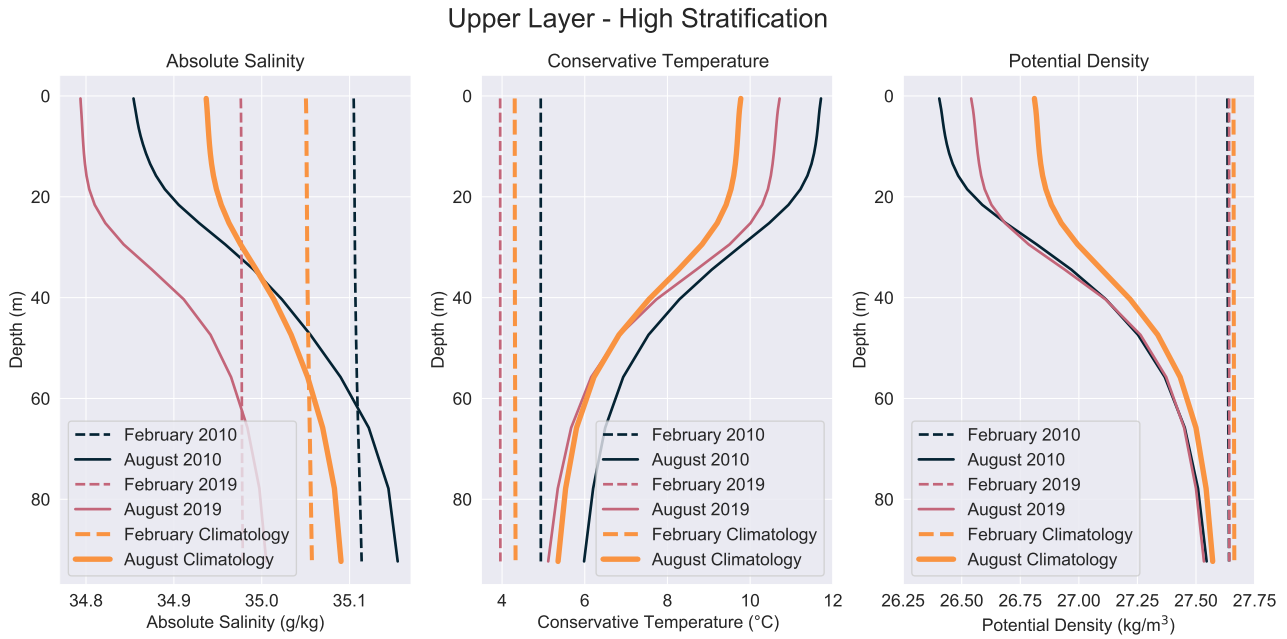


Figure 23: Vertical profiles of absolute salinity, conservative temperature, and potential density in the upper layer of the DCA for February and August in 2010 and 2019, compared with the 1993–2019 climatology, from the CMEMS reanalysis.

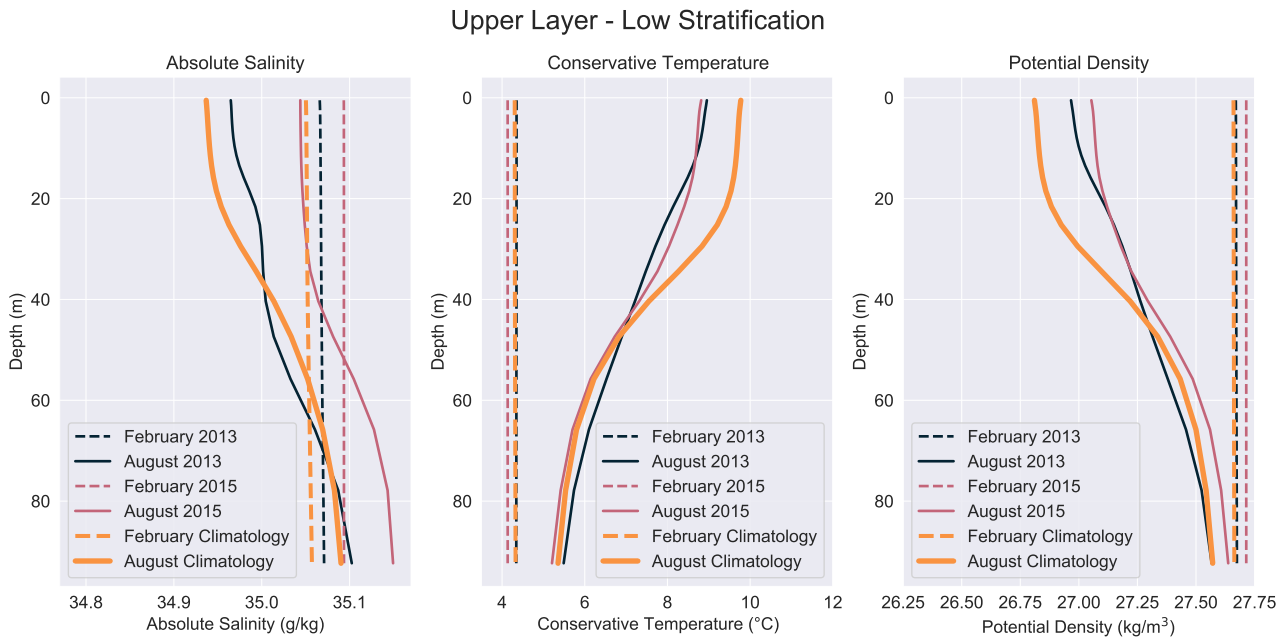


Figure 24: Vertical profiles of absolute salinity, conservative temperature, and potential density in the upper layer of the DCA for February and August in 2013 and 2015, compared with the 1993–2019 climatology, from the CMEMS reanalysis.

4.1.1.2 Low Stratification - 2013 & 2015

The case studies for the two low stratification years in the upper layer, 2013 and 2015, are shown in Figure 24. The months February of both years were more saline than usual, and close to the climatology in terms of temperature. In August, 2015 had a saline anomaly in the whole upper layer, whereas 2013 had a saline anomaly in the upper 40 m but a fresh anomaly below. For both years the vertical salinity gradient in August

was low compared to the climatology. In terms of temperature, both years had a cold anomaly in August in the upper 40 m, and were very similar to the temperature climatology below; thus the vertical temperature gradients were also decreased. The density in August was anomalously high in the upper 40 m and close to the climatology below for both years. The low stratification in 2013 and 2015 was thus a result of the weak vertical gradients in both salinity and temperature.

4.1.1.3 Discussion Upper Layer

In all these four case studies, in August of the considered year, there were anomalies in salinity and/or temperature which had a different sign above 40 m than below. In the high stratification year 2010, the upper 40 m were fresher than the climatology, whereas the part below 40 m was more saline. In the low stratification year 2013, this was the other way around. Furthermore, the high stratification year 2019 had a warm anomaly in the upper 40 m and a cold anomaly below; the opposite was true for the low stratification years 2013 and 2015. These anomalies of opposing sign either enhanced or weakened the vertical gradient in these properties, thus contributing to the observed increased or reduced stratification. This different behaviour between the layers above and below 40 m suggests a strong influence of surface effects that only impact a thin surface layer.

Furthermore, the deviations in salinity and temperature always had the same impact on density. That is, the stratification was either increased in terms of both salinity and temperature, or decreased. In 2010 and 2019, the upper 40 m were warmer and fresher than usual; in 2013 and 2015, they were colder and saltier. As there are no water masses near the DCA with a warm and fresh or cold and saline signature, this also indicates that restratification in the upper layer is not the result of lateral exchanges with nearby water masses (warm and saline IC water or cold and fresh EGC/EGCC water).

Note, moreover, that the restratification for the high stratification years 2010 and 2019 was also very high, as we can see in Figure 22a. This is an indication that the minimum stratification in these years was not anomalously high; in that case the restratification (difference maximum and minimum stratification) would not have been so large. Similarly, restratification was low in the low stratification years 2013 and 2015, so the minimum stratification in these years was not anomalously low. Indeed, it can be seen in Figure 21a that the minimum stratification is every year approximately zero, with little variation visible. In Figures 23 and 24 it is also visible that in February of each year, the salinity and temperature may differ from the climatology, but are always uniform throughout the upper layer. This shows that processes during the summer of the considered years were responsible for the observed high or low stratification values, rather than processes that were already going on for a longer time.

Since we expect surface processes to play a role in restratification of the upper layer, we will look at the surface freshwater and heat fluxes of the indicated years, to see if these can explain the salinity and/or temperature anomalies that led to the high or low stratification. For this we study the net result of surface fluxes over the DCA during the upper layer restratification period of each year. We define this restratification period to start in the month after the occurrence of the minimum winter stratification, and to end in the month of the next maximum stratification in the upper layer. The net precipitation, net evaporation, and net freshwater flux are defined to be the sum of the values of these variables over the indicated period; the net heat flux is defined not as the sum but as the integral over time of the heat fluxes. These net fluxes are shown in Figure 25.

We see that the high stratification years 2010 and 2019 were both characterized by high freshwater gain during the restratification period due to low values of evaporation. Furthermore, 2019 had a very high heat gain during restratification. In 2010 the heat gain was also quite large, but not as far from the average as in 2019. Recall that the presence of a fresh surface layer, which already increases stratification, restricts warming to only this thin layer, thereby further increasing stratification (Section 3.2.1). So the combination of high freshwater gain and high heat gain contributed to the high stratification in 2010 and 2019. In 2013 and 2015, both net freshwater flux and heat flux were close to the average value during the restratification period. So in these years there were likely other processes that contributed to the observed cold and saline anomalies.

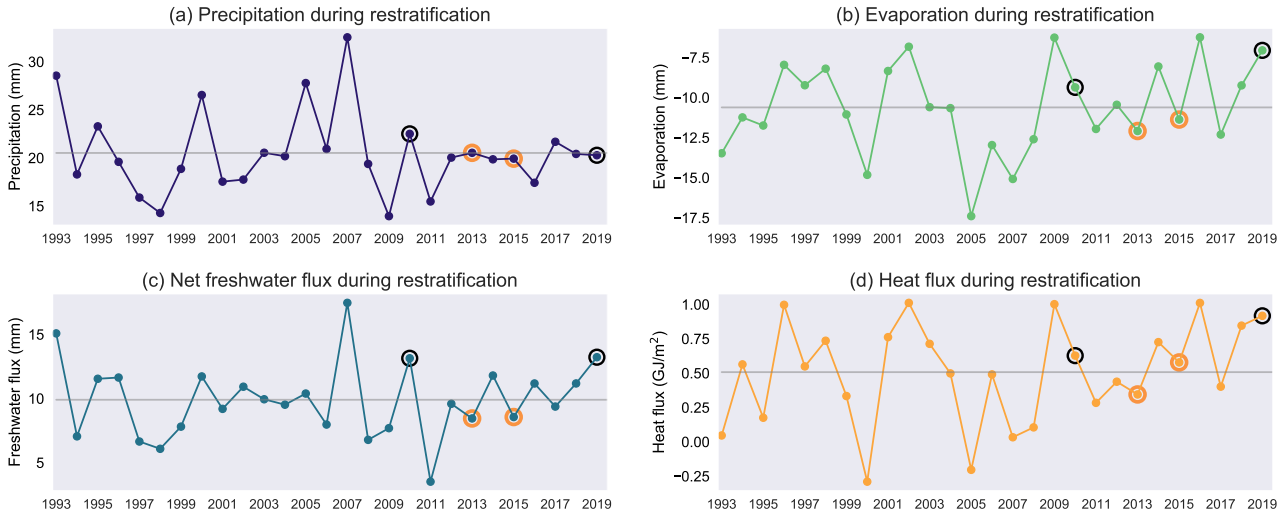


Figure 25: The net values of (a) precipitation, (b) evaporation, (c) net surface freshwater flux and (d) surface heat flux over the DCA during the restratification period of the upper layer of each year, from ERA5 monthly reanalysis data. The restratification period starts in the month after the occurrence of the minimum winter stratification and ends in the month of the next maximum stratification in the upper layer. Grey lines indicate the average value of the time series. Black dots mark years with high stratification and orange dots mark years with low stratification that are used in case studies.

4.1.2 Lower layer

4.1.2.1 High Stratification - 2004 & 2006

Figure 26 shows the case studies for the high stratification years in the lower layer, 2004 and 2006. In both years, in March there was a saline and warm anomaly compared with the climatology. In November, the warm anomaly was still present in both years, and the vertical temperature gradient was increased. However, in terms of salinity there was a difference. In 2006 there was still a saline anomaly, but in 2004 there was a fresh anomaly, with two inversions between 100 and 300 m depth. Still, for both years the November salinity profiles had lower vertical gradients than the climatological profile. Note that in this climatological profile for November there is more saline water above fresher water. Therefore the salinity has a destabilising effect on the stratification. The lower vertical salinity gradients in November 2004 and 2006 thus mean that salinity is less stabilising than usual in these years. So in both years, stratification was increased in terms of both salinity and temperature. This is visible in the November density profiles: they have an increased vertical gradient compared to the climatology. Also they both have a light anomaly. The fact that in November 2006 the result of a saline and warm anomaly was a light anomaly indicates that temperature is dominant in determining the sign of the density anomaly, and thus plays a dominant role in determining the stratification.

4.1.2.2 Low Stratification - 2009 & 2015

The case studies for the low stratification years 2009 and 2015 are shown in Figure 27. In both years, March had a saline anomaly. March had a warm anomaly in 2009 and a cold anomaly in 2015. However the vertical gradients in salinity and temperature were in both years close to the climatology; the lower layer was well-mixed and the vertical gradients were almost zero. In November 2009, salinity was anomalously high and had an increased vertical gradient, but temperature was very similar to the climatology. In November 2015, there was a saline anomaly between 100–300 m and a fresh anomaly below, but both were small in magnitude. The temperature was anomalously low and had a weakened vertical gradient. Both Novembers had anomalously low density and weaker vertical density gradients than usual. In 2009 this was the result of the saline anomaly; in 2015 it was the result of the cold anomaly.

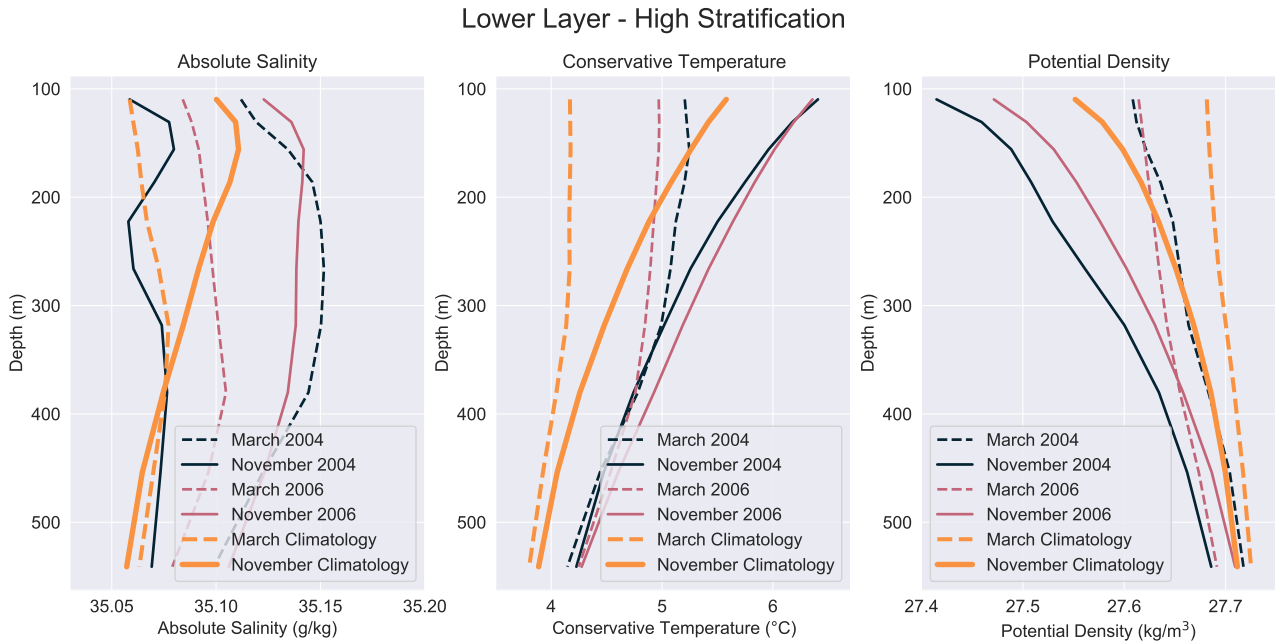


Figure 26: Vertical profiles of absolute salinity, conservative temperature, and potential density in the lower layer of the DCA for March and November in 2004 and 2006, compared with the 1993–2019 climatology, from the CMEMS reanalysis.

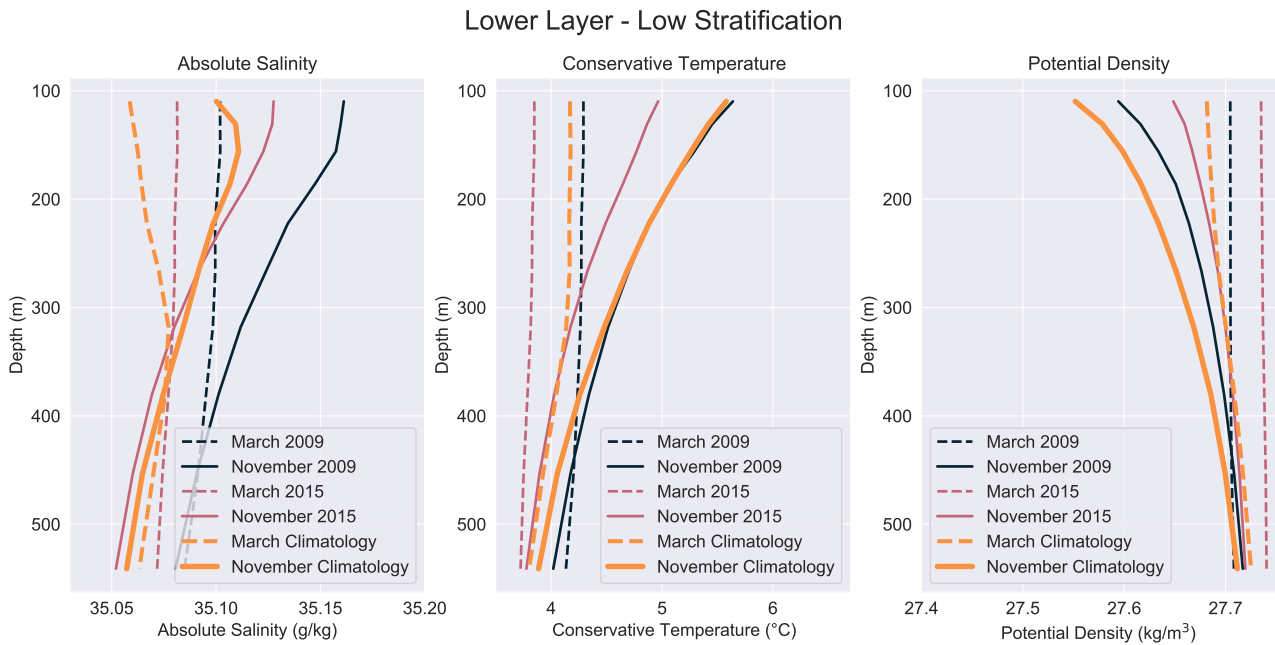


Figure 27: Vertical profiles of absolute salinity, conservative temperature, and potential density in the lower layer of the DCA for March and November in 2009 and 2015, compared with the 1993–2019 climatology, from the CMEMS reanalysis.

4.1.2.3 Discussion Lower Layer

In the lower layer we found different combinations of salinity and temperature anomalies during in the case study years. In November 2004 conditions were fresh and warm compared with the climatology; in 2006, saline and warm; in 2009, saline with no temperature deviation; and in 2015, cold with only a small salinity deviation (saline above 300 m and fresh below). This is in contrast with what we found for the upper layer, where there

was always a combination of either fresh and warm or saline and cold anomalies resulting in the observed high or low stratification. In some, but not all, cases the properties in the lower layer match the signature of surrounding water masses, such as the warm and saline Irminger Current and the cold and fresh East Greenland Current. If an anomaly is not the result of exchange with surrounding water masses (such as the warm and fresh anomaly in 2004), then it must be caused by mixing of upper layer properties into the lower layer.

We hypothesized that the (re)stratification in the lower layer is mainly determined by the strength of convection and by lateral exchange with other water masses. To check this hypothesis for the years of our case studies, we consider the mixed layer depth and the eddy kinetic energy in these years.

With Figure 28a we can study the influence of the MLD. It shows the maximum value of the MLD averaged over the DCA between the end of restratification in the preceding year and the start of restratification in the indicated year. As for the upper layer, the restratification phase is here defined as the period from the month after the minimum winter stratification until the month of the next maximum stratification in the lower layer. In the high stratification years 2004 and 2006 the MLD was low. In 2004 the MLD reached approximately 210 m in winter, in 2006 it was 300 m; so in neither year did the mixed layer (averaged over the DCA) extend beyond the upper half of the lower layer. By contrast, in 2009 the mean MLD reached 680 m during winter, and in 2015 even 950 m (see also de Jong and de Steur, 2016). Comparing 2009 and 2015 with the high stratification years 2004 and 2006, we see that not only the maximum SI during summer, but also the minimum SI during winter was much lower in the former two years than in the latter (Fig. 21b). This can also be seen when comparing the March profiles of the high and low stratification years in Figures 26 and 27. In 2009 and 2015, the deeper mixed layers caused lower minimum SI and therefore lower maximum SI than in 2004 and 2006.

Figure 28b shows the mean surface EKE during the restratification phase, averaged over the portion of the hydrographic section line from Figure 6 that lies eastward of the eastern DCA boundary. As we saw in Figures 12d and 14d in this region there is high EKE, which is associated with eddies that bring warm and saline Irminger Current water into the DCA (Fan et al., 2013). Considering that the eddies are surface-intensified and that the high EKE signature is visible throughout the upper 600 m (Fig. 14d), we need only study the surface EKE values in order to learn something about their impact on the whole upper 600 m. In 2004 and 2006 the mean EKE during restratification was high. So here eddies could have contributed to the enhanced stratification. Note, though, that in 2004 other processes must have also played a role, since there was a fresh and not a saline anomaly. In 2009 and 2015, the EKE during restratification was quite low; in 2015 it was even the lowest of the whole time series. The low EKE might mean that there were fewer eddies contributing to restratification, and that therefore the stratification in November was weaker than usual.

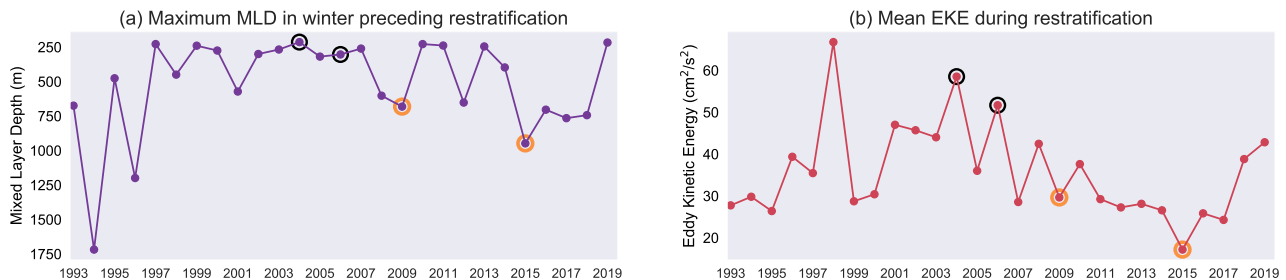


Figure 28: (a) The maximum value of the MLD averaged over the DCA between the end of restratification in the preceding year and the start of restratification in the indicated year. (b) The surface eddy kinetic energy averaged over the portion of the hydrographic section line from Figure 6 that lies eastward of the eastern DCA boundary, averaged over the restratification period in the lower layer for each year. The restratification period starts in the month after the occurrence of the minimum winter stratification and ends in the month of the next maximum stratification in the lower layer. Black dots mark years with high stratification and orange dots mark years with low stratification that are used in case studies.

4.2 Influence of Salinity and Temperature on (Re)Stratification

From the case studies we got some ideas about the role of salinity and temperature in the process of restratification. Often both properties have either an increased or a decreased vertical gradient, so that both lead to stronger or weaker stratification. In the lower layer, it seemed that temperature was dominant in determining the sign of the density anomaly, whereas in the upper layer salinity and temperature always had the same effect on this sign. Furthermore we saw that in the upper layer both salinity and temperature are stabilising, with warm/fresh water above cold/saline water, but in the lower layer salinity is destabilising, with saline water overlaying fresher water.

In this section we will study the influence of salinity and temperature on (re)stratification in detail to see if these conclusions hold for the whole time series, and if we can find more conclusions. We do this by considering time series of SI_T and SI_S as introduced in Section 2.2.3, shown in Figure 29. Recall that they are given in different units than the total stratification index SI (determined from the density profile), and therefore their magnitudes cannot be compared with the magnitude of the total SI .

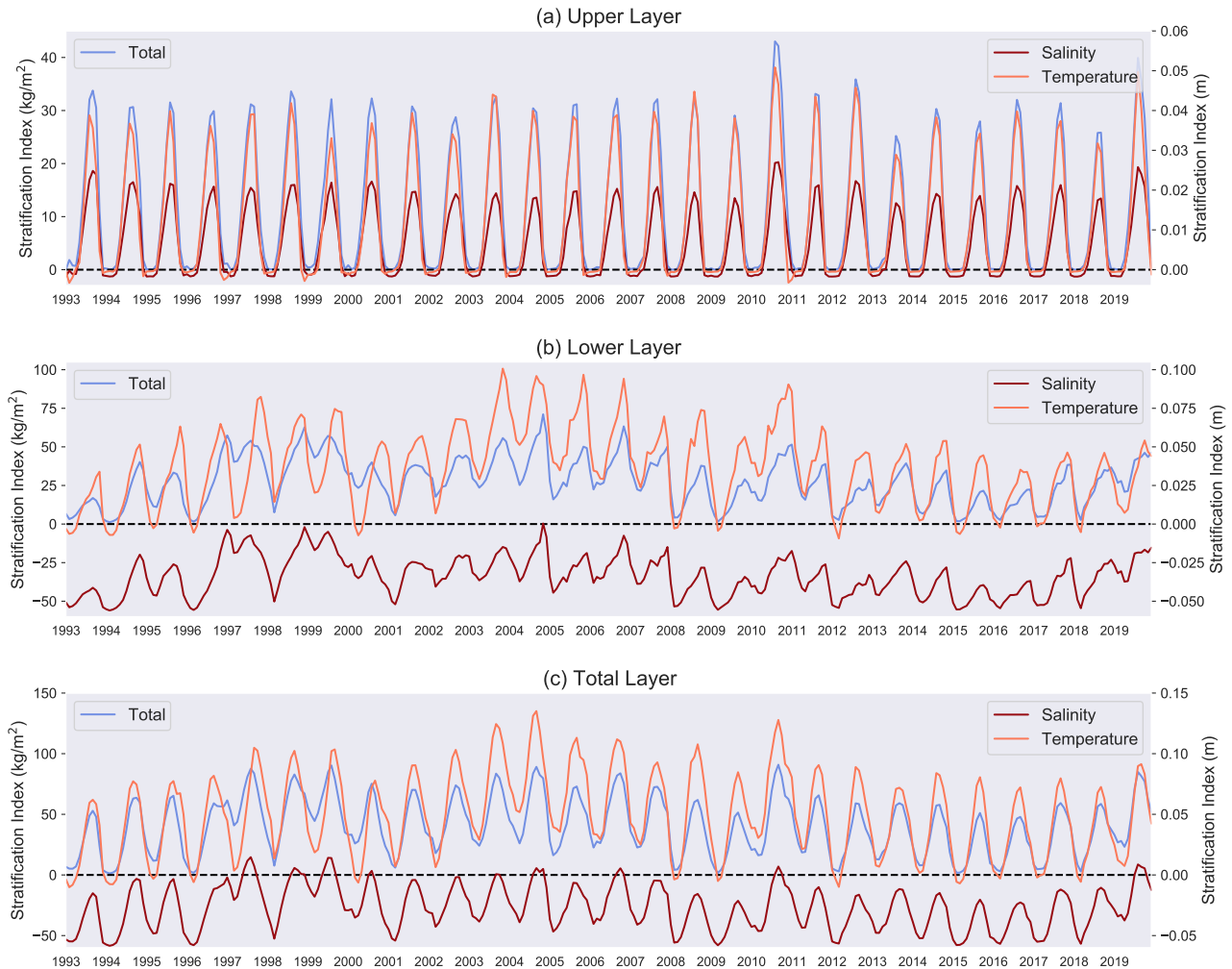


Figure 29: The stratification index (SI) for a density profile that is only determined by salinity or by temperature in the DCA for (a) the upper layer from 0–100 m, (b) the lower layer from 100–600 m, and (c) the total water layer from 0–600 m. The total SI determined from the actual density profile is also shown.

In the upper layer, the SI_T , SI_S and SI all follow a very similar pattern with a strong seasonal cycle. During the winter months, the values of the different stratification indices are sometimes slightly smaller than zero, indicating unstable stratification during the deep convection phase. For the remainder of the year, the upper layer is always stably stratified. The maximum SI_T is always larger than the maximum SI_S .

In the lower layer, the salinity and temperature contribution and the total SI still largely show the same variability, although there are also some differences (e.g. in 1997 the temperature contribution has a clear winter minimum, whereas the salinity contribution and the total SI have only a small local minimum). In this layer, SI_S is always negative, indicating a destabilising effect of salinity. This is the result of more saline water overlying fresher water within this layer as can be seen in Figures 18 and 19. Again, the stratification contribution of temperature is always larger than that of salinity in absolute value.

Over the total 0–600 m layer, the total SI, SI_S and SI_T still have similar variability. Salinity almost always has a destabilising effect; in the lower layer, where SI_S is negative, SI_S has larger absolute values than in the upper layer (since the lower layer is thicker), making the SI_S over the total layer negative as well. Where the SI_S and SI_T variability differ over the total layer, the total SI tends to follow the SI_S variability. The correlation coefficient between the total SI and the SI_S over the total layer is 0.989, whereas that between the total SI and the SI_T is 0.896 (both significant at a 95% significance level). So our observation from the case studies that stratification is often either increased or decreased in terms of both salinity and temperature, can be generalised to the whole time series.

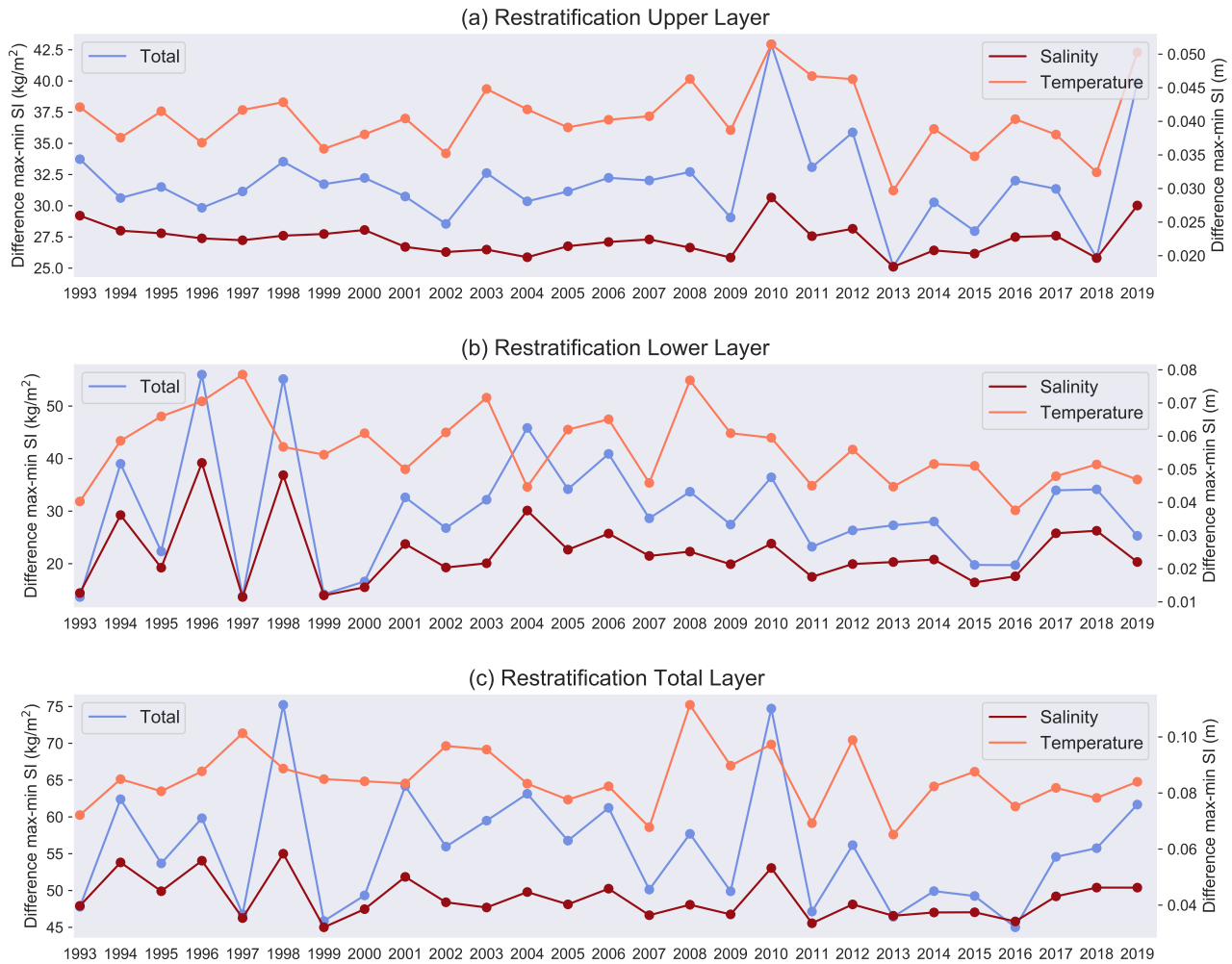


Figure 30: The annual restratification in the DCA, defined as the difference between the maximum stratification index (SI) reached in the summer of a certain year and the minimum stratification index reached in the preceding winter, for (a) the upper layer from 0–100 m, (b) the lower layer from 100–600 m, and (c) the total water layer from 0–600 m. Restratification values are derived from timeseries of total SI as well as of SI for a density profile that is only determined by salinity or by temperature.

Figure 30 shows the annual values of restratification (difference maximum and minimum SI per year) for the temperature and salinity contributions. As for the stratification (Fig. 29), the restratification contribution of temperature is always larger than that of salinity. The patterns of the different contributions are very similar in

the upper layer, but not always in the lower and total layer; in the latter two, the total restratification mainly follows the variability of the salinity restratification. For example, in the high stratification year 2004 the total restratification and the restratification contribution of salinity had local maxima, whereas the contribution of temperature had a local minimum. Indeed, the total restratification is significantly correlated with both the salinity and temperature contributions to restratification in the upper layer. However, in the lower and total layer, it is not significantly correlated with the temperature contribution, but very strongly with the salinity contribution (Table 1). So even though the *values* of the annual restratification are mainly determined by the temperature contribution (which has the largest values), the *variability* in restratification is mainly determined by the salinity contribution.

	Salinity & Total	Temperature & Total
Upper Layer	0.887	0.896
Lower Layer	0.973	0.188
Total Layer	0.868	0.368

Table 1: Correlation coefficients between the salinity and temperature contribution to restratification and the total restratification per layer. Values printed in bold are significant at a 95% significance level.

4.3 Physical Processes Contributing to (Re)Stratification

In Section 4.1 we already investigated possible effects of surface fluxes on restratification in the upper layer, and effects of MLD and EKE on restratification in the lower layer. In this section we will try to generalise these results. As was mentioned already, the CMEMS reanalysis includes ARGO data since 2001 for the Irminger Sea. Thus we have less confidence in the accurate representation of variability by the data from before 2001. Therefore we will focus here on the period 2001–2019. Unless explicitly stated otherwise, any mentions of correlation coefficients between time series in this section will refer to only the 2001–2019 time series. All correlation coefficients are tested for significance at a 95% significance level.

We start with the upper layer. First of all we consider the relation between minimum stratification, the following maximum stratification, and the restratification. The winter minima of SI in the upper layer are always approximately zero, with negligible interannual variation. The reason is that the winter mixed layer always extends below the bottom of the upper layer (Figures 19, 28a) so that the upper layer is always well-mixed in winter. Indeed, there is no significant correlation between the maximum and the minimum stratification. By contrast, the restratification is very strongly and significantly correlated with the maximum stratification, with a correlation coefficient of almost one; the two are almost exactly equal. This result shows that the maximum stratification in the upper layer is fully determined by the restratification. Thus it can only be influenced by processes occurring during the restratification period in summer.

For the upper layer, the timing of the restratification matches the timing of surface heat fluxes being positive and negative (Section 3.3.3). For the case studies, we found that net freshwater and heat fluxes during the restratification phase could explain the high stratification in 2010 and 2019, but not the low stratification in 2013 and 2015. To see if we can identify any connection between restratification, surface freshwater fluxes and surface heat fluxes, we compare the time series of all three in Figure 31. Data from before 2001 is also shown but is not included in any correlation coefficients mentioned here. The surface freshwater and heat fluxes during restratification largely follow the same temporal trends from 2011 onward. However these trends cannot fully explain the trends in restratification: more freshwater or heat gain do not always result in more restratification. Before 2011 the trends are even less clear: despite strong variations in surface fluxes there is only weak variation in restratification. The restratification is not significantly correlated with the freshwater flux nor with the heat flux. In the high stratification years 2010 and 2019, it was the combination of the two that resulted in the strong restratification. The strong freshwater gain caused a fresh anomaly in the upper 40 m, restricting the strong heat gain to only this layer and thus causing a considerable warm anomaly. However in 2016 the values of the freshwater and heat gain were comparable with those in 2019, whereas the restratification was much lower in 2016. So the strength of the surface fluxes during restratification alone cannot explain the interannual variability in restratification in the upper layer; there must be other summertime processes playing a role. The part that cannot be explained by surface fluxes must come from advection, which we did not include in our analysis here. Considering the different behaviour in the upper and lower layer, this likely concerns advection of saline or thermal anomalies which are restricted to the upper layer. An example could be surface freshwater

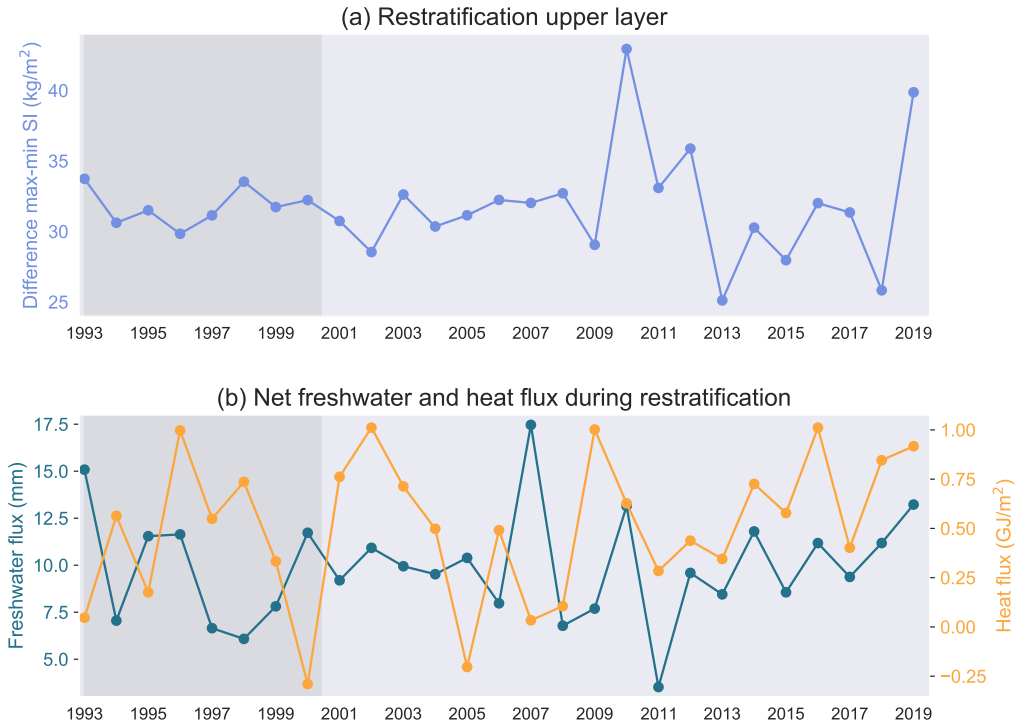


Figure 31: Annual time series of (a) restratification and (b) net freshwater and heat flux during the restratification period in the upper layer over the DCA. The shaded area marks the period before 2001, when the CMEMS data did not include ARGO data.

anomalies resulting from meltwater from Greenland. Such a freshwater anomaly would then restrict surface heating to a thin layer and could thus also cause a warm anomaly.

In the lower layer, we found considerable interannual variability in the minimum stratification (Figure 21b). Here the restratification and the maximum stratification are again significantly correlated, with a correlation coefficient of 0.803. The restratification is again not significantly correlated with the minimum stratification. As opposed to the upper layer, there is a significant correlation of 0.885 between the maximum and the minimum stratification. So the maximum stratification reached in the lower layer is influenced both by wintertime processes which determine the minimum stratification, and by summertime processes which determine the restratification. For the lower layer we found that the high stratification years 2004 and 2006 were preceded by shallow mixed layers, whereas the low stratification years 2009 and 2015 were preceded by deep mixed layers. Figure 32a shows the time series of restratification in the lower layer together with the time series of the maximum MLD averaged over the DCA. The values are so that the MLD always corresponds with the deep convection phase preceding the restratification in the indicated year. The variability in restratification roughly corresponds with the variability in MLD after 2001, with stronger restratification after years with shallower mixed layers. However this is not true for every year. For example, in 2012 the mixed layer extended below the lower layer, whereas in 2011 and 2013 it did not even extend halfway through the lower layer. However, restratification was comparable in all three years. Another example is that in 2019 the mixed layer was much shallower than in 2018, but the restratification was also weaker. The correlation between the restratification in the lower layer and the MLD is not significant. However, there is a significant correlation between the maximum stratification and the MLD, with a value of -0.752 . This is because the minimum stratification is directly influenced by the MLD; correlation between these two is also significant with a value of -0.877 . So the strength of convection influences the interannual variability in minimum stratification and therefore also in maximum stratification, but it does not influence the restratification itself.

Figure 32b compares the time series of restratification in the lower layer with the time series of EKE eastward of the DCA during the restratification phase. These two time series follow each other's temporal variability remarkably well. They are significantly correlated with a correlation coefficient of 0.733. This can be explained as follows. If the EKE east of the DCA is higher, this indicates the presence of more eddies travelling westward

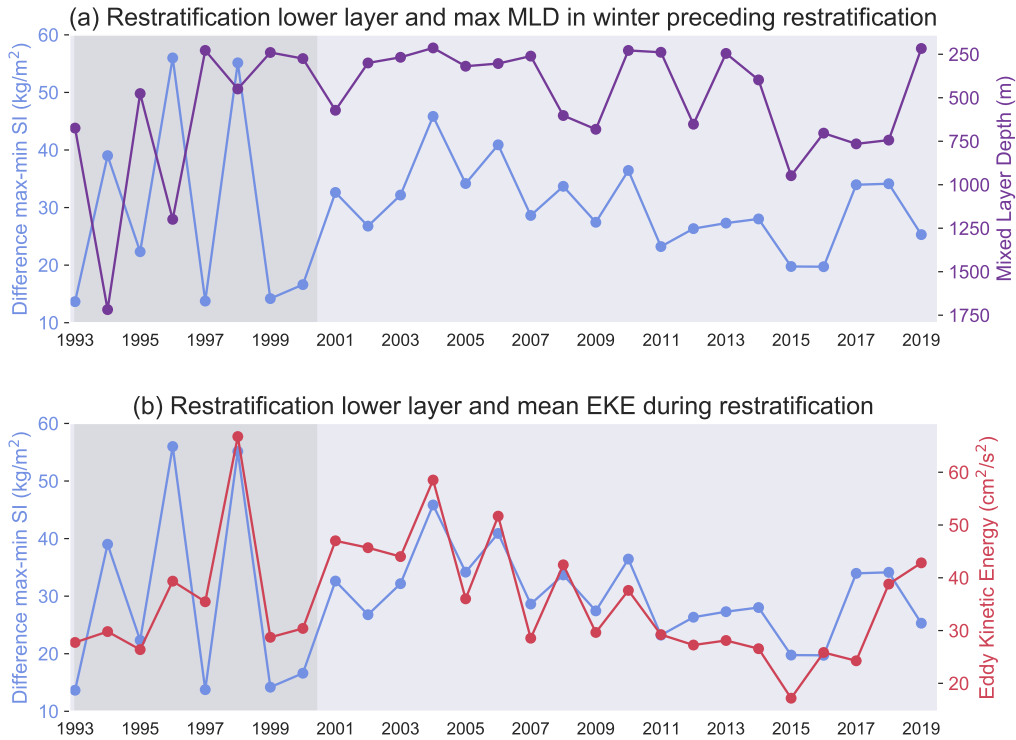


Figure 32: (a) Restratification and maximum MLD preceding the restratification period in the lower layer of the DCA. (b) Restratification in the lower layer of the DCA and surface EKE eastward of the DCA during the restratification phase. The shaded area marks the period before 2001, when the CMEMS data did not include ARGO data.

which can move into the DCA. These eddies are shed by the IC and thus have warm and saline cores. They are anticyclonic and therefore buoyant (Fan et al., 2013). Therefore they can contribute to restratification of the DCA. The higher the EKE, the more eddies there are, and thus the stronger the restratification.

5 Summary and Discussion

5.1 Summary

With all the results presented in this study we can answer the research questions stated in Section 1.5.

1. *What is the vertical structure of restratification in the Irminger Sea?*

We partitioned the upper 600 m of the water column into an upper layer from 0–100 m and a lower layer from 100–600 m, and found distinct restratification behaviour in both layers. The contributions of the upper and lower layer SI to the total SI are of the same order of magnitude, with on average higher values in the lower layer, which is thicker. However the peaks in SI in the upper layer are also clearly visible over the total layer.

2. *What are the characteristics of interannual variability in restratification in the Irminger Sea?*

In the upper layer a strong seasonal cycle dominates in the stratification index, but in some years the maximum SI is notably higher (e.g. 2010 and 2019) or lower (e.g. 2013 or 2015) than average. The SI is always approximately zero in winter because the mixed layer always extends below the bottom of the upper layer, so there is no interannual variability in the minimum SI in the upper layer. In the lower layer the seasonality is also exhibited, but we mainly see considerable interannual variability, in the minimum as well as the maximum SI. Over the total layer the superposition of this seasonality and interannual variability is visible.

3. *What is the influence of salinity and temperature on restratification in the Irminger Sea?*

Salinity and temperature play different roles in both layers. The upper layer is warming and freshening during summer and becoming colder and more saline during winter. The salinity and temperature contributions to stratification both have a stabilising effect during most of the year, and a destabilising effect in the winter months; they follow the same seasonal cycle. By contrast, the lower layer is getting warmer and more saline during summer, and colder and fresher during winter. Salinity has a destabilising effect on the stratification. The density in the lower layer is decreasing during summer and increasing during winter. The fact that density decreases while salinity is increasing indicates a dominant role for temperature in determining the stratification. The temperature contribution determines the values of the annual restratification, whereas the salinity contribution determines the interannual variability in restratification in the lower layer.

4. *Which physical processes contribute to restratification in the Irminger Sea?*

Restratification in the upper layer is influenced by surface freshwater and heat fluxes. The timing of minimum and maximum stratification in the upper layer matches the timing of surface heat fluxes becoming positive and negative, respectively. The high stratification years 2010 and 2019 had a warm and fresh anomaly, which could be linked to strong surface freshwater and heat gain. However the surface fluxes cannot fully account for the interannual variability in maximum stratification. This indicates that there is also a role for lateral advection, which must concern advection of anomalies restricted to the upper layer. In the lower layer, stratification often keeps increasing for months after the surface heat flux has become negative. The minimum stratification is determined by the strength of convection: deeper mixed layers lead to weaker stratification. The restratification itself is not influenced by the mixed layer depth. Instead, it is strongly linked to the eddy kinetic energy in the eastern Irminger Sea, suggesting that warm, saline eddies shed by the Irminger Current play an important role in restratifying the DCA.

5.2 Discussion

The results we found regarding restratification in the Irminger Sea are very similar to results for the Labrador Sea as described by Straneo (2006a). As was already discussed in Section 1.3, a similar vertical partitioning of the water column was made, with a surface layer between 0–200 m and a lower layer from 200–1300 m. Both layers are warming in summer and cooling in winter, but the surface layer freshens in summer and gets more saline in winter, whereas for the lower layer this is the other way around. The surface layer properties exhibit a strong seasonal cycle and are driven by surface fluxes. The lower layer is dominated by interannual variability and is mainly affected by lateral exchange with other water masses. All these results were also found in our study of the Irminger Sea. Nevertheless, there is an important difference. In the Labrador Sea, eddies shed from the boundary current contributing to restratification also show distinct behaviour in the vertical: they have a cold and fresh upper layer extending until 100 to 400 m depth and a warm and saline layer below (De Jong et al., 2014). Therefore distinct behaviour in hydrographic properties and stratification between the upper and lower layer in the interior are to be expected. However, in the Irminger Sea such a vertical structure in eddies is not observed. Eddies shed by the Irminger Current, which contribute to restratification, are warm and saline throughout, and do not have a cold and fresh surface layer (Fan et al., 2013). Therefore it is surprising that a similar vertical structure as in the Labrador Sea is found in the Irminger Sea.

For the upper layer we expected the restratification behaviour to be determined by the surface freshwater and heat fluxes. However we could not fully explain the restratification with only these fluxes. Therefore there must be other processes in the upper layer playing a role. For the high stratification years of our case studies, 2010 and 2019, there exist studies revealing such processes. Oltmanns et al. (2018) studied the summer of 2010 in the Irminger Sea and the impact of its strong warm and fresh anomaly on weakening convection in the 2010–2011 winter. As was already discussed here, the water masses surrounding the DCA do not match the hydrographic properties of the warm and fresh surface anomaly. We found that a combination of strong freshwater and heat gain likely contributed. However, Oltmanns et al. (2018) speculate that the fresh surface layer had a continental origin and was modified by surface heating. They found that surface temperatures were high in a broad area near the southeast Greenland shelf, where meltwater is expected. There are currently no estimates of freshwater exported from Greenland into the Irminger Sea, so we could not take this into account in our study. In the CMEMS reanalysis only climatological runoff is taken into account, but no interannual variability. However, freshening due to ice melt is a plausible cause for freshwater anomalies near the East Greenland shelf, which we know can be exported to the DCA (Foukal et al., 2020; Duyck and De Jong, 2021; Duyck et al., prep) and thus

increase stratification there. In 2019 there might have been another process playing a role in the observed fresh anomaly. As was already briefly mentioned at the end of Section 3.3.1, between 2012 and 2016 a freshwater anomaly formed in the eastern subpolar North Atlantic, as described by Holliday et al. (2020). This was the largest freshening event of 120 years. The freshwater anomaly went on to propagate northward into the Irminger and Labrador Seas and the Nordic Seas. Their expectation was that the anomaly would take about 4–6 years to reach these areas. The observed freshening of the upper and intermediate layers from 2017 onward (Fig. 19a), as well as the strong freshwater anomaly in 2019, are thus the result of the circulating freshwater anomaly. Possibly in other years there were also laterally advected freshwater anomalies impacting stratification in the upper layer. An interesting subject for further study would be the relation between (re)stratification, melt of the Greenland Ice Sheet or Arctic sea ice, and export of meltwater towards the DCA.

For the lower layer we found a strong relation between the strength of annual restratification and EKE in the eastern Irminger Sea. Anticyclonic eddies with warm and saline cores shed by the Irminger Current move westward into the DCA, thus restratifying it (Fan et al., 2013). The higher the EKE, the stronger the maximum stratification in the lower layer. A limitation of the study presented here is that we only studied EKE, but not individual eddies and their properties. We did not check how many eddies actually moved into the DCA in each year, and we did not consider interannual variability in the temperature and salinity shed by the Irminger Current, which can be caused by variability of the IC properties (Fan et al., 2013; de Jong et al., 2020). The CMEMS monthly data set has the disadvantage that its spatial and temporal resolution are not optimal to study eddy properties. Fan et al. (2013) describe the observation of anticyclonic eddies by a mooring in the Irminger Sea between 2002 and 2009. For 16 of the observed eddies, estimates of their length scales and velocity structure were made. These eddies had a mean core diameter of 12 km, and a mean peak observed azimuthal speed of 0.1 m/s. With the spatial resolution of $1/12^\circ$ and the temporal resolution of one month of the CMEMS reanalysis used here, the occurrence or crossing of the DCA boundary of eddies might therefore be missed. A suggestion would be to use the CMEMS daily data set and apply eddy detection algorithms (see e.g. Fan et al., 2013; De Jong et al., 2014; de Jong et al., 2016) for certain fixed locations, for example along the WOCE AR7E section or along the DCA boundary, to study the movement and properties of individual eddies and their effect on restratification of the lower layer.

Another suggestion is to quantify the lateral fluxes of salt and heat across the boundary of the DCA. An explicit calculation of the fluxes over segments of the boundary would allow us to study not only the vertical structure and interannual variability but also the source of salt and heat fluxes. Unfortunately the CMEMS reanalysis is not suitable for this. The variables from the reanalysis are interpolated and therefore lose their conservation properties, making it impossible to close budgets. An alternative option would be the approach from Straneo (2006a), who computed the heat and salt content of both layers in the Labrador Sea using float data. In the upper layer (0–200 m in that study), the lateral fluxes during restratification were then defined as the difference between change in heat and salt content and the surface heat and freshwater fluxes. In the lower layer (200–1300 m), any change in heat and salt content during restratification was assumed to result from lateral fluxes, since surface fluxes only impact the upper layer and the exchange between the upper and lower layer is negligible during restratification. However this is a highly idealised approach for which a high amount of float or mooring data within the DCA would be required to accurately compute heat or salt contents of the DCA. Furthermore a disadvantage of this method is that it does not explicitly compute the lateral fluxes per location along the DCA boundary, and can therefore not provide any information about the source of the fluxes.

5.3 Implications for the Future

A very relevant question is how stratification of the Irminger Sea will change in the coming decades. Since the stratification is part of the preconditioning for deep convection, changes in stratification might lead to changes in deep convection and thereby impact the AMOC.

On the short term, effects of the extreme freshwater anomaly described by Holliday et al. (2020) are already observed. This anomaly is still present the Irminger Sea and can thus contribute to increased upper layer stratification. CTD sections from the summer of 2021 show that the freshwater anomaly is currently mixing down in a very shallow layer (De Jong and Middag, personal communication). There are accounts of similar extreme surface freshwater anomalies in the subpolar North Atlantic, so-called Great Salinity Anomalies (GSAs), in the 1970s and 1980s (Belkin et al., 1998). They could have great impacts: for example from 1969 to 1971 convection in the Labrador Sea shut down due to surface freshening induced by a GSA (Gelderloos et al., 2012).

Further study of the current freshwater anomaly in the Irminger Sea is thus important to understand convection and restratification in the next few years, and is a work in progress.

On the long term, effects of anthropogenic climate change need to be taken into consideration. Due to climate change, ocean surface temperatures have been increasing from the 19th century, and are projected to continue doing so in this 21st century. Furthermore, there are major changes in Arctic sea ice and freshwater distribution, and the Greenland Ice Sheet is losing mass: both processes will also continue throughout the 21st century (Sévellec et al., 2017; Fox-Kemper et al., 2021). Thus the Irminger Sea’s surface ocean will likely become fresher and warmer in the future. As we found in this study, this will increase stratification in the upper layer. Strengthened upper layer stratification could impact mixing strength and result in shallower mixed layers. This could, in turn, increase the stratification in the lower layer, as we showed in this study.

Increased stratification and weakened deep convection in the Irminger Sea will have important consequences for the global climate. Weaker convection implies less anthropogenic carbon uptake by the Irminger Sea. Also it will result in less overturning, for which the Irminger Sea plays an important role (Petit et al., 2020). This could contribute to a slow-down of the AMOC. Given these possible impacts, it is very important to have more in-depth studies of the processes contributing to restratification in the Irminger Sea and their expected changes in the coming decades.

Data Availability Statement

The CMEMS monthly mean data is available at https://resources.marine.copernicus.eu/?option=com_csw&view=details&product_id=GLOBAL_REANALYSIS_PHY_001_030. The files for 1993–2012 were last accessed on 29-10-2020; the files for 2013–2019 were last accessed on 21-05-2021. The file with the static fields for the CMEMS data (such as layer thicknesses) was downloaded from ftp://nrt.cmems-du.eu/Core/GLOBAL_ANALYSIS_FORECAST_PHY_001_024/global-analysis-forecast-phy-001-024-statics/ on 04-05-2021 (this is actually the file for a different data set, but it uses the same bathymetry as the [global-reanalysis-phy-001-030-monthly](https://resources.marine.copernicus.eu/?option=com_csw&view=details&product_id=GLOBAL_REANALYSIS_PHY_001_030) product).

The ERA5 monthly averaged data on single levels is available at <https://cds.climate.copernicus.eu/cdsapp#!/dataset/reanalysis-era5-single-levels-monthly-means?tab=overview> and was last accessed on 16-09-2021.

Data was processed using Python 3.6.13. All code used for processing data and making figures for this report is available at <https://github.com/MiriamSterl/RestratificationIrmingerSea>.

Acknowledgements

Many people supported me during the time I worked on this project. First, I would like to thank Dr. Femke de Jong, my main supervisor. Thank you for all the long online meetings, for your valuable feedback and advice about this project and about being a woman in science, and for reassuring me when I was feeling insecure. Second, I also thank my supervisors from UU, Dr. Erik van Sebille and Prof. Dr. Leo Maas, for their valuable input and feedback. Third, a big thank you to Elena from the Copernicus Marine Service help desk for always friendly, patiently and thoroughly answering all my questions about CMEMS.

It was a strange experience to do a research internship at an institute that I could not physically go to. Therefore a huge thanks to everyone at the department of Ocean Systems who helped to make me feel part of NIOZ. I would like to thank Nora, Elodie and Niek for all the nice discussions we had. In particular, I thank Nora for welcoming me into the group even before I had started the project, for her feedback on my thesis, all the fun chats we had, and of course for her great pep talks whenever I needed them. I look forward to continuing to work at NIOZ with all of you (now finally in real life!).

Writing a thesis can feel lonely, and even more so during a lockdown. Luckily all the interaction with my fellow Climate Physics students did not make it a lonely experience at all. Our online study group meetings, and later our many hours spent in the IMAU Master's room, always helped me to realise that I was not the only one struggling with certain things and that everything would be just fine. Apart from that I hugely enjoyed our coffee and lunch breaks. Thanks to all of you!

In all the months working from home, I was lucky enough to have three lovely home office colleagues. Jillis, Lieke and Erki, thank you for making my home an amazing place to be, and for all the dinners and *Heel Holland Bakt* evenings. I will miss you a lot, but promise to come back to haunt the house.

Finally, a huge thanks for my amazing family, for always being there for me. To my parents, Andreas and Caroline (a.k.a. Vati and Mutti), for all of your support with everything in my life. Of course, in particular, thank you Vati for your feedback on my thesis, and thank you Mutti for the beautiful painting you made for the cover. To my boyfriend Angelo, thank you for always calming me down whenever I feel stressed (which is quite often in a period of finishing a thesis, moving to an island, and starting a PhD), for making me feel safe, and for making me laugh. I am extremely grateful for having you in my life. And of course, thank you to my siblings(-in-law), Florian, Sebastian, Xenia, and Mereke. I can learn so much from all of you, and you mean the world to me.

References

- Assmann, K. M. and Timmermann, R. (2005). Variability of dense water formation in the Ross Sea. *Ocean Dynamics*, 55(2):68–87.
- Bailey, D. A., Rhines, P. B., and Häkkinen, S. (2005). Formation and pathways of North Atlantic Deep Water in a coupled ice–ocean model of the Arctic–North Atlantic Oceans. *Climate Dynamics*, 25(5):497–516.
- Bashmachnikov, I. L., Fedorov, A. M., Golubkin, P. A., Vesman, A. V., Selyuzhenok, V. V., Gnatiuk, N. V., Bobylev, L. P., Hodges, K. I., and Dukhovskoy, D. S. (2021). Mechanisms of interannual variability of deep convection in the Greenland sea. *Deep-Sea Research Part I: Oceanographic Research Papers*, 174(April):103557.
- Belkin, I. M., Levitus, S., Antonov, J., and Malmberg, S. A. (1998). ‘Great Salinity Anomalies’ in the North Atlantic. *Progress in Oceanography*, 41(1):1–68.
- Brown, P. J., Mcdonagh, E. L., Sanders, R., Watson, A. J., King, B. A., Smeed, D. A., Baringer, M. O., and Meinen, C. S. (2021). Anthropogenic Carbon Transports and Uptake.
- Chanut, J., Barñier, B., Large, W., Debreu, L., Penduff, T., Molines, J. M., and Mathiot, P. (2008). Mesoscale eddies in the Labrador Sea and their contribution to convection and restratification. *Journal of Physical Oceanography*, 38(8):1617–1643.
- De Jong, M. F., Bower, A. S., and Furey, H. H. (2014). Two years of observations of warm-core anticyclones in the labrador sea and their seasonal cycle in heat and salt stratification. *Journal of Physical Oceanography*, 44(2):427–444.
- de Jong, M. F., Bower, A. S., and Furey, H. H. (2016). Seasonal and interannual variations of irvinger ring formation and boundary-interior heat exchange in FLAME. *Journal of Physical Oceanography*, 46(6):1717–1734.
- de Jong, M. F. and de Steur, L. (2016). Strong winter cooling over the Irminger Sea in winter 2014–2015, exceptional deep convection, and the emergence of anomalously low SST. *Geophysical Research Letters*, 43(13):7106–7113.
- de Jong, M. F., de Steur, L., Fried, N., Bol, R., and Kritsotalakis, S. (2020). Year-Round Measurements of the Irminger Current: Variability of a Two-Core Current System Observed in 2014–2016. *Journal of Geophysical Research: Oceans*, 125(10).
- de Jong, M. F., Oltmanns, M., Karstensen, J., and Society, T. O. (2018). Deep convection in the Irminger Sea observed with a dense mooring array. *Oceanography*, 31(1):50–59.
- De Jong, M. F., Van Aken, H. M., Våge, K., and Pickart, R. S. (2012). Convective mixing in the central Irminger Sea: 2002-2010. *Deep-Sea Research Part I: Oceanographic Research Papers*, 63:36–51.
- Dijkstra, H. A. (2008). *Dynamical oceanography*. Springer US.
- Duyck, E. and De Jong, M. F. (2021). Circulation Over the South-East Greenland Shelf and Potential for Liquid Freshwater Export: A Drifter Study. *Geophysical Research Letters*, 48(5):1–9.
- Duyck, E., Gelderloos, R., and De Jong, M. F. (in prep.). Wind Driven Freshwater Export at Cape Farewell.
- Fan, X., Send, U., Testor, P., Karstensen, J., and Lherminier, P. (2013). Observations of irvinger sea anticyclonic eddies. *Journal of Physical Oceanography*, 43(4):805–823.
- Fernandez, E. and Lellouche, J. M. (2018). Product User Manual For the Global Ocean Physical Reanalysis product GLOBAL_REANALYSIS_PHY_001_030.
- Foukal, N. P., Gelderloos, R., and Pickart, R. S. (2020). A continuous pathway for fresh water along the East Greenland shelf. *Science Advances*, 6(43).

- Fox-Kemper, B., Hewitt, H. T., Xiao, C., Aðalgeirsdóttir, G., Drijfhout, S. S., Edwards, T. L., Golledge, N. R., Hemer, M., Kopp, R. E., Krinner, G., Mix, A., Notz, D., Nowicki, S., Nurhati, I. S., Ruiz, J., Sallée, J.-B., Slangen, A. B. A., and Yu, Y. (2021). Ocean, Cryosphere and Sea Level Change. In Masson-Delmotte, V., Zhai, P., Pirani, A., Connors, S., Péan, C., Berger, S., Caud, N., Chen, Y., Goldfarb, L., Gomis, M., Huang, M., Leitzell, K., Lonnoy, E., Matthews, J., Maycock, T., Waterfield, T., Yelekçi, O., Yu, R., and Zhou, B., editors, *Climate Change 2021: The Physical Science Basis. Contribution of Working Group I to the Sixth Assessment Report of the Intergovernmental Panel on Climate Change*. Cambridge University Press. In Press.
- Frajka-Williams, E., Rhines, P. B., and Eriksen, C. C. (2014). Horizontal stratification during deep convection in the Labrador sea. *Journal of Physical Oceanography*, 44(1):220–228.
- Fratantoni, D. M. (2001). North Atlantic surface circulation during the 1990’s observed with satellite-tracked drifters. *Journal of Geophysical Research*, 106(C10):22,067–22,093.
- Fröb, F., Olsen, A., Våge, K., Moore, G. W., Yashayaev, I., Jeansson, E., and Rajasakaren, B. (2016). Irminger Sea deep convection injects oxygen and anthropogenic carbon to the ocean interior. *Nature Communications*, 7.
- Gelderloos, R., Katsman, C. A., and Drijfhout, S. S. (2011). Assessing the roles of three eddy types in restratifying the Labrador Sea after deep convection. *Journal of Physical Oceanography*, 41(11):2102–2119.
- Gelderloos, R., Straneo, F., and Katsman, C. A. (2012). Mechanisms behind the temporary shutdown of deep convection in the Labrador Sea: Lessons from the Great Salinity Anomaly years 1968-71. *Journal of Climate*, 25(19):6743–6755.
- Georgiou, S., van der Boog, C. G., Brüggemann, N., Ypma, S. L., Pietrzak, J. D., and Katsman, C. A. (2019). On the interplay between downwelling, deep convection and mesoscale eddies in the Labrador Sea. *Ocean Modelling*, 135(August 2018):56–70.
- Herrmann, M., Sevault, F., Beuvier, J., and Somot, S. (2010). What induced the exceptional 2005 convection event in the northwestern Mediterranean basin? Answers from a modeling study. *Journal of Geophysical Research: Oceans*, 115(12):1–19.
- Hersbach, H., Bell, B., Berrisford, P., Hirahara, S., Horányi, A., Muñoz-Sabater, J., Nicolas, J., Peubey, C., Radu, R., Schepers, D., Simmons, A., Soci, C., Abdalla, S., Abellan, X., Balsamo, G., Bechtold, P., Biavati, G., Bidlot, J., Bonavita, M., De Chiara, G., Dahlgren, P., Dee, D., Diamantakis, M., Dragani, R., Flemming, J., Forbes, R., Fuentes, M., Geer, A., Haimberger, L., Healy, S., Hogan, R. J., Hólm, E., Janisková, M., Keeley, S., Laloyaux, P., Lopez, P., Lupu, C., Radnoti, G., de Rosnay, P., Rozum, I., Vamborg, F., Villaume, S., and Thépaut, J. N. (2020). The ERA5 global reanalysis. *Quarterly Journal of the Royal Meteorological Society*, 146(730):1999–2049.
- Holliday, N. P. (2016). RRS Discovery Cruise DY054, 27 Jul - 17 Aug 2016, Reykjavik to Southampton. OSNAP 2016 mooring refurbishment cruise, Leg 2. Technical report, National Oceanography Centre, Southampton.
- Holliday, N. P., Bersch, M., Berx, B., Chafik, L., Cunningham, S., Florindo-López, C., Hátún, H., Johns, W., Josey, S. A., Larsen, K. M. H., Mulet, S., Oltmanns, M., Reverdin, G., Rossby, T., Thierry, V., Valdimarsson, H., and Yashayaev, I. (2020). Ocean circulation causes the largest freshening event for 120 years in eastern subpolar North Atlantic. *Nature Communications*, 11(1).
- Hopkins, J. E., Holliday, N. P., Rayner, D., Houpert, L., Le Bras, I., Straneo, F., Wilson, C., and Bacon, S. (2019). Transport Variability of the Irminger Sea Deep Western Boundary Current From a Mooring Array. *Journal of Geophysical Research: Oceans*.
- Jones, H. and Marshall, J. (1997). Restratification after deep convection. *Journal of Physical Oceanography*, 27(10):2276–2287.
- Katsman, C. A., Spall, M. A., and Pickart, R. S. (2004). Boundary current eddies and their role in the restratification of the Labrador Sea. *Journal of Physical Oceanography*, 34(9):1967–1983.
- Koltermann, K., Gouretski, V., and Jancke, K. (2011). *Hydrographic Atlas of the World Ocean Circulation Experiment (WOCE), Volume 3: Atlantic Ocean*. Southampton, UK.

- Lazier, J., Hendry, R., Clarke, A., Yashayaev, I., and Rhines, P. (2002). Convection and restratification in the Labrador Sea, 1990-2000. *Deep-Sea Research Part I: Oceanographic Research Papers*, 49(10):1819–1835.
- Le Bras, I. A., Straneo, F., Holte, J., de Jong, M. F., and Holliday, N. P. (2020). Rapid Export of Waters Formed by Convection Near the Irminger Sea’s Western Boundary. *Geophysical Research Letters*, 47(3).
- Le Bras, I. A. A., Straneo, F., Holte, J., and Holliday, N. P. (2018). Seasonality of Freshwater in the East Greenland Current System From 2014 to 2016. *Journal of Geophysical Research: Oceans*, 123(12):8828–8848.
- L’Hévéder, B., Li, L., Sevault, F., and Somot, S. (2013). Interannual variability of deep convection in the Northwestern Mediterranean simulated with a coupled AORCM. *Climate Dynamics*, 41(3-4):937–960.
- Li, F., Lozier, M. S., Holliday, N. P., Johns, W. E., Le Bras, I. A., Moat, B. I., Cunningham, S. A., and de Jong, M. F. (2021). Observation-based estimates of heat and freshwater exchanges from the subtropical North Atlantic to the Arctic. *Progress in Oceanography*, 197(June):102640.
- Lilly, J. M., Rhines, P. B., Visbeck, M., Davis, R., Lazier, J. R., Schott, F., and Farmer, D. (1999). Observing deep convection in the labrador sea during winter 1994/95. *Journal of Physical Oceanography*, 29(8 PART 2):2065–2098.
- Lozier, M. S. (2010). Deconstructing the conveyor belt. *Science*, 328(5985):1507–1511.
- Lozier, M. S. (2012). Overturning in the North Atlantic. *Annual Review of Marine Science*, 4:291–315.
- Lozier, M. S., Li, F., Bacon, S., Bahr, F., Bower, A. S., Cunningham, S. A., De Jong, M. F., De Steur, L., DeYoung, B., Fischer, J., Gary, S. F., Greenan, B. J., Holliday, N. P., Houk, A., Houpert, L., Inall, M. E., Johns, W. E., Johnson, H. L., Johnson, C., Karstensen, J., Koman, G., Le Bras, I. A., Lin, X., Mackay, N., Marshall, D. P., Mercier, H., Oltmanns, M., Pickart, R. S., Ramsey, A. L., Rayner, D., Straneo, F., Thierry, V., Torres, D. J., Williams, R. G., Wilson, C., Yang, J., Yashayaev, I., and Zhao, J. (2019). A sea change in our view of overturning in the subpolar North Atlantic. *Science*, 363(6426):516–521.
- Madec, G. (2016). *NEMO Ocean Engine*.
- Margirier, F., Testor, P., Heslop, E., Mallil, K., Bosse, A., Houpert, L., Mortier, L., Bouin, M. N., Coppola, L., D’Ortenzio, F., Durrieu de Madron, X., Mourre, B., Prieur, L., Raimbault, P., and Taillandier, V. (2020). Abrupt warming and salinification of intermediate waters interplays with decline of deep convection in the Northwestern Mediterranean Sea. *Scientific Reports*, 10(1):1–11.
- Marshall, J. and Schott, F. (1999). Open-Ocean Convection: Observations, Theory, and Models. *Reviews of Geophysics*, 37(98):1–64.
- McCarthy, G. D., Smeed, D. A., Cunningham, S. A., and Roberts, C. D. (2017). Atlantic Meridional Overturning Circulation. *Marine Climate Change Impacts Partnership: Science Review*, (July):15–21.
- McDougall, T. J. and Barker, P. (2011). *Getting started with TEOS-10 and the Gibbs Seawater (GSW) Oceanographic Toolbox*. SCOR/IAPSO WG127.
- Oltmanns, M., Karstensen, J., and Fischer, J. (2018). Increased risk of a shutdown of ocean convection posed by warm North Atlantic summers. *Nature Climate Change*, 8(4):300–304.
- Pedro, J. B., Martin, T., Steig, E. J., Jochum, M., Park, W., and Rasmussen, S. O. (2016). Southern Ocean deep convection as a driver of Antarctic warming events. *Geophysical Research Letters*, 43(5):2192–2199.
- Pérez, F. F., Mercier, H., Vázquez-Rodríguez, M., Lherminier, P., Velo, A., Pardo, P. C., Rosón, G., and Ríos, A. F. (2013). Atlantic Ocean CO₂ uptake reduced by weakening of the meridional overturning circulation. *Nature Geoscience*, 6(2):146–152.
- Petit, T., Lozier, M. S., Josey, S. A., and Cunningham, S. A. (2020). Atlantic Deep Water Formation Occurs Primarily in the Iceland Basin and Irminger Sea by Local Buoyancy Forcing. *Geophysical Research Letters*, 47(22):1–9.
- Petit, T., Mercier, H., and Thierry, V. (2019). New Insight Into the Formation and Evolution of the East Reykjanes Ridge Current and Irminger Current. *Journal of Geophysical Research: Oceans*, 124(12):9171–9189.

- Pickart, R. S., Straneo, F., and Moore, G. W. (2003). Is Labrador Sea Water formed in the Irminger basin? *Deep-Sea Research Part I: Oceanographic Research Papers*, 50(1):23–52.
- Robinson, I. S. (2010). *Discovering the Ocean from Space*. Springer Berlin Heidelberg.
- Roquet, F., Madec, G., McDougall, T. J., and Barker, P. M. (2015). Accurate polynomial expressions for the density and specific volume of seawater using the TEOS-10 standard. *Ocean Modelling*, 90:29–43.
- Sabine, C. L., Feely, R. A., Gruber, N., Key, R. M., Lee, K., Büllester, J. L., Wanninkhof, R., Wong, C. S., Wallace, D. W. R., Tilbrook, B., Millero, F. J., Peng, T.-H., Kozyr, A., Ono, T., and Rios, A. F. (2004). The oceanic sink for anthropogenic CO₂. *Science*, 305(July):367–371.
- Sampe, T. and Xie, S. P. (2007). Mapping high sea winds from space: A global climatology. *Bulletin of the American Meteorological Society*, 88(12):1965–1978.
- Sévellec, F., Fedorov, A. V., and Liu, W. (2017). Arctic sea-ice decline weakens the Atlantic Meridional Overturning Circulation. *Nature Climate Change*, 7(8):604–610.
- Somot, S., Houpert, L., Sevault, F., Testor, P., Bosse, A., Taupier-Letage, I., Bouin, M. N., Waldman, R., Cassou, C., Sanchez-Gomez, E., Durrieu de Madron, X., Adloff, F., Nabat, P., and Herrmann, M. (2018). Characterizing, modelling and understanding the climate variability of the deep water formation in the North-Western Mediterranean Sea. *Climate Dynamics*, 51(3):1179–1210.
- Straneo, F. (2006a). Heat and freshwater transport through the central Labrador Sea. *Journal of Physical Oceanography*, 36(4):606–628.
- Straneo, F. (2006b). On the connection between dense water formation, overturning, and poleward heat transport in a convective basin. *Journal of Physical Oceanography*, 36(9):1822–1840.
- Sutherland, D. A. and Pickart, R. S. (2008). The East Greenland Coastal Current: Structure, variability, and forcing. *Progress in Oceanography*, 78(1):58–77.
- Swift, J. H. (1984). The circulation of the Denmark Strait and Iceland-Scotland overflow waters in the North Atlantic. *Deep Sea Research Part A, Oceanographic Research Papers*, 31(11):1339–1355.
- Våge, K., Pickart, R. S., Moore, G. W., and Ribergaard, M. H. (2008). Winter mixed layer development in the central Irminger Sea: The effect of strong, intermittent wind events. *Journal of Physical Oceanography*, 38(3):541–565.
- Våge, K., Pickart, R. S., Sarafanov, A., Knutsen, Ø., Mercier, H., Lherminier, P., van Aken, H. M., Meincke, J., Quadfasel, D., and Bacon, S. (2011). The Irminger Gyre: Circulation, convection, and interannual variability. *Deep-Sea Research Part I: Oceanographic Research Papers*, 58(5):590–614.
- Veth, C. (2005). RV Pelagia Shipboard Report: Cruise 64PE240, Project CLIVARNET, Atlantic Monitoring Programme (CAMP). Technical report, Royal Netherlands Institute for Sea Research.
- Volkov, D. L. (2005). Interannual variability of the altimetry-derived eddy field and surface circulation in the extratropical North Atlantic Ocean in 1993–2001. *Journal of Physical Oceanography*, 35(4):405–426.
- Wang, Z., Wu, Y., Lin, X., Liu, C., and Xie, Z. (2017). Impacts of open-ocean deep convection in the Weddell Sea on coastal and bottom water temperature. *Climate Dynamics*, 48(9-10):2967–2981.
- Yashayaev, I., Bersch, M., and van Aken, H. M. (2007). Spreading of the Labrador Sea Water to the Irminger and Iceland basins. *Geophysical Research Letters*, 34(10):1–8.
- Yashayaev, I. and Loder, J. W. (2017). Further intensification of deep convection in the Labrador Sea in 2016. *Geophysical Research Letters*, 44(3):1429–1438.

A Effect of Averaging CMEMS Data Over DCA

A.1 Choosing a DCA Boundary

In Section 2.2.1, it was explained that to define the Deep Convection Area (DCA), a contour of the smoothed MLD field averaged over months with large MLD values (maximum MLD exceeding 1000 m) was used. Here, we show the comparison between four different contours of this MLD field: the contours corresponding with the values 550 m, 600 m, 650 m, and 700 m. In Figure 33, for each month of the CMEMS 1993–2019 reanalysis in which the maximum MLD was more than 1000 m, the contours corresponding with MLD values of 1000 m are shown (NB: for this the unsmoothed, monthly MLD field is used). This shows where exactly deep convection has taken place throughout the years. Each panel shows one of the aforementioned contours of the smoothed, averaged MLD field. In Figure 34, the mean conservative temperature field averaged over the upper 600 m is shown, again with the four different contours. Based on these figures, the choice for the 650 m contour is made; it contains a larger part of the locations where deep convection occurred than the 700 m contour, mainly in the southeastern part, while not taking as much of the warm Irminger Current with it as the 550 m and 600 m contour do.

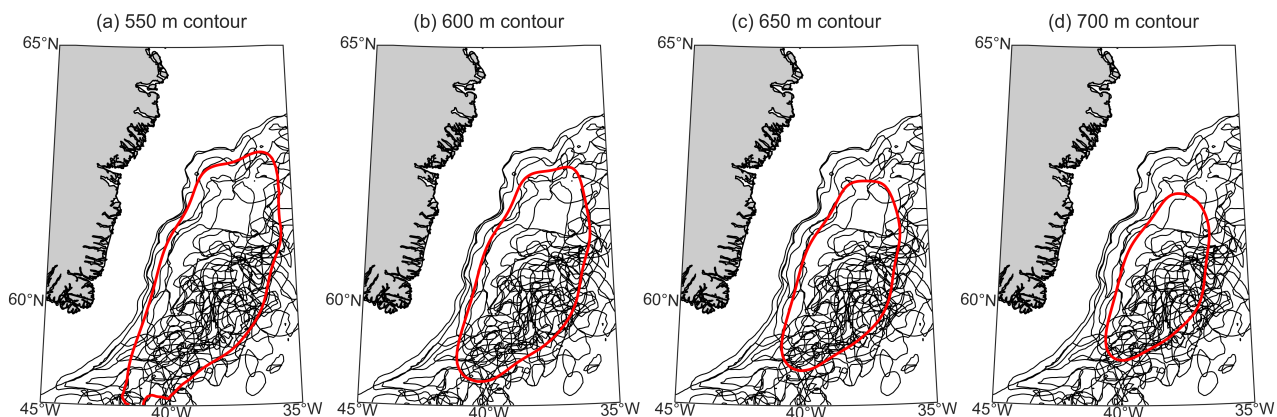


Figure 33: The MLD = 1000 m contours for each month in the 1993–2019 CMEMS reanalysis in which the maximum MLD exceeded 1000 m (black). Each panel shows a different contour (red) of the MLD field averaged over the months from the monthly 1993–2019 CMEMS reanalysis in which the maximum MLD exceeded 1000 m, and smoothed with a Gaussian filter with $\sigma = 5$ grid cells.

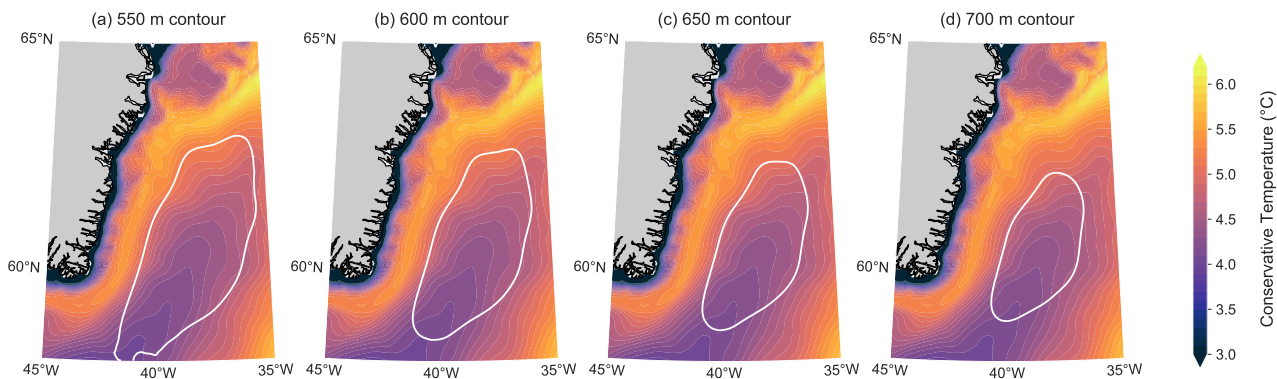


Figure 34: The 1993–2019 mean conservative temperature field from the CMEMS reanalysis, averaged over the upper 600 m. Each panel shows a different contour (white) of the MLD field averaged over the months from the monthly 1993–2019 CMEMS reanalysis in which the maximum MLD exceeded 1000 m, and smoothed with a Gaussian filter with $\sigma = 5$ grid cells.

A.2 Comparison of CMEMS Data at Fixed Location and Averaged Over DCA

In this study we always considered properties averaged over the DCA. Here we compare time series of hydrographic properties over depth from the CMEMS data averaged over the DCA (as in Fig. 19) with time series from the CMEMS data interpolated to the location of the LOCO mooring (as in Fig. 7a,c,e) for 2003–2017. These time series are shown in Figure 35. The figure shows that the time series interpolated to the mooring location and the time series averaged over the DCA are very similar. The time series averaged over the DCA are smoother in time, which makes sense since they are averaged over a large area. Nonetheless, interannual variations at the LOCO location are also visible in the average over the DCA. Examples are the deeper mixed layers in 2015–2017 together with a freshening and cooling of the water column down to approximately 1500 m depth. The similarity between the averaged time series and the time series at a single location give confidence that the averaged data accurately represent the properties and restratification behaviour we are interested in, and that the averaging does not hide significant regional behaviour. To confirm this last statement, comparisons with time series at other locations within the DCA would be needed to compare regional variations in hydrographic properties across the DCA. These findings also give confidence that the choice of a slightly different boundary for the DCA, as discussed in Appendix A.1, would not significantly affect the results as presented in this study.

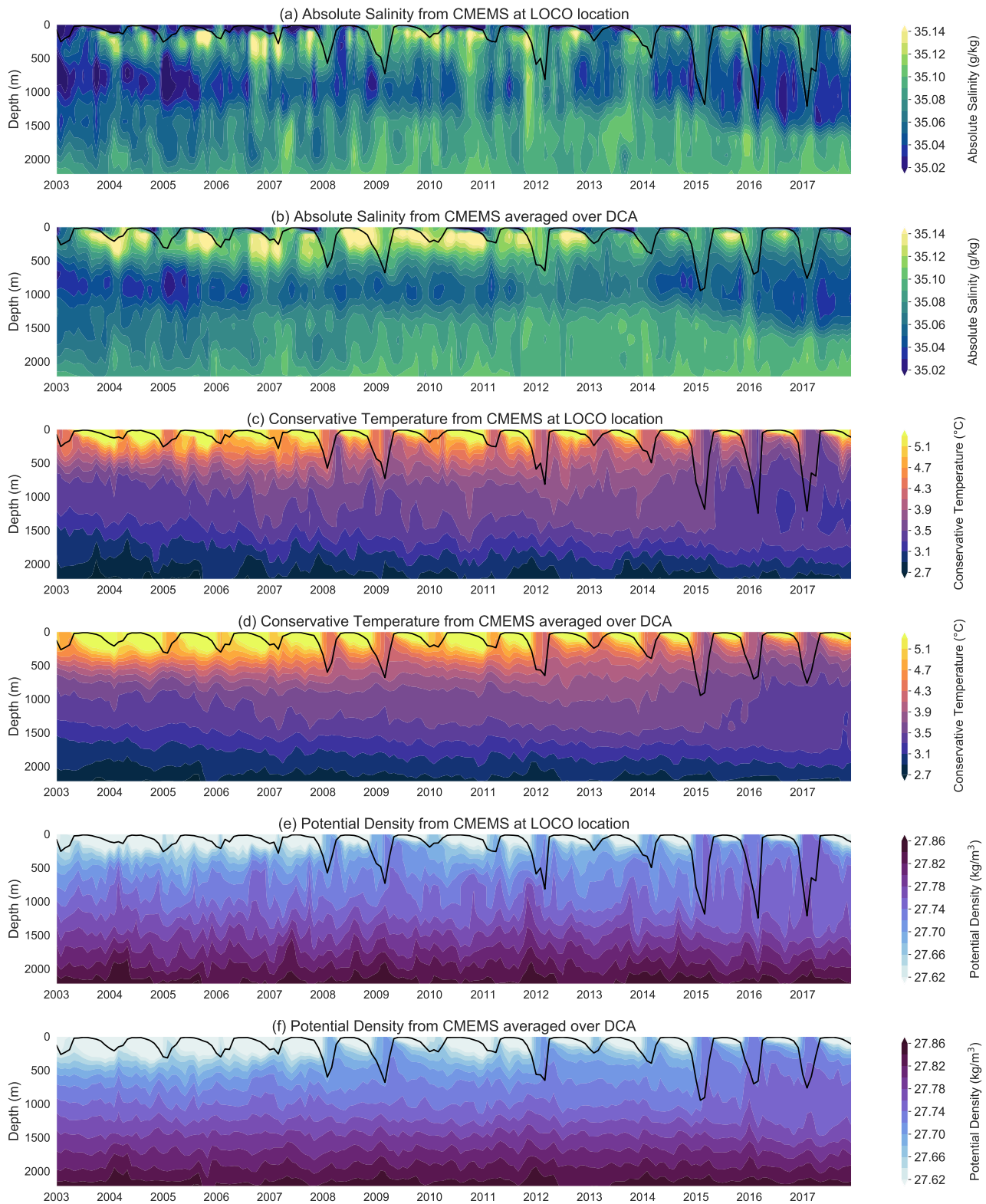


Figure 35: The temporal evolution of profiles of (a)-(b) absolute salinity, (c)-(d) conservative temperature and (e)-(f) potential density from the CMEMS monthly reanalysis data. The mixed layer depth is shown in black. Panels (a), (c) and (e) show the data interpolated to the location of the LOCO mooring (location shown in Figure 6). Panels (b), (d) and (f) show the data averaged over the DCA.